GRI-89/0138

# Falcon Series Data Report

# 1987 LNG Vapor Barrier Verification Field Trials



**FINAL REPORT**

(June 1990)

Gas Research Institute
8600 West Bryn Mawr Avenue
Chicago, Illinois 60631

GRI-89/0138

# Falcon Series Data Report

# 1987 LNG Vapor Barrier Verification Field Trials

Prepared by

**T. C. Brown, R. T. Cederwall, S. T. Chan, D. L. Ermak,**
**R. P. Koopman, K.C. Lamson, J. W. McClure, and L. K. Morris**

Lawrence Livermore National Laboratory
Box 808
Livermore, California 94550

For
GAS RESEARCH INSTITUTE
Contract No. 5085-252-1189
and
U.S. Department of Transportation

GRI Project Manager
Ted A. Williams
Environment, Safety and Distribution Division

June 1990

## DISCLAIMER

**LEGAL NOTICE:** This report was prepared by Lawrence Livermore National Laboratory (LLNL) as an account of work sponsored by the Gas Research Institute (GRI) and the U.S. Department of Transportation (DOT). Neither GRI, Members of GRI, DOT, LLNL, nor any person acting on their behalf:

a. Makes any warranty or representation, express or implied, with respect to the accuracy, completeness, or usefulness of the information contained in this report, or that the use of any apparatus, method, or process disclosed in this report may not infringe upon privately owned rights; or

b. Assumes any liability with respect to the use of, or for damages resulting from, the use of any information, apparatus, method, or process disclosed in this report.

## RESEARCH SUMMARY

| | |
|---|---|
| Title: | Falcon Series Data Report<br>1987 LNG Vapor Barrier Verification Field Trials |
| Prepared by: | T.C. Brown et al. |
| Coauthors: | R.T. Cederwall, S.T. Chan, D.L. Ermak, R.P. Koopman, K.C. Lamson, J.W. McClure, and L.K. Morris |
| Objectives: | The tests summarized in this report were designed: (1) to evaluate the effectiveness of a near full-scale vapor barrier on reducing the hazard distance associated with a large scale release of LNG, (2) to obtain extensive data for validation of wind tunnel and computer models of LNG releases into a vapor barrier. |
| Technical Perspective: | Key variables were examined, including spill rate, spill volume, and fluid velocity for LNG released onto a water pond inside a vapor barrier water spills were performed in order to vaporize LNG at a rate equal to the spill rate. A goal was to conduct all tests at the nominal worst-case atmospheric conditions of 3.5 m/s wind speed and a stable atmosphere. |
| Results: | Five experiments were conducted with spill rates varying from 8.7 $m^3$/min to 30 $m^3$/min, spill volumes from 20 $m^3$ to 63 $m^3$ and fluid velocities from 32 m/s to 146 m/s. Very good and complete data were obtained on three of the five experiments with some data loss on Test 2 and extensive data loss on Test 5 due to accidental ignition of the gas cloud. |
| Technical Approach: | A 44 m by 88 m by 9 m tall vapor barrier was constructed out of fiberglass cloth and erected at the LGF Spill Test Facility. A water pond was constructed inside the vapor barrier to promote rapid vaporization of the spilled LNG. An extensive array of measurement instruments was erected both inside the vapor barrier and downwind of the barrier to gather the extensive data needed for model validation. |
| Project Implications: | The report presents the data from the Falcon Series LNG vapor dispersion experiments conducted by LLNL and sponsored by GRI and the U.S. Department of Transporation. Detailed data from the experiments are maintained by GRI in magnetic tape format. The Falcon Series experiments provide valuable data for vapor dispersion characterization in a complex obstacle field, data for the evaluation of vapor fences as a dispersion mitigation measure, and data for validation of wind tunnel and computer models. Ongoing research activities involve laboratory and computer simulations of these experiments. |

Ted A. Williams

GRI Project Manager

# Table of Contents

50272-101

| REPORT DOCUMENTATION PAGE | 1. REPORT NO. GRI-89/0138 | 2. | 3. Recipient's Accession No. |
|---|---|---|---|

**4. Title and Subtitle**
Falcon Series Data Report
1987 LNG Vapor Barrier Verification Field Trials

**5. Report Date** approved June, 1990

**6.**

**7. Author(s)** T.C. Brown, R.T. Cederwall, S.T. Chan, D.L. Ermak, R.P. Koopman, K.C. Lamson, J.W. McClure, and L.K. Morris

**8. Performing Organization Rept. No.** UCRL-

**9. Performing Organization Name and Address**
Lawrence Livermore National Laboratory, L-262
Box 808, 7000 East Ave.
Livermore, CA 94550

**10. Project/Task/Work Unit No.**

**11. Contract(C) or Grant(G) No.**
(C) GRI 5085-252-1189
(G)

**12. Sponsoring Organization Name and Address**
Gas Research Institute
8600 West Bryn Mawr Avenue
Chicago, IL 60631

**13. Type of Report & Period Covered**
Data Report
1/86 - 11/89

**14.**

**15. Supplementary Notes**

**16. Abstract (Limit: 200 words)**

A series of five Liquefied Natural Gas Spills up to 66 $m^3$ in volume were performed on water within a vapor barrier structure at Frenchman Flat on the Nevada Test Site as a part of a joint government/industry study. This data report presents a description of the tests, the test apparatus, the instrumentation, the meteorological conditions, and the data from the tests.

**17. Document Analysis a. Descriptors**

**b. Identifiers/Open-Ended Terms**

**c. COSATI Field/Group**

| 18. Availability Statement | 19. Security Class (This Report) | 21. No. of Pages |
|---|---|---|
| Release unlimited.<br>Available from GRI or LLNL | Unclassified | 661 |
| | 20. Security Class (This Page) Unclassified | 22. |

(See ANSI-Z39.18) See Instructions on Reverse

OPTIONAL FORM 272 (4-77)
(Formerly NTIS-35)
Department of Commerce

## Abstract

A series of five Liquefied Natural Gas spills up to 66 $m^3$ in volume were performed on water within a vapor barrier structure at Frenchman Flat on the Nevada Test Site as a part of a study funded by the Gas Research Institute and the U.S. Department of Transportation. This data report presents a description of the tests, the test apparatus, the instrumentation, the meteorological conditions, and the data from the tests.


## 1.0 Introduction

The Lawrence Livermore National Laboratory (LLNL) conducted a series of five large scale (up to 66 $m^3$) pressurized Liquefied Natural Gas (LNG) spill tests for the Department of Transportation (DOT) and the Gas Research Institute (GRI) as part of a joint government/industry study. These tests were code named the "Falcon" Series. These tests were performed to evaluate the effectiveness of vapor fences as a mitigation technique for accidental releases of LNG, and to provide a data base for the validation of wind tunnel and computer model simulations of vapor fence effects on LNG dispersion. To assist in evaluating the effectiveness of vapor fences as a mitigation technique the experimental apparatus was designed to be sufficiently large to represent realistic vapor fence geometries and the tests designed to be of sufficient length to establish steady state conditions inside the vapor lower flammability limit (LFL) region. Spills were made onto a specially designed water pond equipped with a circulation system to maximize evaporation thus attempting to make the source evaporation rate as nearly equal to the spill rate as possible. The tests were performed over flat terrain under stable and neutral wind conditions at the Department of Energy (DOE) Liquefied Gaseous Fuels Spill Test Facility (LGFSTF) in the Frenchman Flat Area of the Nevada Test Site (NTS) which is under the jurisdiction of the DOE Nevada Operations Office (DOE/NV).

Two previous large scale experimental field test series (the Burro and Coyote series) were conducted with LNG by LLNL and the Naval Weapons Center (NWC) at China Lake, California, under the joint sponsorship of the DOE and the GRI. The purpose of the Burro Series, conducted in the summer of 1980, was to determine the transport and dispersion of vapor from spills of LNG on water. The Coyote series was conducted in the summer and fall of 1981, to investigate Rapid Phase Transition (RPT) explosions and to determine the characteristics of fires resulting from ignition of vapor clouds from LNG spills.

The purpose of this report is to describe the spill tests, test apparatus, instrumentation, meteorological conditions, and to make the data from the Falcon Test Series available to the sponsors. The bulk of the data are presented graphically to facilitate user assimilation of the several million words of digital data stored in the LLNL data base. This report is intended to report the data only, and therefore contains little analysis. The analysis of selected data from these tests will be published in future reports. Copies of the data tapes have been given to the sponsors.

The operational information necessary for conducting these spill tests was presented in the LGF Program Test Plan (Brown et al., 1987), Test Management Summary (Brown et al., 1987), Safety Assessment Document (Brown et al., 1987), and the Environmental Assessment (EA) (Patton et al., 1986).

## 2.0 LNG Vapor Barrier Verification Field Trials Description

The purpose of this section is to describe the experimental apparatus, experimental procedures, diagnostic instrumentation, control systems, data acquisition systems, and data processing systems to the extent necessary to allow the reader to understand the measurements used to produce the final results and their accuracy. Descriptions will be summary in nature and, where more detailed information exists, it will be referenced in the text. The exact position and operational status of each diagnostic instrument and instrument tower for each individual test is given in the Experiment Summary section. Tables 1–3 summarize the type and number of sensors employed during the test series. Figures 1–12 graphically depict the location of each sensor type, the $x$, $y$, and $z$ coordinates are with respect to an origin at the working point located in the middle of the downwind (NE) wall of the vapor barrier. The spill array was oriented parallel with the most prevalent wind direction with the positive $x$-axis forming an azimuth of 45° East of True North 1from the working point (positive $x$ runs downwind with a wind direction of 225°).

**Table 1.** Gas dispersion instrumentation.

| Measurement | Instrument | Quantity |
|---|---|---|
| Gas concentration measurements | MSA | 38 |
| | LLNL-IR | 35 |
| | JPL-IR | 4 |
| Wind field measurements | Met-One | 19 |
| Turbulence measurements | Gill bivane | 18 |
| Temperature measurements | Thermocouple | 100 |
| | RTD | 9 |
| Heat flux measurements | HY-CAL | 6 |
| Humidity measurements | ONDYNE | 4 |
| Absolute air pressure | Barometer | 1 |

**Table 2.** Spill facility instrumentation.

| Measurement | Quantity |
|---|---|
| Storage tank pressure | 4 |
| Drive gas pressure | 1 |
| Spill line pressure | 1 |
| Instrument gas pressure | 1 |
| Storage tank temperature | 5 |
| Spill line temperature | 10 |
| Storage tank level | 4 |
| Spill line flow | 1 |

Table 3. Photographic documentation.

| Instrument | Quantity |
|---|---|
| 35mm Still Frame Camera | 3 |
| 16mm 24 Frame/second Motion Picture Camera | 4 |
| Color Video Camera | 2 |
| CCD type Color Video Camera | 1 |

## 2.1 The Liquefied Gaseous Fuels Spill Test Facility

The Liquefied Gaseous Fuels Spill Test Facility (LGFSTF) was used for the first time during the Falcon Series. The LGFSTF was designed by Bechtel National, Inc., and constructed by Holmes and Narver Engineering and REECo as subcontractors to the USDOE. Complete detailed descriptions of the facility are available at the facility and at the NTS Engineering Library. The most comprehensive document is the LGFSTF, Nevada Test Site, Holmes & Narver/Department of Energy, Mechanical Design Record Book. A simpler description, plus a discussion of design criteria, the data acquisition system, and the meteorological instrumentation may be found in Johnson and Thompson (1986). The Facility is located on Frenchman Flat, an extremely flat playa with little vegetation.

The baseline facility consists of two generally separate process systems. The larger and more complex of the two systems is designed to handle cryogenic fluids, such as LNG, and was the system used for the Falcon Test Series. The cryogenic spill system consists of two independent 100-$m^3$ (26,000-gal) cryogenic storage tanks connected to 500-ft-long spill pipes that lead northwest to the spill area. Test fluid is pressure driven out of the storage tanks and through the spill pipes by means of nitrogen ($N_2$) drive gas at 5 to 140 psig. The drive gas is supplied from a 2000 psig, 2400 $ft^3$ (67 $m^3$) pressure vessel. The source of this gas is an $LN_2$ storage tank provided with a vaporizer and pumping system.

The operation and performance of the LGFSTF was controlled and monitored from a remote data recording control point located a safe distance upwind from the LGFSTF process systems location. The general location and intrasystem relationships of the LGFSTF are shown in the site plan in Figure 13.

The nitrogen storage and supply system that provided drive, cooldown, and purge gas to the facility is shown schematically in Figure 14. This system provided nitrogen drive gas at controlled pressures from 35 to 140 psig to force LNG out of the storage tanks and through the spill pipes to the spill point. Nitrogen was also supplied for purging tanks and piping prior to their use and after testing was completed, as well as for remote controlled valve actuation.

The drive gas system consists of piping, pressure control, and valving that feed the high pressure gas into the storage tanks or the upstream end of the spill pipes. The piping and valves were designed to provide the flow rates and pressures required to drive LNG at the rates specified for the Falcon Series. The control levels on the pressure control stations were varied and appropriate orifices inserted to provide the different spill rates for each test. Drive gas was routed to the upstream end of the spill pipes to drive residual LNG out of the spill pipe during the later stages (blowdown phase) of a test. The procedure involves isolating and bypassing the storage tanks after the predetermined volume of LNG had been discharged from the storage tank into the spill pipe.

Liquid nitrogen was used to chill the cryogenic piping and tankage prior to introducing LNG into these systems. Pre-test cooling of the spill pipe was accomplished by introducing $LN_2$ into

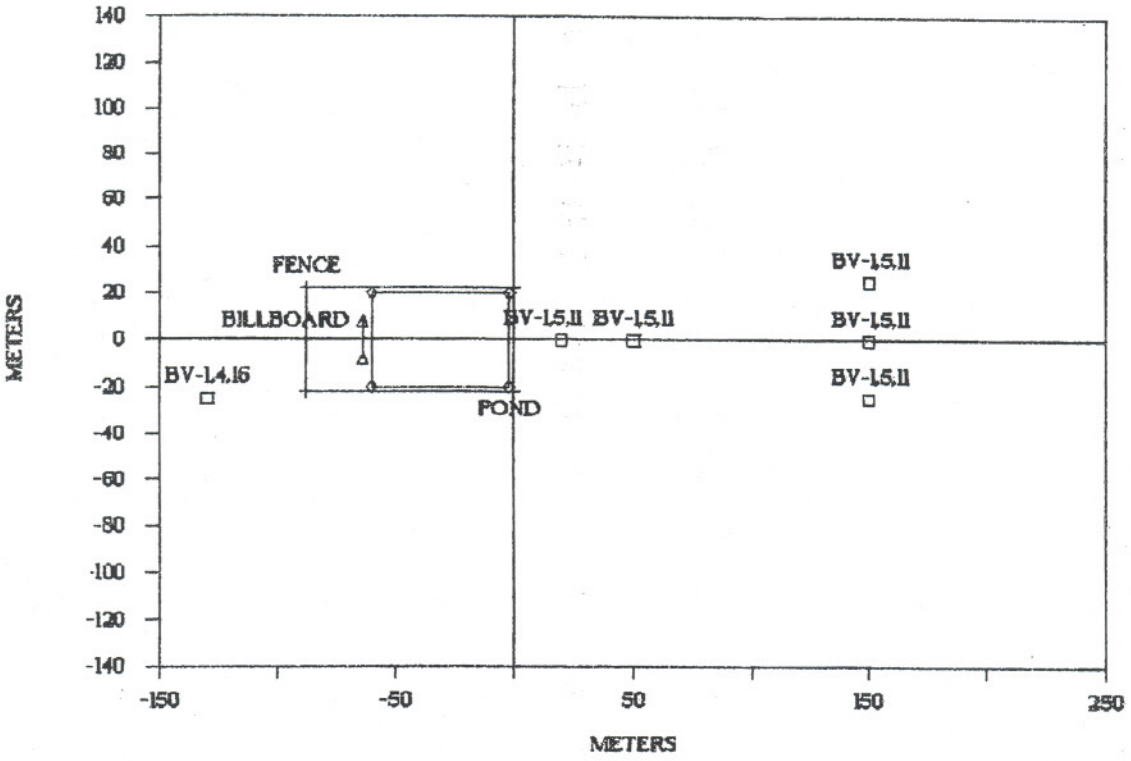


**Figure 1.** Falcon Series bivane array.

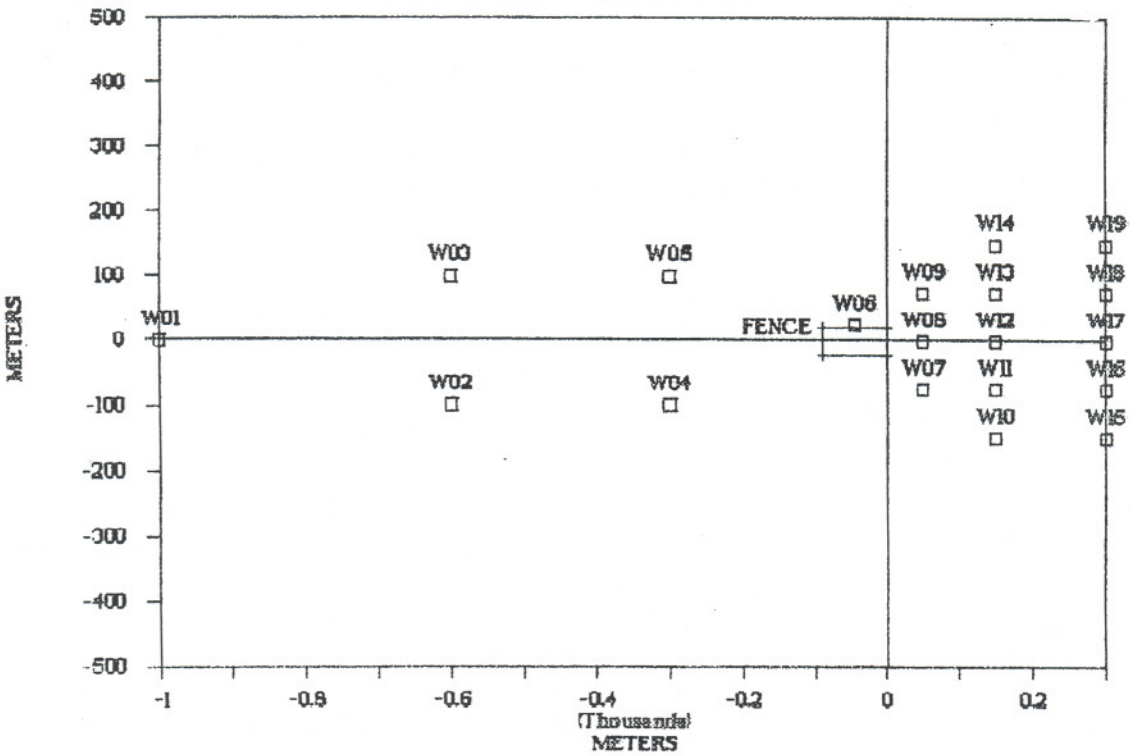


**Figure 2.** Falcon Series windfield array.

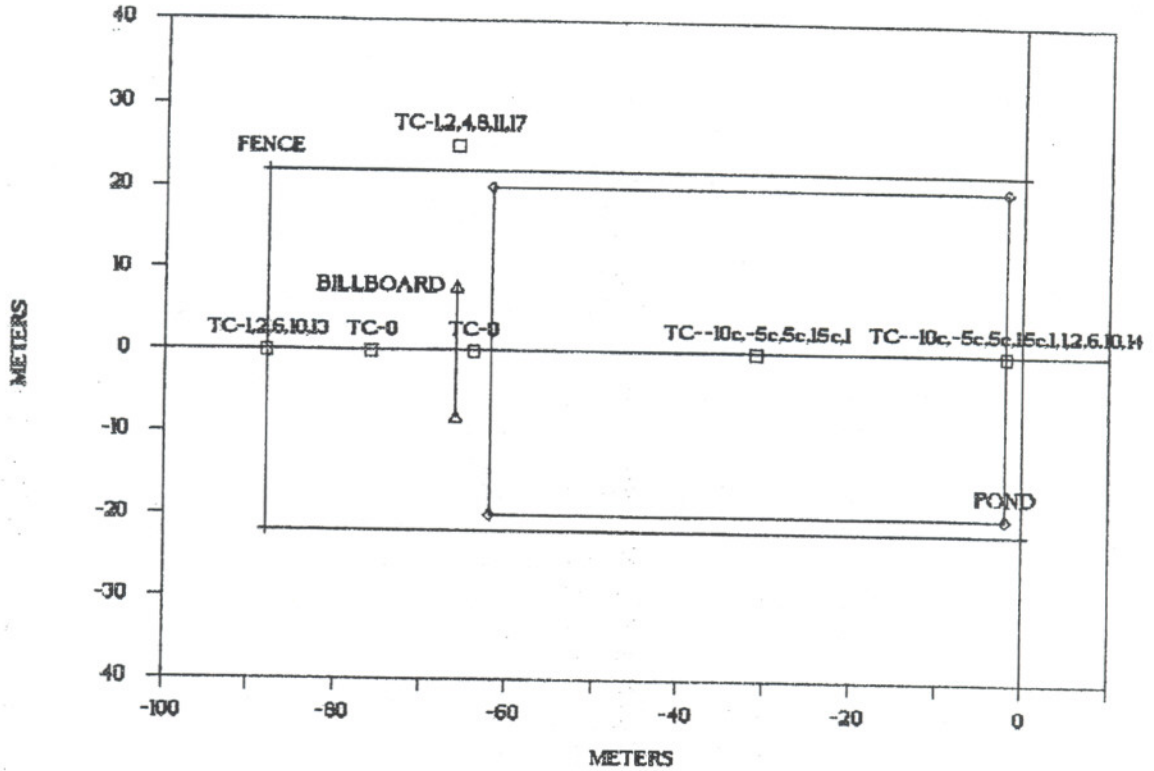


**Figure 3.** Falcon 1–2 spill area temperature array.

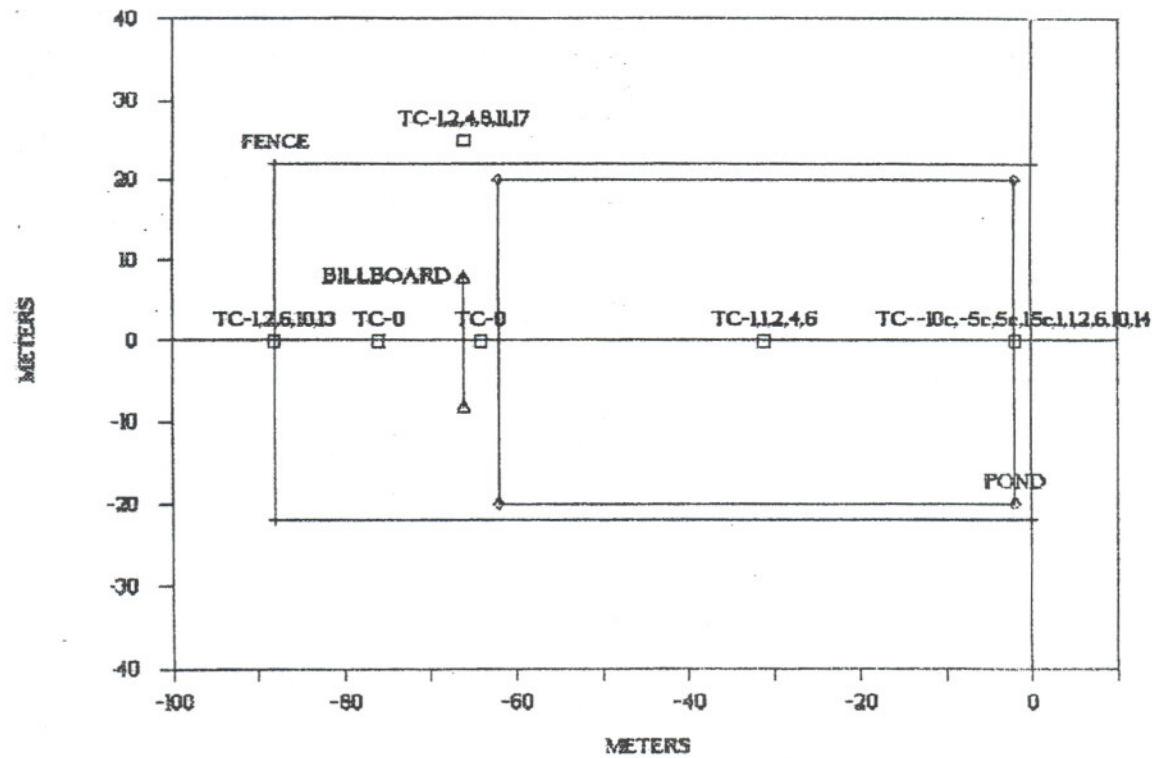


**Figure 4.** Falcon 3–5 spill area temperature array.

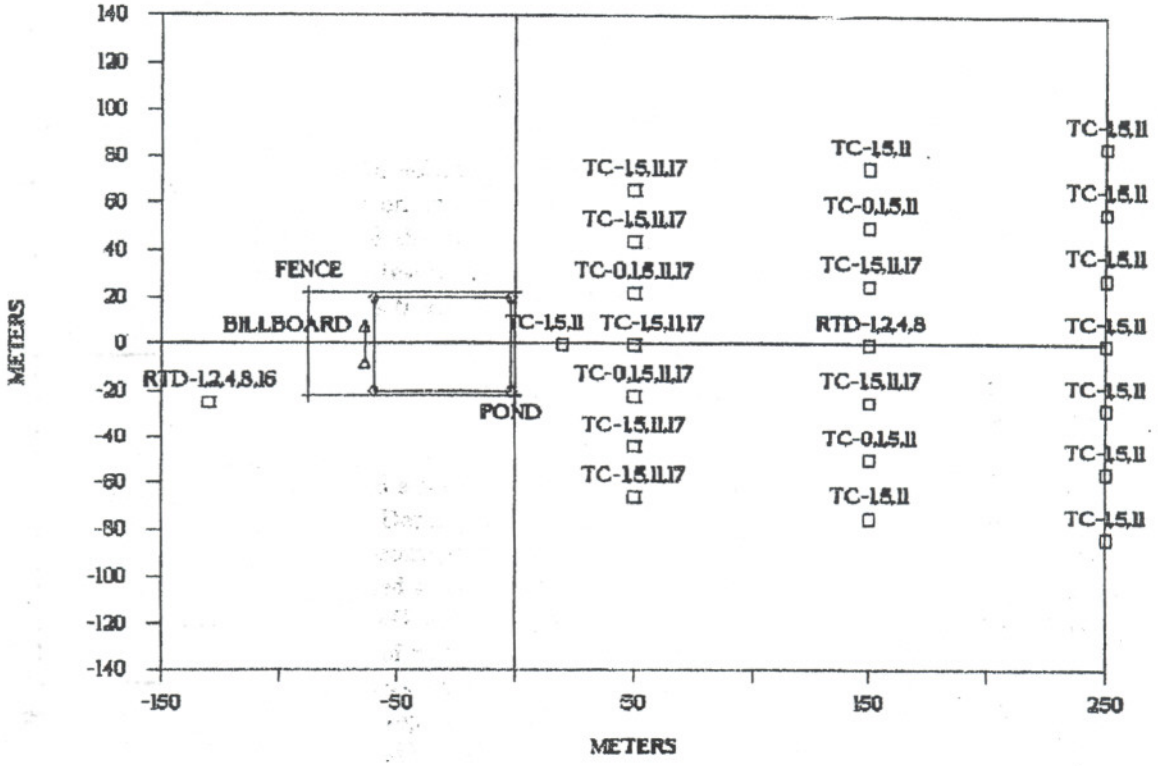


**Figure 5.** Falcon 1–3 temperature array.

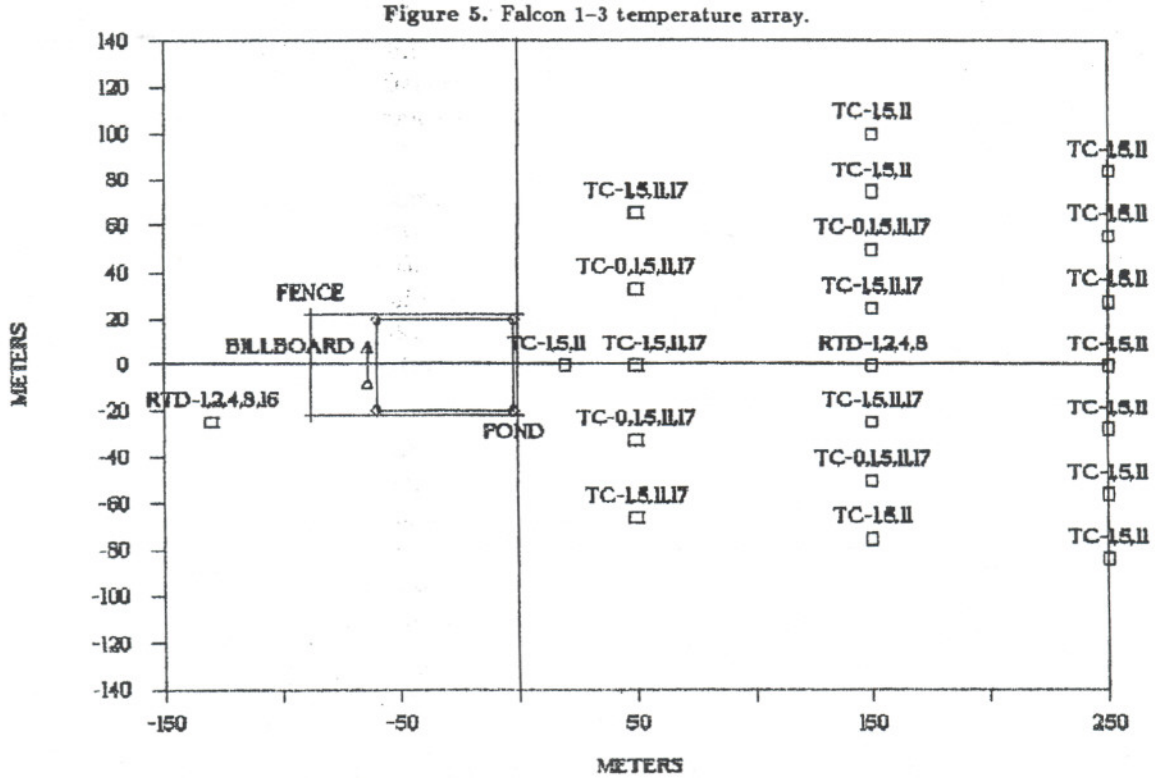


**Figure 6.** Falcon 4–5 temperature array.

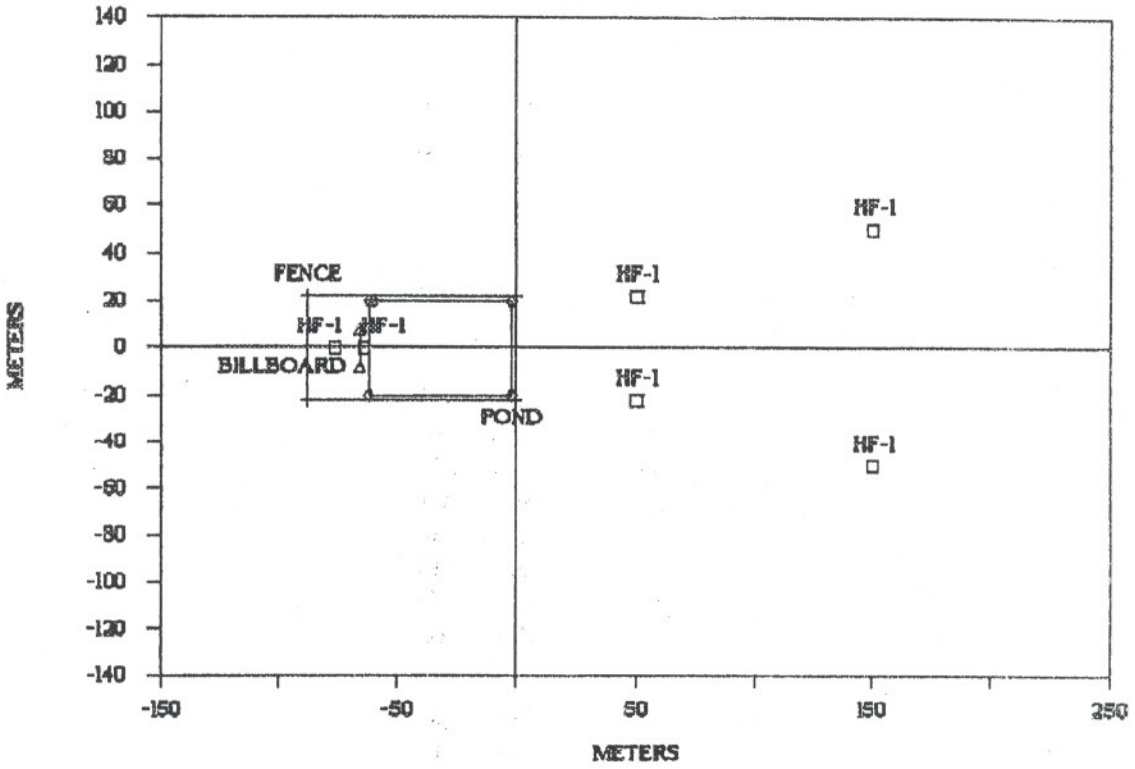


**Figure 7.** Falcon Series heat flux array.

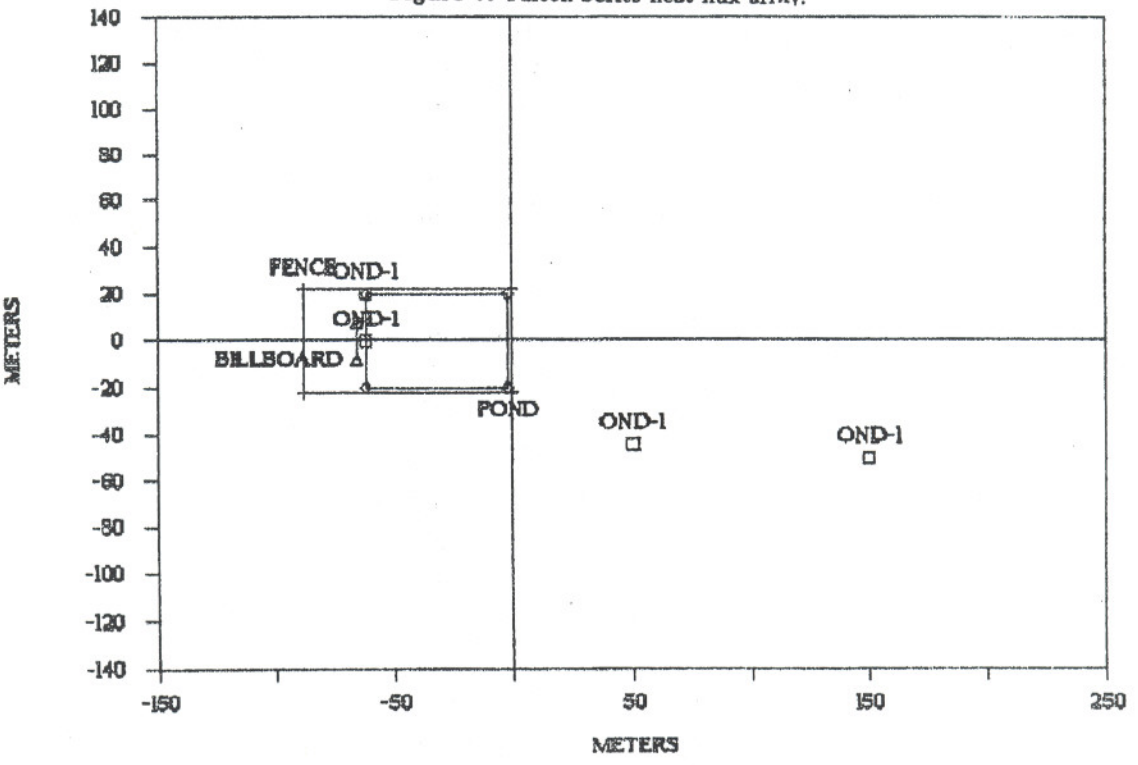


**Figure 8.** Falcon Series humidity array.

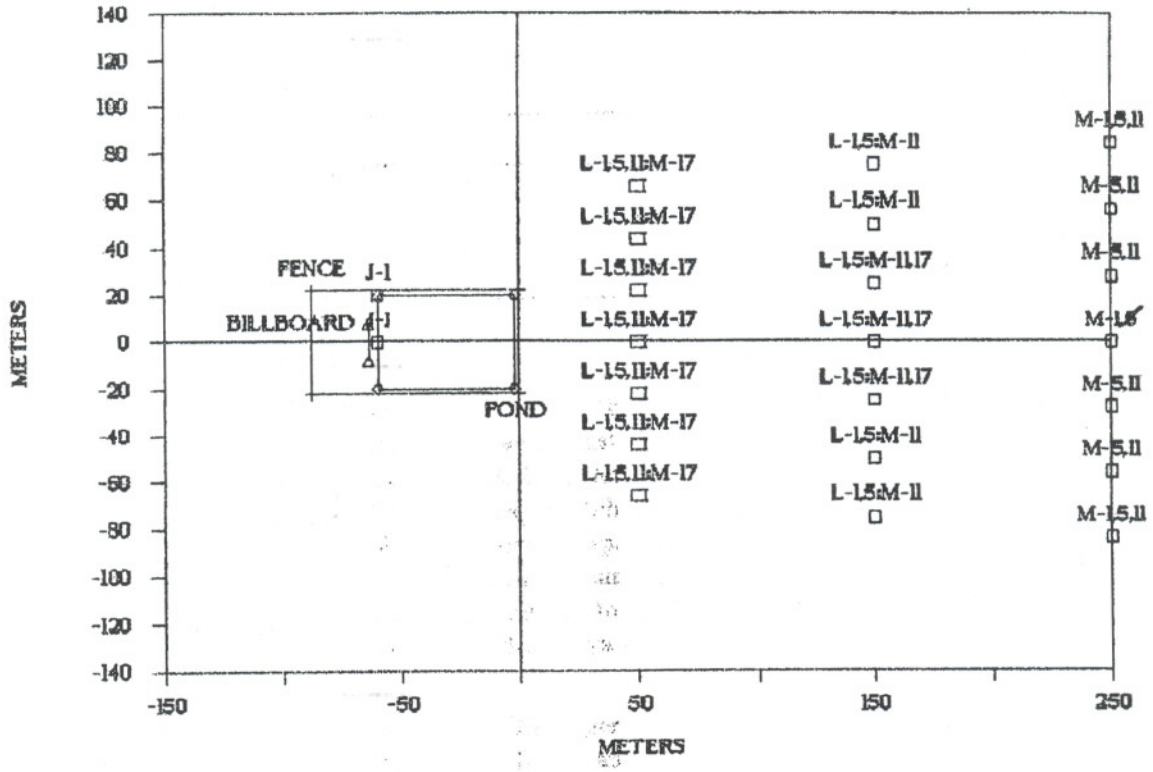


**Figure 9.** Falcon 1 gas array.

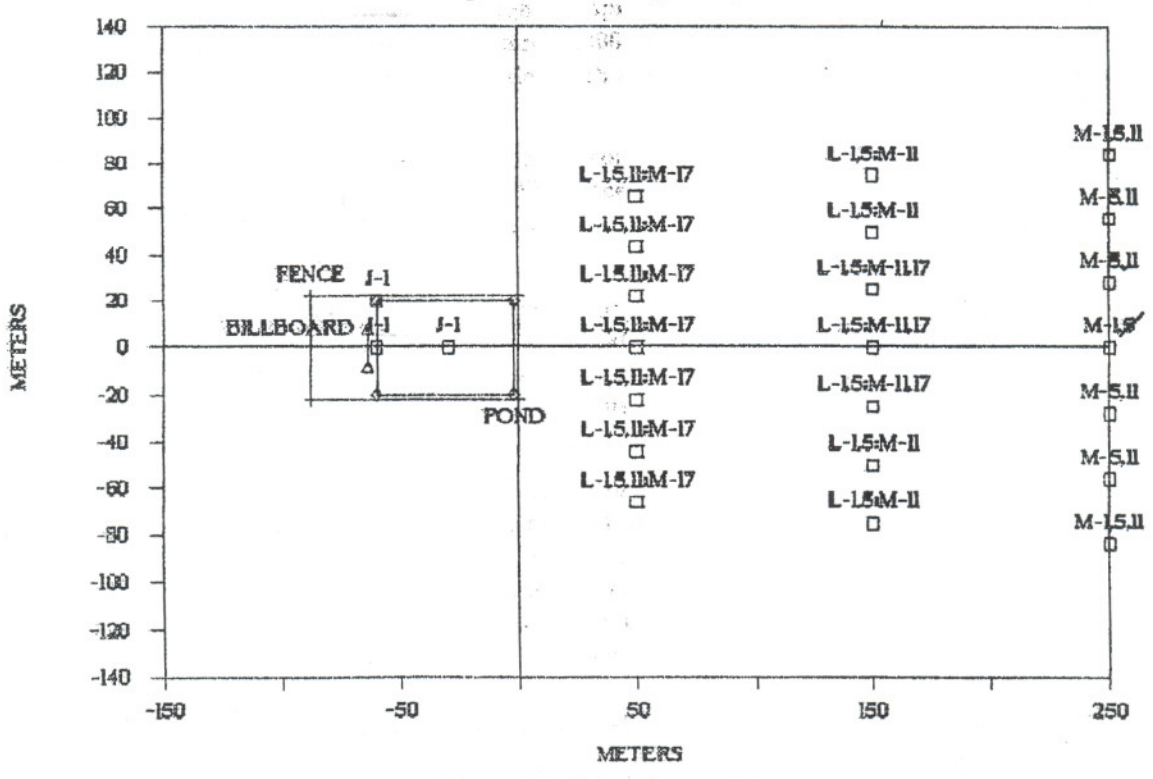


**Figure 10.** Falcon 2 gas array.

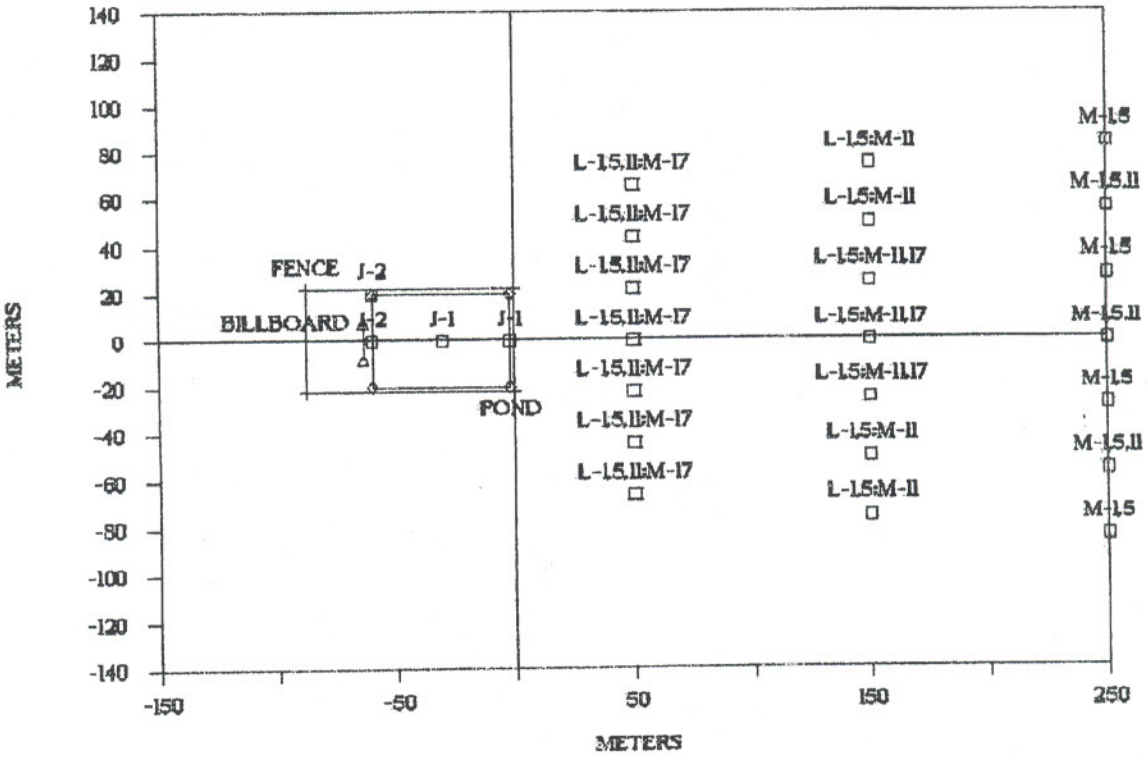


**Figure 11.** Falcon 3 gas array.

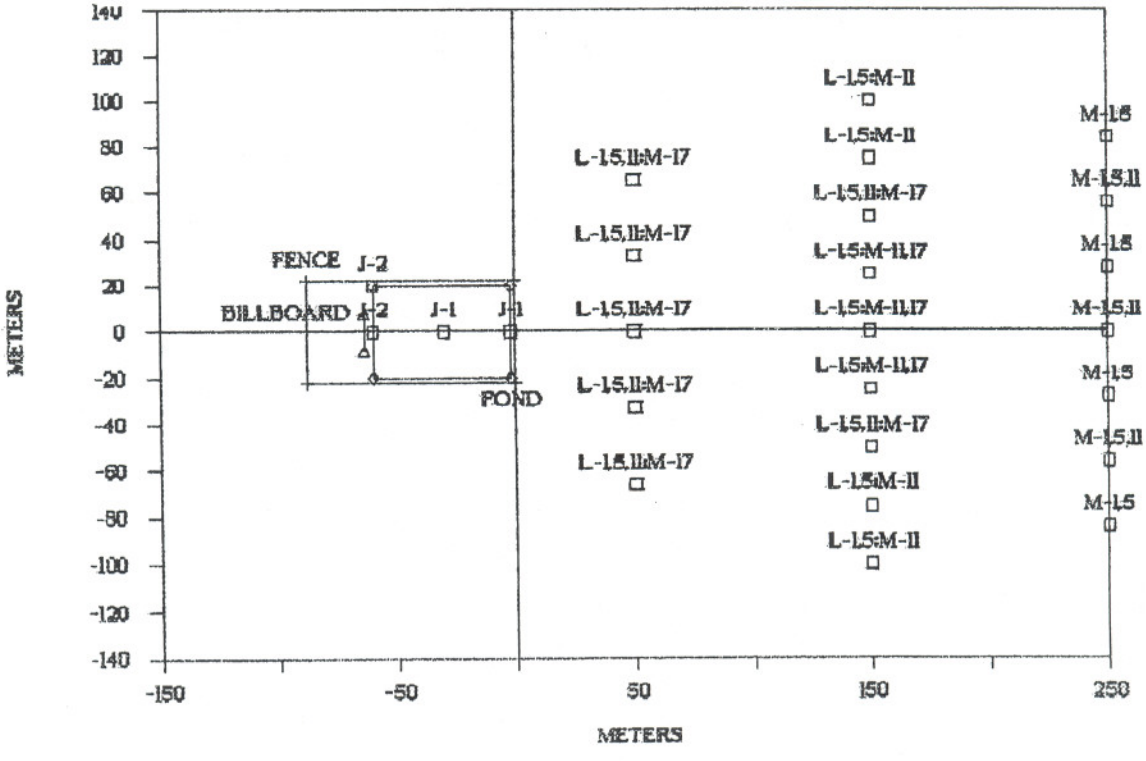


**Figure 12.** Falcon 4–5 gas array.

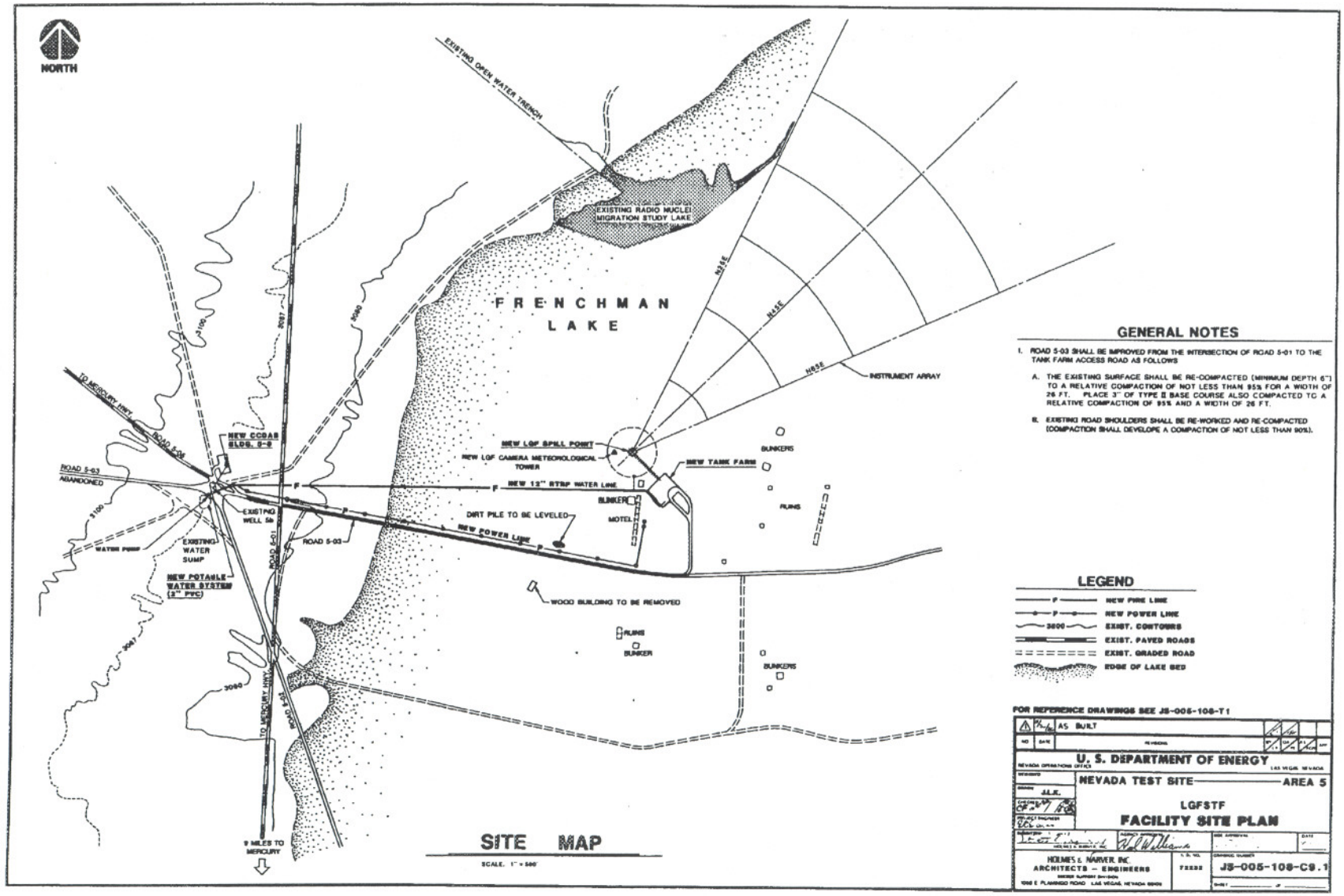


Figure 13. Site plan of LGF Spill Test Facility.

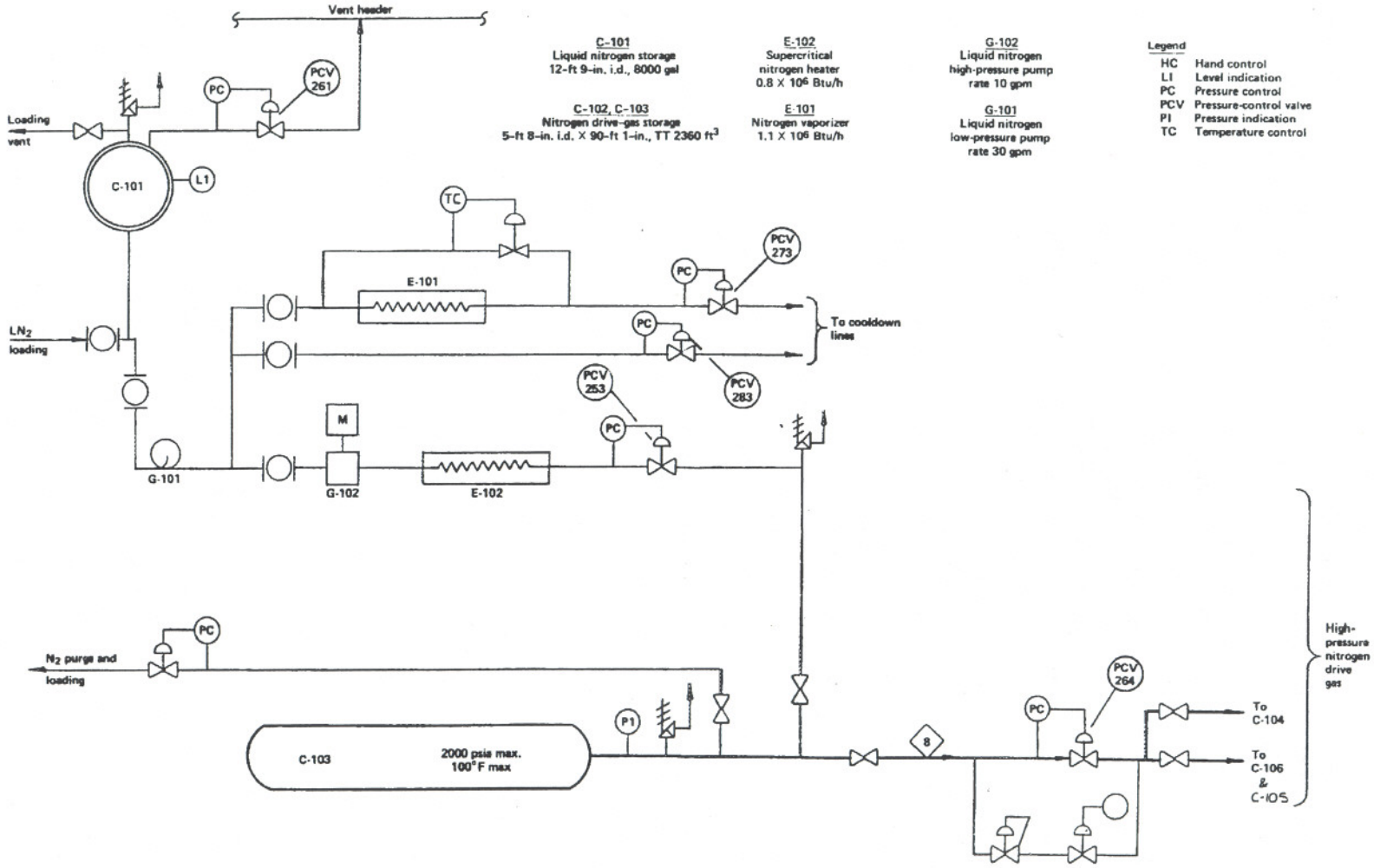


Figure 14. Nitrogen storage and supply system.



Figure 4. Nitrogen storage and supply system.

the spill pipe and venting the boil-off through the spill valve and/or the high point vent valve. Temperature monitoring of the spill pipe was used to determine the flow of $LN_2$ into the spill pipe during cooldown and to determine when LNG could be introduced into the spill pipe.

The cryogenic spill system, shown in Figure 15, provided the means for receiving, storing, and discharging LNG. The system received LNG delivered by tanker truck (supplied by Trussville Utilities Board, Trussville, Alabama) and provided storage between tests. The two cryogenic tanks are provided with valves and piping for receiving LNG deliveries, for discharging LNG, and for transferring LNG from one tank to the other. The tanks are instrumented with vacuum and pressure gauges, thermocouples, and liquid level sensors. Tank C-105 is connected to two separate lines; a 12-inch diameter line to provide high flow capability, and a 6-inch diameter line, which was not utilized in this test series. Tank C-106 is connected separately to a single 12-inch diameter line.

Each spill pipe is equipped with control valves at each end. To provide uniform LNG distribution on the pond surface a multi-exit spill "spider" was used. The spill "spider" was used, the spill pond, and the water circulation system are schematically depicted in Figure 16. Each arm of the spider was approximately 11.6 m in length, was oriented 90° from adjacent arms, and was fitted with a restrictive orifice at the downstream end of the horizontal portion to prevent flashing in the pipe. The spill pond was 40 m by 60 m and was filled to a depth of approximately 76 cm. Detailed mechanical drawings are available from the Liquified Gaseous Fuels Program at LLNL. The spill pond, the "spider" and the water circulation system were designed to vaporize the LNG at a high rate so that the vapor source rate was nearly equal to the spill rate. A known vapor source rate is very important for modeling purposes, especially when the data are to be used for model validation. RPTs were a known hazard for spills on water, but the requirement for a high (and known) vaporization rate was primary and the water pond was the only practical way of obtaining it.

The vapor fence structure (depicted in Figure 17) was fabricated from a proprietary fiberglass cloth impregnated with a mixture of silicon, Teflon and graphite. The fabric was reinforced by aluminum battens and suspended from a series of 9.1 m aluminum pillars by stainless steel cable. The barrier was 44 m by 88 m and was raised to a height of 8.7 m. The "billboard" structure, located upwind of the pond was employed to generate turbulence typical of a storage tank inside the fence. It was made from the same material as the vapor fence, reinforced with the same batten material and suspended from 13.7 m aluminum pillars. The structure was 17.1 m wide and was raised to a height of 13.3 m (see Figure 17).

## 2.2 Command, Control, and Data Acquisition

The Command, Control, and Data Acquisition System (CCDAS) provides remote and local control for the spill process, monitors important parameters and status information within the spill process, and provides a central location where all spill data are collected and stored. The system consists of the LGF Data Acquisition System (LGFDAS) and industrial control computer hardware and software. A block diagram of the CCDAS is shown in Figure 18. At the spill site, a local microcomputer-based subsystem provides signal conditioning for both input and output, provides local monitoring and control for manual operation and checkout, and supports communications with the remote subsystem. The operators' console and main control hardware are located at the remote site (CCDAS building), approximately one mile to the west. By means of a high speed data

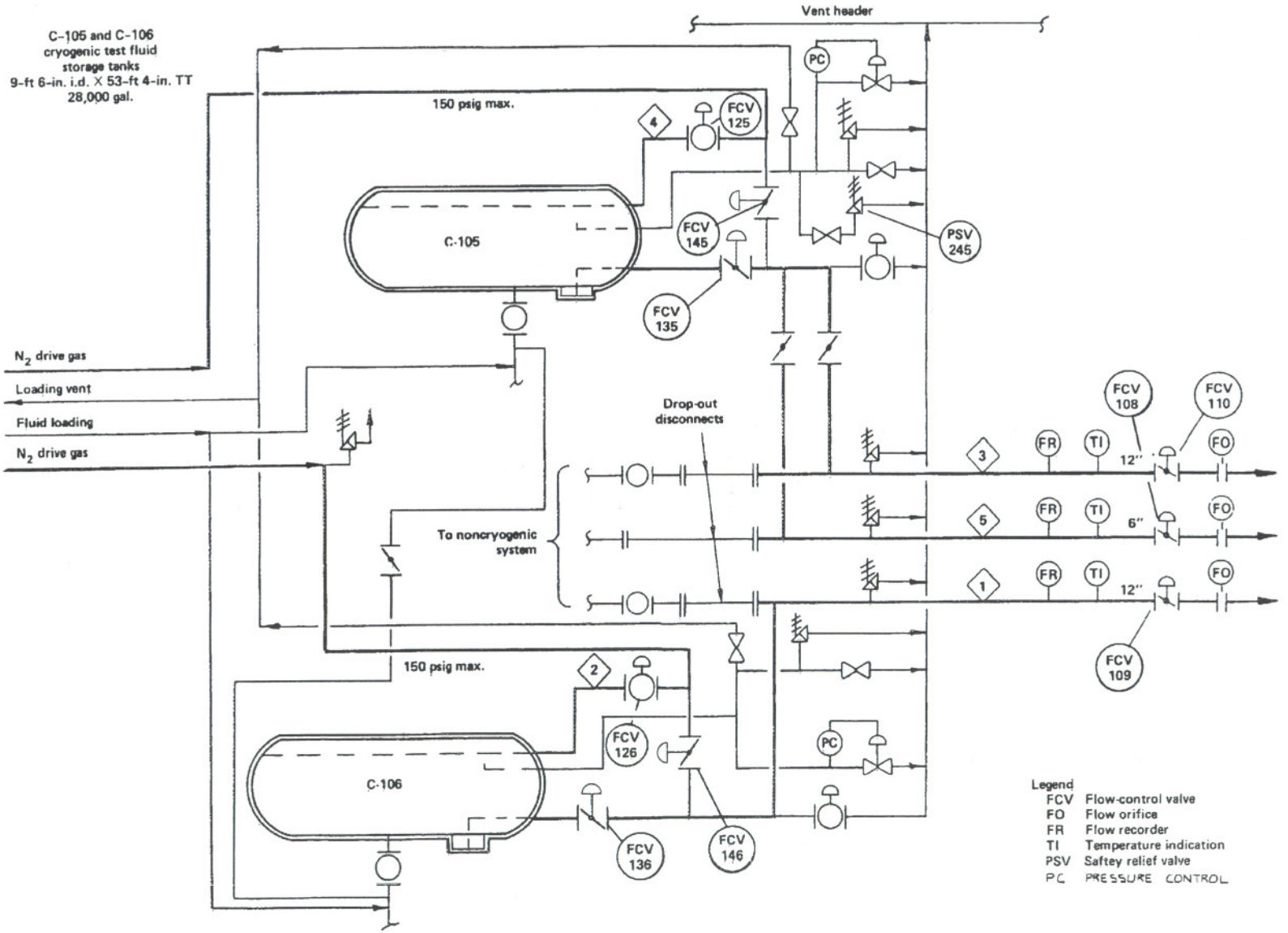


Figure 15. Cryogenic spill system.

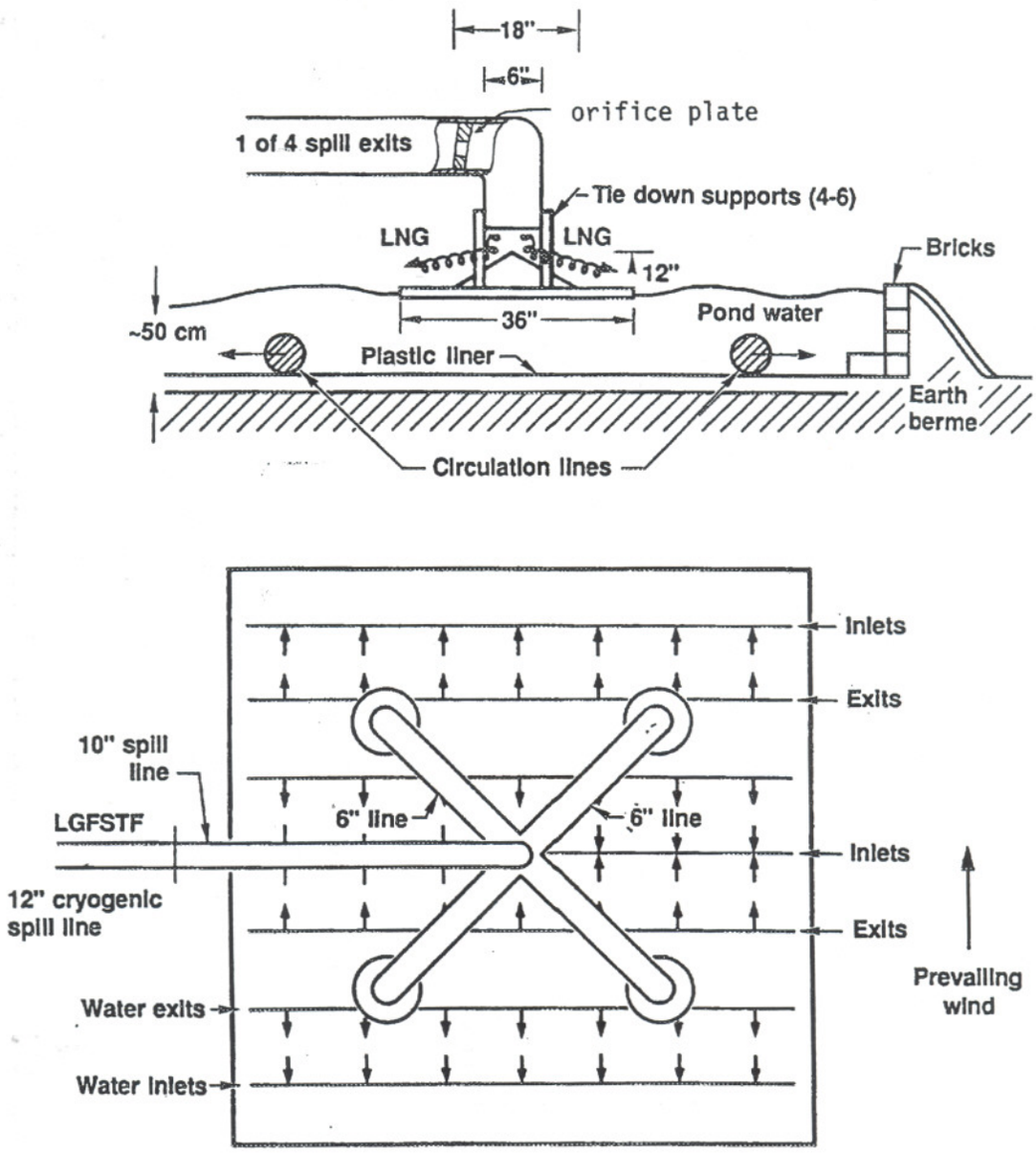


**Figure 16.** The vapor source multi-exit spill configuration.

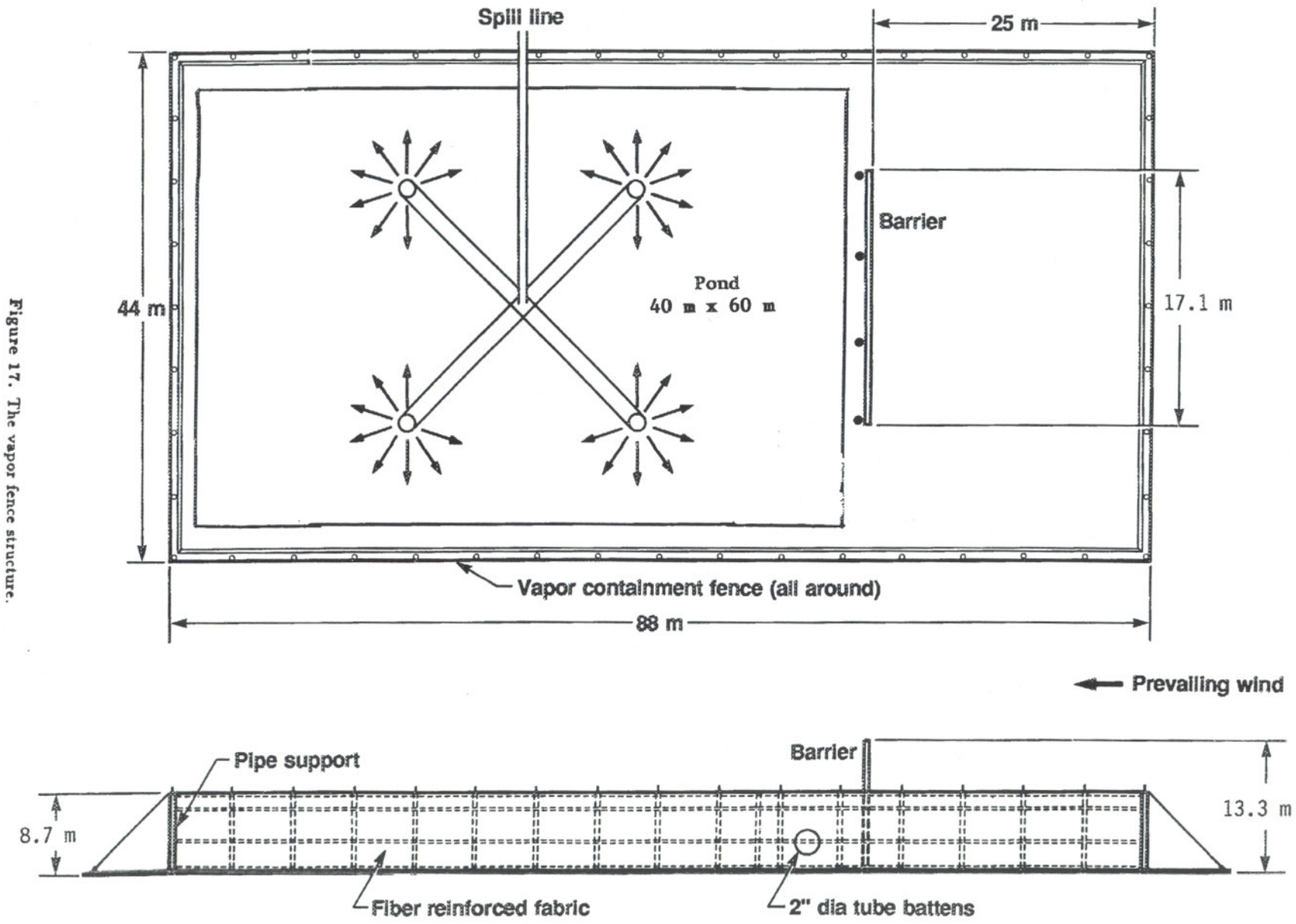


Figure 17. The vapor fence structure.

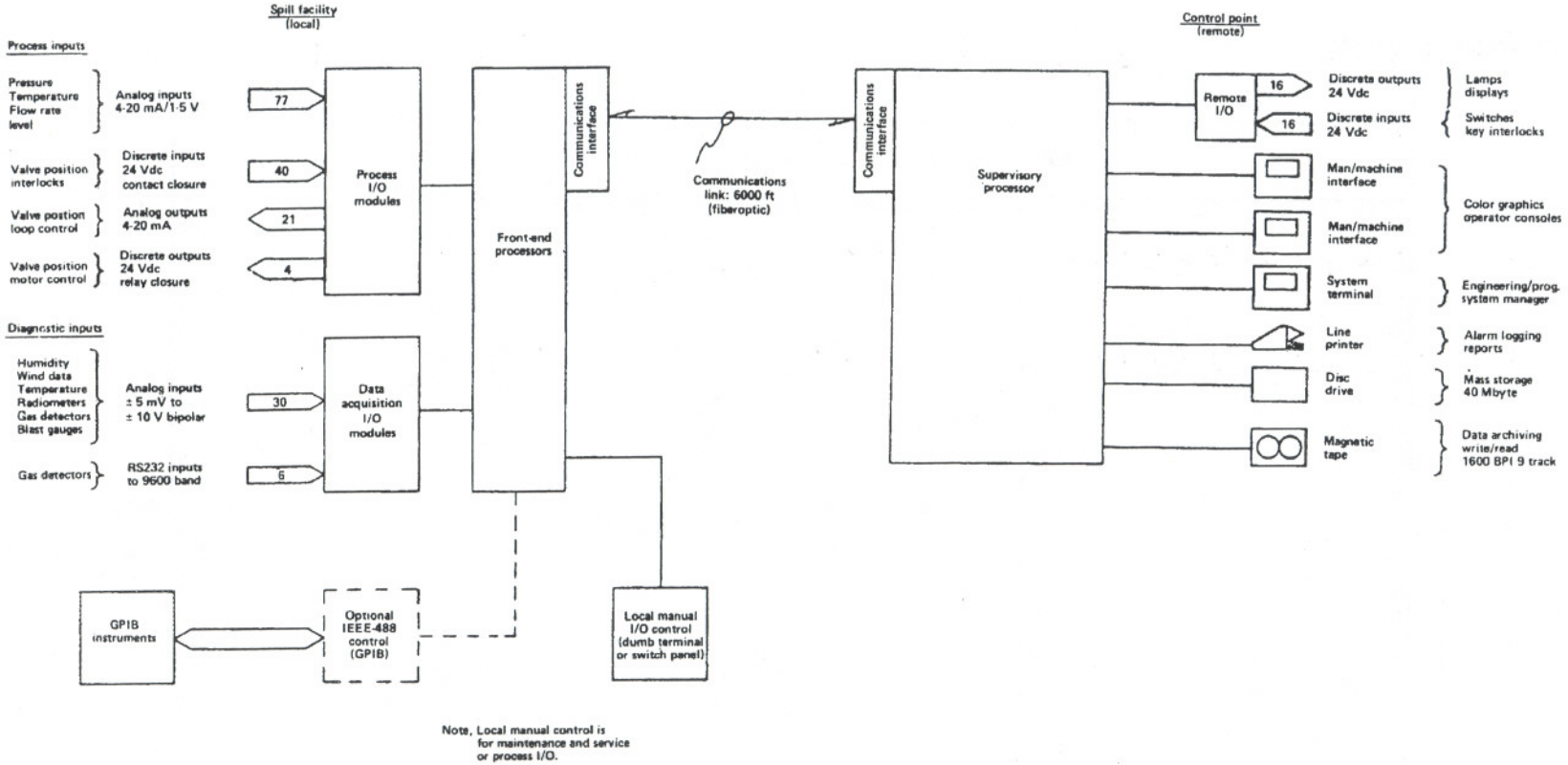


Note, Local manual control is for maintenance and service or process I/O.

**Figure 18.** Command, control, and data acquisition system.

link, the operators are able to observe and control the spill procedure and to acquire diagnostic data from the downwind sensor array, all in real time.

All facility operations not otherwise under direct manual control are conducted through the remote/local parts of the process control subsystem. The center of the system is the supervisory processor at the CCDAS building. Operators communicate with the process control system by means of man/machine interfaces (MMIs). These high resolution color MMIs are capable of displaying system status, alarms, messages, piping and flow diagrams, and data in the form of trend plots. To confirm process status, operators can view the real time MMI displays.

The process control subsystem also collects and stores status and measurement information relevant to facility operation. Analog measurements include multiple thermocouples, pressure transducers, flow meters, level indicators, etc. Signals from these transducers are converted to a current by a field mounted transmitter and sent to the process I/O modules. The current is converted to a digital word and sent over the high speed data link to the supervisory processor. The data are processed for display on the MMIs and are stored on disk. Certain data were integrated by the computer and displayed on the MMIs for parameters such as total flow. The parameters of each input, such as gain, linearization data, alarm limits, and sample rates, are stored on disk as part of the system data base. Each input is calibrated, linearized, checked for alarm limit, and time stamped as it is displayed and stored.

Data transmitted from the front-end processor to the CCDAS supervisory processor are stored on computer disk for short-term storage and processing. High capacity computer disk storage is provided, due to the large number of data points to be sampled and to allow monitoring data points as often as once per second. All data are time stamped to reconstruct a time history and to compare the occurrence of events on a temporal basis. When testing was completed, the data was archived on magnetic tape and saved for long-term storage and analysis.

Acquisition and storage of sensor field data were accomplished by the LGF Data Acquisition System (LGFDAS) located in the CCDAS building. The LGFDAS was developed by the LGF Program, over a period of several years, specifically for large-scale spill tests. The system utilizes two way UHF radio telemetry for command and data transmission, and is designed to acquire data from microprocessor controlled sensor stations at ranges up to ten miles from the receiving antenna (at the CCDAS building for these tests). The remote data acquisition stations are battery powered, portable, and ruggedized. Batteries are recharged by solar panels, which are collocated with the remote station. During the Falcon Series, a network of 44 stations were employed recording nearly 400 data channels at a rate of one sample per second from nearly 350 gas field channels and one sample every 10 sec from 38 wind field channels. Each station consisted of a Pacific Cyber/Metrix Model PPS-1201 microprocessor (CMOS PDP-8 equivalent), up to 8 k words of RAM, instrumentation amplifiers, relays to turn on sensors, radio transmitter and receiver, solar cells, and battery. Data acquired from the various sensors were packed alternately into one of two 2 kbyte buffers. The DEC LSI-11 minicomputers at the CCDAS building sequentially poll the remote stations in their network (gas field or wind field) requesting their full data buffers at 4.8 or 19.2 kbaud. Wind field data were presented in real time to help determine when test conditions were optimal. Raw data were recorded on disk for later processing.

After each test the raw data were converted to calibrated data sets using experimentally determined sensor calibration tables on the LSI-11 minicomputers. Calibrated data sets, sensor calibration files, data acquisition control files, and dayfiles are written to ASCII magnetic tape and

transferred to the LLNL Computation Center for archival. Data are stored on an off line mass storage system and are readily available for analysis.

Data manipulation, IR sensor data processing, and plotting were done on a CDC 7600 computer, using the high quality computational and graphics output devices available at LLNL. Gas concentration contour generation, mass flux analysis, and meteorological analysis were done using programs written specifically for this purpose. Acquisition and processing of the calibration data were done on a dedicated LSI-11 minicomputer, and the resulting files used at both LLNL and NTS for conversion of raw sensor data to calibrated data in engineering units.

## 2.3 Diagnostic Instrumentation

The purpose of this section is to describe each instrument used to measure the physical parameters necessary to evaluate the effectiveness of vapor barriers on dispersion of LNG. Discussion of each sensor is intended to be sufficient to appraise the reader of the sensor type, measurement technique employed, and estimated accuracy. More detailed descriptions are referenced in the text.

### 2.3.1 Meteorological Sensors

#### 2.3.1.1 Turbulence Anemometers

A total of 18 standard, commercially available Gill bivane anemometers (R.M. Young Company) were employed on the Falcon series of tests as depicted in Figure 1. These anemometers have a threshold of 0.1–0.2 m/s and a response distance constant of 1.0 m. Factory supplied calibration curves were used, and data taken every 1 sec. Absolute pointing accuracy was estimated to be better than $\pm 5°$ horizontally. Vertical error was generally larger, but data were corrected by subtracting the apparent pre-zero vertical mean angle. Speed and horizontal direction were generally in good agreement with the two-axis anemometers.

#### 2.3.1.2 Wind Field Anemometers

The wind field measurements were made using commercially available two-axis cup and vane anemometers (Met-One) located at 19 stations, 2 m above ground, both upwind and downwind of the spill point, as shown in Figure 2. They have a starting threshold of 0.2 m/s and a response distance constant of 1.5 m. Data were taken at 1 sec intervals, then vector averaged by the instrument for 10 sec prior to transmitting to the LGFDAS. The standard deviation of the individual directions about the 10 sec scalar mean were also transmitted. The wind field anemometers were calibrated with respect to three other 'standard' sensors selected from the same product group. The standards were then sent to the National Bureau of Standards for calibration in a wind tunnel, and the results used for final calibration of the field instruments. The uncertainty in wind speed for these instruments is the larger of $\pm 1\%$ or 0.07 m/s. Pointing accuracy was estimated to be $\pm 2°$.

#### 2.3.1.3 Thermocouples

Standard Chromel-Alumel (type $k$) thermocouples were collocated with each gas sensor to provide temperature measurement of the gas cloud. As shown in Figures 3–6, additional thermocouples were installed at other locations both inside and outside the vapor curtain and in the ground at some stations. The 20 mil thermocouples had a response time of about 1 sec, corresponding roughly to the gas sensors which averaged data for 1 sec. Improvements in amplifier design have eliminated the amplifier drift problems experienced on previous test series, and the RTD array at station G11 (center station, 150 m row) allowed elimination of most thermocouple baseline uncertainty by adjusting individual data sets to the pre-test temperature profile measured by the RTD array. Relative temperature variations measured during the test are believed accurate to $\pm 0.5°C$.

#### 2.3.1.4 Resistive Temperature Devices

The sensing element for the resistive temperature device (RTD) is an 1000 ohm platinum resistor mounted in an aspirated solar shield. Five RTD's were mounted on the upwind met tower (station G24) at elevations of 1, 2, 4, 8, and 16 m. Four additional RTDs were mounted at station G11 at elevations of 1, 2, 4, and 8 m (see Figures 5 and 6). The accuracy after calibration is estimated to be $\pm 0.1°C$.

#### 2.3.1.5 Ground Heat-Flux Sensors

The ground heat-flux sensors were standard, commercially available heat-flux plates manufactured by HY-CAL Engineering. They consisted of two layers of thermopiles separated by material of known thermal conductivity, forming a thin rectangular wafer that was buried just below the soil surface. These devices were installed at two locations inside the vapor curtain and four downwind locations, as depicted in Figure 7. Factory calibration curves were employed. Sensor to sensor variation was less than $\pm 2\%$ at full scale.

#### 2.3.1.6 Humidity Sensors

The four humidity sensors deployed during the Falcon Series (see Figure 8) were commercially available Ondyne dew point hygrometers. Several problems were encountered early in the test series, and as a result, dependable humidity data were not recorded for Falcon 1 and 2 by these sensors. Data reported for the first two tests were obtained from the Weather Service Nuclear Support Office (WSNSO). Accuracy of humidity measurements made during Falcon 3–5 are estimated at $\pm 10\%$.

### 2.3.2 Gas Concentration Sensors

During the Falcon Series, a total of 77 gas concentration sensors were employed, as depicted in Figures 9 through 12. Included in this total were 39 infrared sensors (35 LLNL-IR and 4 JPL-IR) and 38 MSA catalytic sensors. The JPL-IR sensors measured samples from inside the vapor fence, where the highest concentrations were expected. These samples were warmed to evaporate any water droplets or ice particles formed by the cold LNG vapor. The LLNL-IR sensors were at lower elevations at 50 and 150 m downwind, where intermediate concentrations were expected. The MSA

sensors were deployed at higher elevations at 50 and 150 m and at 250 m downwind where, gas concentrations were not expected to exceed 5%.

#### 2.3.2.1 LLNL-IR Gas Sensor

The LLNL-IR gas concentration sensor was developed at LLNL (Bingham et al., 1983) for use in the Burro Series of LNG spill tests. They were again used to detect LNG in the Coyote Series, Ammonia in the Desert Tortoise Series, and $N_2O_4$ in the Eagle Series. Pre- and post-test calibration and several field checks over the years of use have shown the LLNL-IR to be a stable and dependable sensor for use in the extremes of the desert environment.

A schematic drawing of the LLNL-IR sensor is presented in Figure 19. Infrared radiation from the source passes through an optical path open to the atmosphere. If hydrocarbons are present, then absorption occurs, and the amount of absorption specific to methane, ethane plus propane, and cold-induced water or ice particle fog are detected at the pyroelectric detector. Absorption specific to these species is defined by four narrow-band pass filters between 3.0 and 4.0 $\mu$m. The optical paths exposed to the atmosphere were either 5 or 15 cm in length, thus the instrument readings were for average concentrations in volumes of 19.4 and 58.1 $cm^3$, respectively. The 5 cm optical paths were employed where higher gas concentrations were anticipated.

In the absence of fog, two channels serve primarily to determine the methane and ethane concentrations. The other two channels are used as reference channels to compensate for shifts in system throughput due to dust on the lenses or to temperature-induced baseline shifts. Relatively little cross-gas sensitivity is experienced within the two main channels. The instruments were calibrated using methane concentrations of 0–30%, ethane concentrations of 0–10%, and a methane/ethane mixture of 11.2/2.2%. Calibration uncertainties were consistent with those observed for the Burro and Coyote series. A detailed discussion of these uncertainties and other aspects of the LLNL-IR may be found in Bingham et al. (1983).

The overall uncertainty of the total hydrocarbons reading is estimated to be within 10% for readings above 2.5% concentration. Below 2.5% the readings begin to be dominated by noise introduced into the ethane channel arising from instrument noise and deficiencies in the fog correction algorithm. The ethane noise was observed to average around 0.1% concentration with peak values around 0.25% concentration and persisted even when the methane readings indicated concentrations as low as 10. Since the total hydrocarbons reading is a simple sum of the methane and ethane readings the ethane noise makes low level readings look larger than they actually are and for very low levels can totally dominate the readings.

Fog affects the sensitivity of the LLNL-IR sensor, since fog absorbs at about the same wavelength as the gas being measured. Hence the sensor must be calibrated to acount for fog in the absorption path. Details of this calibration are presented in Section 2.3.2.4.

#### 2.3.2.2 JPL-IR Gas Sensor

The JPL-IR sensors are four band radiometers similar to the LLNL-IR sensors, except they are designed to operate in fog-free regions and to detect separately methane, ethane, and propane. The sensor was developed by Jet Propulsion Laboratory (JPL) for use on the Burro and Coyote tests. One prototype model was fielded on the last two Burro Tests, eight units were fielded on Coyote,

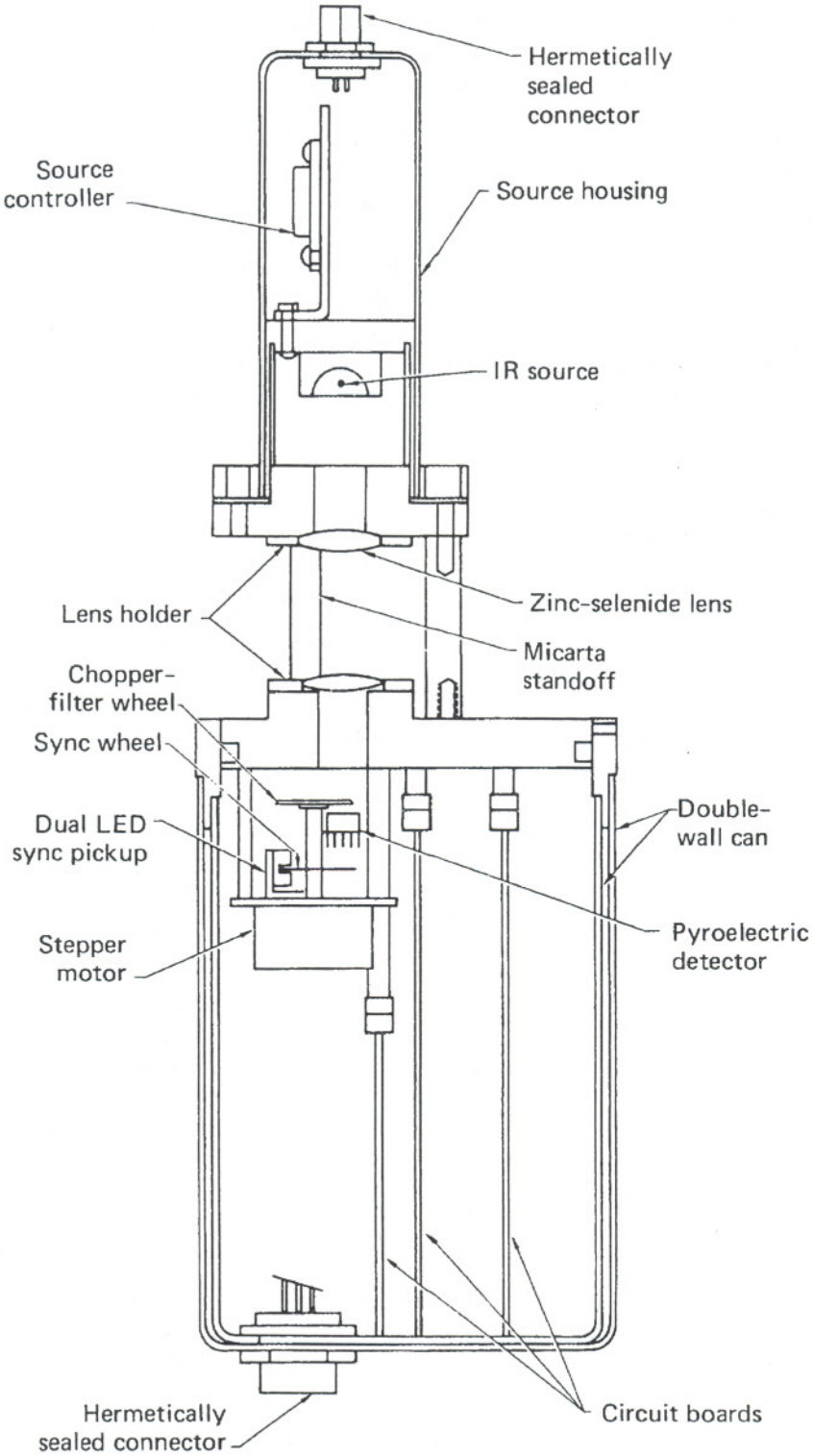


Figure 19. Cross section of the LLNL-IR sensor.

and four units were employed on the Falcon Series. All four units sampled gas concentrations within the vapor curtain. To eliminate fog, the sensors themselves were placed outside the vapor curtain and samples were drawn by air pumps through long tubes run underwater to warm the samples.

JPL selected the spectral region of the 2.0 to 2.5 $\mu$m bands of methane, ethane, and propane, due to the availability of inexpensive components and high performance room temperature detectors. The four bands centered at 2.02, 2.36, 2.46, and 2.51 m were chosen to enable detection of any of the three species down to 0.4% with an accuracy of 0.2% or 10% of concentration, whichever is greater. Figure 20 shows a schematic of the sensor, which used four crossings of a 15 cm path to give an effective path length of 60 cm. An incandescent lamp, operating at approximately 1850 K, provides a source beam which was chopped by a motor driven blade. After exiting the unit and passing through the LNG vapor sample, the beam reenters the housing, is split by a partially silvered mirror to produce four beams which are focused on the interference filters and PbS detector. The detector assembly was cooled with a thermoelectric cooler in order to stabilize the detector response and the filter pass bands.

#### 2.3.2.3 MSA Catalytic Sensor

MSA sensors are well understood, standard commercial units that operate on the catalytic principal and work well as long as they are not exposed to flame, high wind, or gas concentrations approaching the stoichiometric mixture (10% for methane). The sensor response is very linear, and the uncertainty is approximately 10% of the reading. Sensors were individually calibrated, and post-test calibrations were used to correct for changes in sensor response.

#### 2.3.2.4 Fog Calibration of the Multispectral LLNL Infrared Gas Sensors

Because of the high concentration fog experienced during this test series, particularly on Falcon 1, it was necessary to do additional fog calibration of the sensors. This required that an extensive laboratory program be conducted after the test series was over.

As has been mentioned earlier, the LLNL IR gas sensor utilizes the principle of molecular absorption in the middle of the infrared region, between 3 and 4 microns, to detect the presence of hydrocarbon gas. Methane, ethane and propane have strong molecular absorption bands in this spectral region. The four filters used in the sensors have center frequency wavelengths of:

| | |
|---|---|
| Methane | 3.20 microns |
| Ethane | 3.66 microns |
| Reference | 3.90 microns |
| Fog | 3.03 microns |

Dense fog in the absorption path complicated the measurement problem. The sensitivity of the detector is affected by such factors as fog particle size, density, index of refraction, and wavelength of incident radiation. Absorption and scattering by the water droplets produce the same effect as gas absorption, and must be corrected for when processing the measured gas concentration data.

The sapphire-rod IR source is separated from the pyroelectric sensor by a 5 or 15 centimeter open path, a zinc selenide lens, and a rotary chopper wheel with the four narrow bandpass filters.

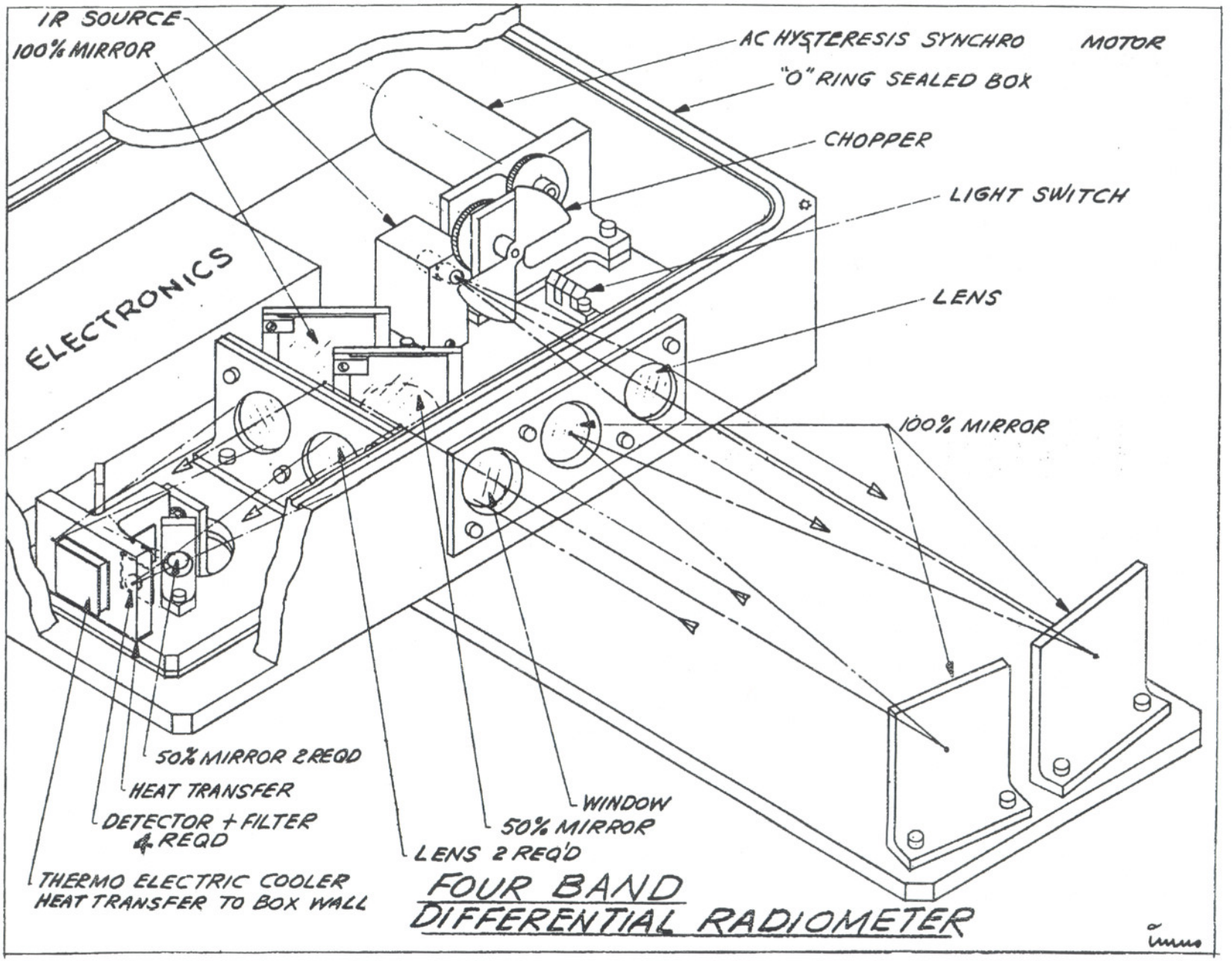


Figure 20. Pictorial sketch of the JPL-IR sensor.

The gas-air-fog sample passes through a small mesh stainless steel screen to prevent aliasing from high frequency fluctuations. Figure 19 shows a schematic drawing of the sensor assembly.

To obtain the fog correction coefficients, all sensors were individually exposed in a fog chamber to varying concentrations of fog, generated by pouring liquid nitrogen onto a water reservoir contained within the insulated fog chamber. A low wattage heater was used to maintain constant water temperature, and prevent freezing.

Because of the dense fog, the original fog correction program did not perform satisfactorily either. A new numerical algorithm had to be developed for calculating the concentrations of hydrocarbons from field measurements. This algorithm involves solving the following four coupled equations for unknowns $C_M$, $C_E$, $C_F$, and $C_R$:

$$\alpha_M = A(C_M)^{XA} + D(C_E)^{XD} + S_{13}C_F \ , \tag{1}$$

$$\alpha_E = B(C_M)^{XB} + E(C_E)^{XE} + S_{24}C_R \ , \tag{2}$$

$$\alpha_F = H(C_M)^{XH} + F(C_E)^{XF} + C_F \ , \tag{3}$$

$$\alpha_R = C(C_M)^{XC} + G(C_E)^{XG} + C_R \ , \tag{4}$$

In the above $\alpha_M$, $\alpha_E$, $\alpha_F$, and $\alpha_R$, are the extinction coefficients (deduced from field data) for the methane, ethane, fog, and reference channels, respectively. A, B, C, D, E, F, G, H, XA, XB, XC, XD, XE, XF, XG, and XH are the various influence coefficients of methane and ethane gases on the extinction coefficients and are determined in laboratory calibrations; $C_M$ and $C_E$ are respectively the volumetric fraction of methane and ethane; the terms involving $C_F$, $C_R$ represent the contribution of fog to each of the extinction coefficients. The values of $S_{13}$ and $S_{24}$ are determined from the laboratory fog calibration tests described subsequently. The above equations are solved iteratively, subjected to the constraints that the values of $C_M$, $C_E$, $C_F$, and $C_R$ should be non-negative, until the residuals of these equations fall within an acceptable tolerance.

As an example, Figure 21 shows the experimental results from the exposure of the infrared sensor to liquid nitrogen/water fog. Superimposed on the top graph are the light intensities recorded by the methane channel (dotted) and the fog channels (solid) respectively; the curves on the lower plot correspond to the readings of the ethane (dotted) and reference (solid) channels during the same LN spill. The data points (in $*$) are calculated by the following formula:

$$\text{top}: \quad S_{13} = \frac{ln(M/M_o)}{ln(F/F_o)}$$

$$\text{lower}: \quad S_{24} = \frac{ln(E/E_o)}{ln(R/R_o)}$$

Where $M$ Light intensity measured by the methane channel
$M_o$ Methane baseline reading
$E$ Light intensity measured by the ethane channel
$E_o$ Ethane baseline reading
$F$ Light intensity measured by the fog channel
$F_o$ Fog baseline reading
$R$ Light intensity measured by the reference channel

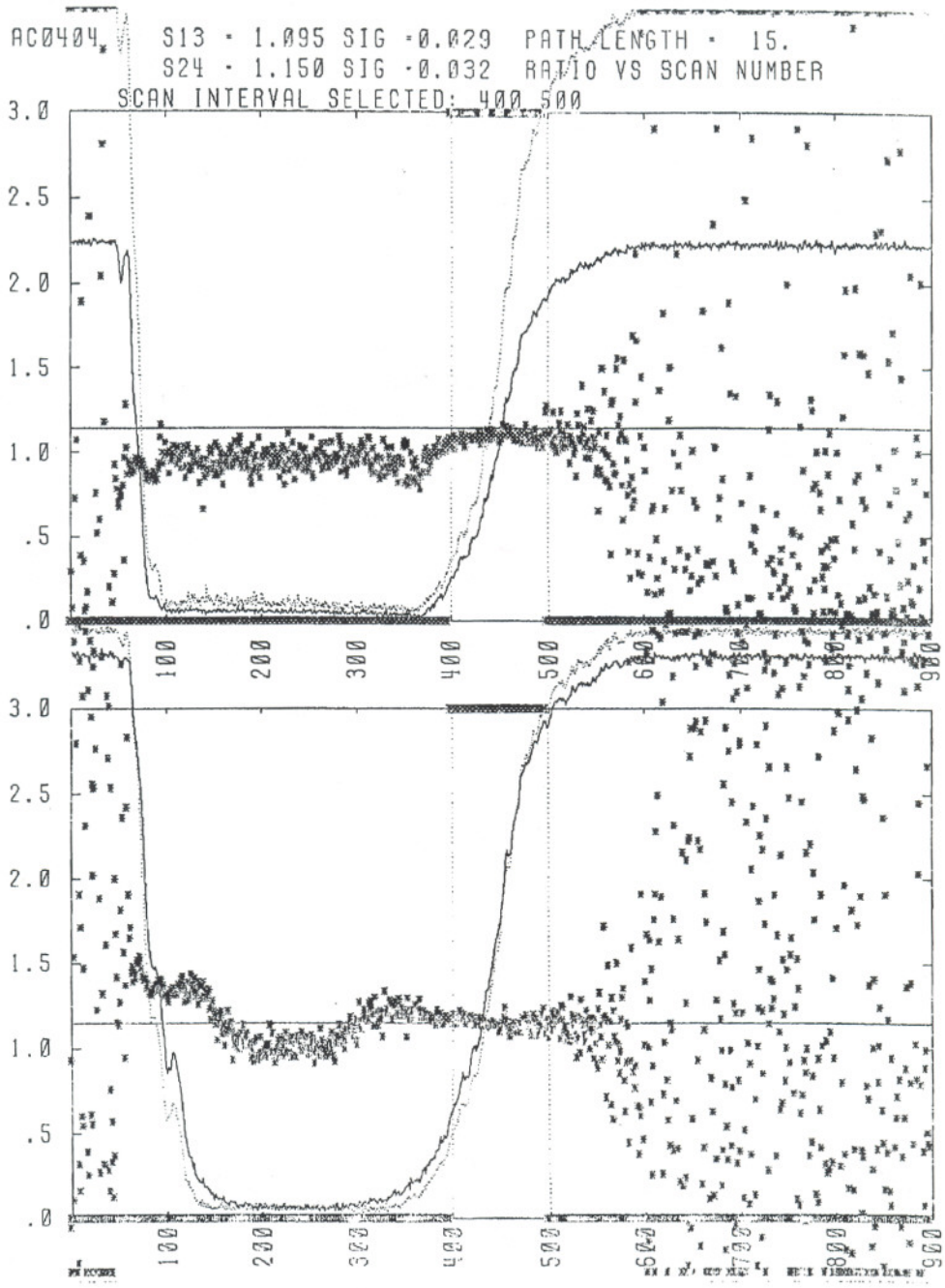


**Figure 21.** LLNL IR sensor fog response and fog ratios.

$R_o$ Reference baseline reading

Based on estimates of fog intensity in the field tests being mostly less than 10%, the mean values and standard deviations of $S_{13}$ and $S_{24}$ were determined for fog intensity in the range of 1 to 10% within the vertical lines of the graph (outside of this range, the variations are much larger and thus not as appropriate). Results for all the sensors used in the field tests are summarized in Table 4. As is seen, the fog coefficients vary noticeably among sensors. For this reason, values for individual sensors were used in the data reduction program to obtain the concentrations of hydrocarbons.

## 2.4 Photographic Coverage

Photographic coverage was provided by LLNL Nevada Photo Applications Group and video coverage was provided by the LGF Program field team. Table 3 summarizes the equipment employed during the test series and Figure 22 graphically depicts the camera locations. The 35 mm framing cameras were programmed with variable framing rates, and took 36 frames over a period of 15 min (from $t$ = 10 sec to $t$ = 904 sec). The crosswind location contained two 35 mm cameras, one with a telephoto lens and one with a wide angle lens. The upwind location had one 35 mm camera with a wide angle lens. Both locations had two motion picture cameras set at two different light settings to insure good exposure. The motion picture cameras operated at 24 frames per second. The CCD type television camera was located next to the vapor curtain at a height of 60 ft looking down into the enclosed area. The two remaining video cameras were located at an elevation of 80 ft on the met tower (collocated with the 35 mm and two movie cameras), and on top of the $LN_2$ storage tank at the rear of the tank farm (elevation = 60 ft, range = 600 ft).

TABLE 4: FALCON LLNL-IR SENSOR FOG COEFFICIENTS
(DARK CURRENT NOT SUBTRACTED)

| SENSOR NUMBER | PATH LENGTH (cm.) | S13 | | S24 | |
|---|---|---|---|---|---|
| | | RATIO | SIGMA | RATIO | SIGMA |
| 2 | 15 | 1.153 | 0.024 | 1.120 | 0.026 |
| 3* | 15 | 1.137 | 0.034 | 1.138 | 0.031 |
| 4 | 15 | 1.101 | 0.028 | 1.143 | 0.032 |
| 5 | 15 | 1.160 | 0.035 | 1.188 | 0.035 |
| 6 | 15 | 1.144 | 0.048 | 1.138 | 0.037 |
| 7 | 15 | 1.151 | 0.016 | 1.201 | 0.019 |
| 8 | 15 | 1.158 | 0.008 | 1.100 | 0.023 |
| 9 | 15 | 1.143 | 0.025 | 1.117 | 0.021 |
| 10* | 15 | 1.171 | 0.012 | 1.104 | 0.017 |
| 11 | 15 | 1.165 | 0.025 | 1.134 | 0.024 |
| 12 | 15 | 1.123 | 0.028 | 1.173 | 0.026 |
| 13* | 15 | 1.162 | 0.023 | 1.152 | 0.024 |
| 14 | 15 | 1.159 | 0.021 | 1.169 | 0.024 |
| 15* | 15 | 1.133 | 0.013 | 1.166 | 0.026 |
| 16 | 15 | 1.120 | 0.024 | 1.161 | 0.021 |
| 17 | 15 | 1.157 | 0.016 | 1.164 | 0.030 |
| 18 | 15 | 1.149 | 0.024 | 1.146 | 0.025 |
| 19 | 15 | 1.157 | 0.024 | 1.214 | 0.028 |
| 21 | 15 | 1.149 | 0.015 | 1.094 | 0.013 |
| 22 | 15 | 1.168 | 0.019 | 1.134 | 0.021 |
| 23 | 15 | 1.129 | 0.013 | 1.172 | 0.015 |
| 24 | 15 | 1.184 | 0.015 | 1.109 | 0.011 |
| 25 | 15 | 1.056 | 0.017 | 0.976 | 0.029 |
| 26 | 15 | 1.163 | 0.020 | 1.190 | 0.026 |
| 27 | 15 | 1.159 | 0.033 | 1.120 | 0.025 |
| 28 | 15 | 1.148 | 0.024 | 1.100 | 0.023 |
| 29 | 15 | 1.124 | 0.035 | 1.165 | 0.037 |
| 30 | 15 | 1.169 | 0.017 | 1.168 | 0.024 |
| 31 | 5 | 1.128 | 0.012 | 1.186 | 0.021 |
| 32+ | 5 | 1.152 | 0.017 | 1.199 | 0.022 |
| 33 | 5 | 1.156 | 0.024 | 1.221 | 0.021 |
| 34 | 5 | 1.155 | 0.020 | 1.195 | 0.025 |
| 35 | 5 | 1.134 | 0.015 | 1.210 | 0.027 |
| 36+ | 5 | 1.152 | 0.017 | 1.199 | 0.022 |
| 37 | 5 | 1.189 | 0.016 | 1.184 | 0.017 |

* Sensor damaged by fire. Coefficients represent the averaged values of the undamaged sensors having the same kind of filters.

\+ Sensor damaged by fire. Coefficients are the averaged values of sensors 31, 33, 34, 35, and 37.

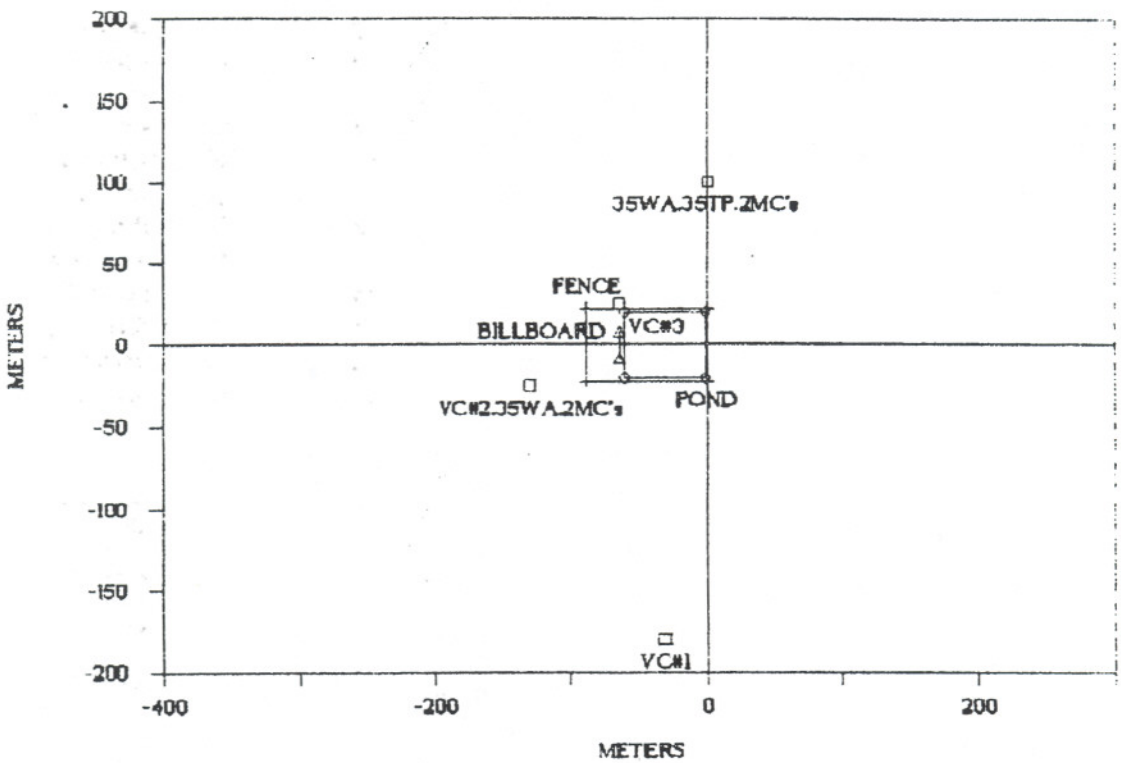


**Figure 22.** Falcon Series camera array.

## 3.0 Experiment Summaries

A total of five tests were conducted in the Falcon Series; three were conducted in June 1987 and two were conducted in late August 1987. The tests were conducted at the DOE's permanent Spill Test Facility (LGFSTF) on Frenchman Lake at the Nevada Test Site. Frenchman Lake is a normally dry lakebed measuring approximately 3.5 km by 5.0 km. The lakebed is extremely flat with the difference between average surface layer elevation at the lakebed center and at the lakebed edge being of the order of 0.3 m (one foot). Weather conditions were generally typical of summertime conditions in the high desert with predictable, highly directional, thermally-driven winds arising about midday at 10 to 20 m/s and gradually dropping off to 3 to 5 m/s as sunset approached. High temperatures coupled with the influx of some tropical moisture produced localized thundershower activity in the higher terrain surrounding Frenchman Lake on some occasions.

A summary of test parameters is given in Table 5. Spill valve open and close times reflect the time that the signals were sent from the CCDAS to the valve. Zero time for all data plots is the spill valve open time. The spill valve required 8 sec to fully open and 11 sec to fully close from the time it received the signal. Spill rate and spill volume were calculated using time history data of drive gas pressure within an orifice flow calculation and verified by pre- and post-test liquid level readings from the storage tanks. Drive gas pressures stated reflect the average system pressure, more detailed temporal history of drive gas pressure is available in the LLNL database. Fluid velocity was calculated from orifice size and flow rate data. Water temperature was measured directly using thermocouples submerged in the pond (relative accuracy estimated at $\pm 0.5°C$). Gas analysis was done at the pickup point at Trussville, Alabama, for Falcon 1 and 2, performed post-test taking samples from facility storage tanks at NTS and analyzing with a mass spectrometer at LLNL for Falcon 3, and performed pre-test from NTS storage tank samples analyzed at LLNL for Falcon 4 and 5.

**Table 5.** Falcon Series test parameters.

| Test Name | Falcon-1 | Falcon-2 | Falcon-3 | Falcon-4 | Falcon-5 |
|---|---|---|---|---|---|
| Date of test | 12 Jun 87 | 18 Jun 87 | 29 Jun 87 | 21 Aug 87 | 29 Aug 87 |
| Spill valve open time | 19:47:56 | 18:09:09 | 18:52:02 | 19:27:04 | 18:58:00 |
| Spill valve close time | 19:50:07 | 18:10:27 | 18:54:36 | 19:32:05 | 18:59:18 |
| Spill tank | C-105 | C-105 | C-105 | C-106 | C-106 |
| Spill rate | 28.7 $m^3$/min | 15.9 $m^3$/min | 18.9 $m^3$/min | 8.7 $m^3$/min | 30.3 $m^3$/min |
| Spill volume | 66.4 $m^3$ | 20.6 $m^3$ | 50.7 $m^3$ | 44.9 $m^3$ | 43.9 $m^3$ |
| Drive gas pressure | 65 psig | 35 psig | 40 psig | 125 psig | 70 psig |
| Orifice diameter | 4.5 in | 4.5 in | 4.5 in | 1.5 in | 4.5 in |
| Fluid velocity | 65 m/s | 32.5 m/s | 32.5 m/s | 146 m/s | 65 m/s |
| Water temperature (pre/post-°C) | 28.4/22.4 | 23.6/20.6 | no data | 23.2/22.0 | 26.0/nd |
| Gas analysis (Meth/Heavy-%) | 94.7/3.9 | 95.6/3.7 | 91/8.0 | 91/8.0 | 88/10 |

Table 6 presents a detailed instrumentation plan for each test, which provides the exact location of each sensor fielded in each experiment. In addition, the comments column reflects the operating condition of each sensor during the test. A legend of sensor nomenclature and status codes appears at the end of the table. In general, there were only minor variations in instrument plans from test to test; however two changes are large enough to mention here:

1. Between Falcon 3 and Falcon 4, two entire stations were moved from the 50 meter row to the 150 meter row to provide a wider mass flux row, due to a wider than anticipated vapor cloud observed in Falcon 1 and Falcon 3.
2. Between Falcon 2 and 3, certain JPL-IR sensors were increased in sample height from 1 to 2 m and some thermocouples, previously submerged in the pond or near the pond surface, were distributed over elevations from 1 to 6 meters to study temperature profiles within the vapor curtain.

Additional remarks specific to each test are listed at the end of each instrumentation plan in Table 6.

**Table 6.** Falcon Series instrumentation deployment plan.

Instrumentation Plan—Falcon 1

| Station | Instrument | $x$ | $y$ | $z$ | S/N | Comments |
|---|---|---|---|---|---|---|
| G01 | TC | 50 m | −66 m | 1 m | NSN | |
| | TC | 50 m | −66 m | 5 m | NSN | |
| | TC | 50 m | −66 m | 11 m | NSN | |
| | TC | 50 m | −66 m | 17 m | 215 | |
| | MSA | 50 m | −66 m | 17 m | 010 | |
| | LLNL-IR | 50 m | −66 m | 1 m | 031 | |
| | LLNL-IR | 50 m | −66 m | 5 m | 029 | |
| | LLNL-IR | 50 m | −66 m | 11 m | 022 | |
| G02 | TC | 50 m | −44 m | 1 m | NSN | |
| | TC | 50 m | −44 m | 5 m | NSN | |
| | TC | 50 m | −44 m | 11 m | NSN | |
| | TC | 50 m | −44 m | 17 m | 216 | |
| | MSA | 50 m | −44 m | 17 m | 513 | |
| | LLNL-IR | 50 m | −44 m | 1 m | 033 | |
| | LLNL-IR | 50 m | −44 m | 5 m | 004 | |
| | LLNL-IR | 50 m | −44 m | 11 m | 009 | |
| G03 | TC | 50 m | −22 m | 0 | NSN | |
| | TC | 50 m | −22 m | 1 m | NSN | DNF |
| | TC | 50 m | −22 m | 5 m | NSN | |
| | TC | 50 m | −22 m | 11 m | NSN | |
| | TC | 50 m | −22 m | 17 m | 211 | |
| | MSA | 50 m | −22 m | 17 m | 172 | |
| | LLNL-IR | 50 m | −22 m | 1 m | 032 | |
| | LLNL-IR | 50 m | −22 m | 5 m | 003 | |
| | LLNL-IR | 50 m | −22 m | 11 m | 010 | |
| | heat flux | 50 m | −22 m | 0 | NSN | |
| G04 | TC | 50 m | 0 | 1 m | NSN | |
| | TC | 50 m | 0 | 5 m | NSN | |
| | TC | 50 m | 0 | 11 m | NSN | |
| | TC | 50 m | 0 | 17 m | 121 | |
| | MSA | 50 m | 0 | 17 m | 522 | |
| | LLNL-IR | 50 m | 0 | 1 m | 036 | |
| | LLNL-IR | 50 m | 0 | 5 m | 015 | |
| | LLNL-IR | 50 m | 0 | 11 m | 013 | |
| | bivane | 50 m | 0 | 1 m | 378 | |
| | bivane | 50 m | 0 | 5 m | 377 | |
| | bivane | 50 m | 0 | 11 m | 386 | |
| | humidity | 50 m | 0 | 1 m | 393 | |
| G05 | TC | 50 m | 22 m | 0 | NSN | |
| | TC | 50 m | 22 m | 1 m | NSN | |
| | TC | 50 m | 22 m | 5 m | NSN | |
| | TC | 50 m | 22 m | 11 m | NSN | |
| | TC | 50 m | 22 m | 17 m | 213 | |
| | MSA | 50 m | 22 m | 17 m | 012 | |
| | LLNL-IR | 50 m | 22 m | 1 m | 034 | |
| | LLNL-IR | 50 m | 22 m | 5 m | 008 | |
| | LLNL-IR | 50 m | 22 m | 11 m | 030 | |
| | heat flux | 50 m | 22 m | 0 | 025 | |

**Table 6.** Continued.

Instrumentation Plan—Falcon 1

| Station | Instrument | $x$ | $y$ | $z$ | S/N | Comments |
|---|---|---|---|---|---|---|
| G06 | TC | 50 m | 44 m | 1 m | NSN | |
| | TC | 50 m | 44 m | 5 m | NSN | |
| | TC | 50 m | 44 m | 11 m | NSN | DNF |
| | TC | 50 m | 44 m | 17 m | 214 | |
| | MSA | 50 m | 44 m | 17 m | 009 | |
| | LLNL-IR | 50 m | 44 m | 1 m | 037 | |
| | LLNL-IR | 50 m | 44 m | 5 m | 016 | |
| | LLNL-IR | 50 m | 44 m | 11 m | 006 | |
| G07 | TC | 50 m | 66 m | 1 m | NSN | |
| | TC | 50 m | 66 m | 5 m | NSN | |
| | TC | 50 m | 66 m | 11 m | NSN | |
| | TC | 50 m | 66 m | 17 m | 201 | |
| | MSA | 50 m | 66 m | 17 m | 013 | |
| | LLNL-IR | 50 m | 66 m | 1 m | 035 | |
| | LLNL-IR | 50 m | 66 m | 5 m | 017 | |
| | LLNL-IR | 50 m | 66 m | 11 m | 014 | |
| G08 | TC | 150 m | −75 m | 1 m | NSN | |
| | TC | 150 m | −75 m | 5 m | NSN | |
| | TC | 150 m | −75 m | 11 m | 217 | |
| | MSA | 150 m | −75 m | 11 m | 020 | |
| | LLNL-IR | 150 m | −75 m | 1 m | 028 | |
| | LLNL-IR | 150 m | −75 m | 5 m | 005 | |
| G09 | TC | 150 m | −50 m | 0 | NSN | |
| | TC | 150 m | −50 m | 1 m | NSN | |
| | TC | 150 m | −50 m | 5 m | NSN | |
| | TC | 150 m | −50 m | 11 m | 218 | |
| | MSA | 150 m | −50 m | 11 m | 519 | |
| | LLNL-IR | 150 m | −50 m | 1 m | 018 | |
| | LLNL-IR | 150 m | −50 m | 5 m | 025 | |
| | heat flux | 150 m | −50 m | 0 | 023 | |
| G10 | TC | 150 m | −25 m | 1 m | NSN | |
| | TC | 150 m | −25 m | 5 m | NSN | |
| | TC | 150 m | −25 m | 11 m | 203 | |
| | TC | 150 m | −25 m | 17 m | 204 | |
| | MSA | 150 m | −25 m | 11 m | 004 | |
| | MSA | 150 m | −25 m | 17 m | 016 | |
| | LLNL-IR | 150 m | −25 m | 1 m | 021 | |
| | LLNL-IR | 150 m | −25 m | 5 m | 002 | |
| | bivane | 150 m | −25 m | 1 m | 384 | |
| | bivane | 150 m | −25 m | 5 m | 392 | |
| | bivane | 150 m | −25 m | 11 m | 387 | |
| G11 | MSA | 150 m | 0 | 11 m | 007 | |
| | MSA | 150 m | 0 | 17 m | 512 | |
| | LLNL-IR | 150 m | 0 | 1 m | 007 | |
| | LLNL-IR | 150 m | 0 | 5 m | 026 | |
| | bivane | 150 m | 0 | 1 m | 380 | |
| | bivane | 150 m | 0 | 5 m | 385 | |
| | bivane | 150 m | 0 | 11 m | 379 | |

**Table 6.** Continued.

Instrumentation Plan—Falcon 1

| Station | Instrument | $x$ | $y$ | $z$ | S/N | Comments |
|---|---|---|---|---|---|---|
| | RTD | 150 m | 0 | 1 m | 006 | |
| | RTD | 150 m | 0 | 2 m | 007 | |
| | RTD | 150 m | 0 | 4 m | 008 | |
| | RTD | 150 m | 0 | 8 m | 009 | |
| G12 | TC | 150 m | 25 m | 1 m | NSN | |
| | TC | 150 m | 25 m | 5 m | NSN | |
| | TC | 150 m | 25 m | 11 m | 205 | |
| | TC | 150 m | 25 m | 17 m | 206 | |
| | MSA | 150 m | 25 m | 11 m | 520 | |
| | MSA | 150 m | 25 m | 17 m | 515 | |
| | LLNL-IR | 150 m | 25 m | 1 m | 024 | |
| | LLNL-IR | 150 m | 25 m | 5 m | 023 | |
| | bivane | 150 m | 25 m | 1 m | 391 | |
| | bivane | 150 m | 25 m | 5 m | 389 | |
| | bivane | 150 m | 25 m | 11 m | 373 | |
| G13 | TC | 150 m | 50 m | 0 | NSN | |
| | TC | 150 m | 50 m | 1 m | NSN | |
| | TC | 150 m | 50 m | 5 m | NSN | |
| | TC | 150 m | 50 m | 11 m | 220 | |
| | MSA | 150 m | 50 m | 11 m | 011 | |
| | LLNL-IR | 150 m | 50 m | 1 m | 011 | |
| | LLNL-IR | 150 m | 50 m | 5 m | 027 | |
| | heat flux | 150 m | 50 m | 0 | 029 | |
| G14 | TC | 150 m | 75 m | 1 m | NSN | |
| | TC | 150 m | 75 m | 5 m | NSN | |
| | TC | 150 m | 75 m | 11 m | 230 | |
| | MSA | 150 m | 75 m | 11 m | 017 | |
| | LLNL-IR | 150 m | 75 m | 1 m | 012 | |
| | LLNL-IR | 150 m | 75 m | 5 m | 019 | |
| G15 | TC | 250 m | −84 m | 1 m | 225 | |
| | TC | 250 m | −84 m | 5 m | 226 | |
| | TC | 250 m | −84 m | 11 m | 227 | |
| | MSA | 250 m | −84 m | 1 m | 014 | |
| | MSA | 250 m | −84 m | 5 m | 006 | |
| | MSA | 250 m | −84 m | 11 m | 015 | |
| G16 | TC | 250 m | −56 m | 1 m | 228 | |
| | TC | 250 m | −56 m | 5 m | 229 | |
| | TC | 250 m | −56 m | 11 m | 231 | |
| | MSA | 250 m | −56 m | 5 m | 001 | |
| | MSA | 250 m | −56 m | 11 m | 018 | |
| G17 | TC | 250 m | −28 m | 1 m | 232 | |
| | TC | 250 m | −28 m | 5 m | 233 | |
| | TC | 250 m | −28 m | 11 m | 234 | |
| | MSA | 250 m | −28 m | 5 m | 173 | |
| | MSA | 250 m | −28 m | 11 m | 518 | |
| G18 | TC | 250 m | 0 | 1 m | 235 | |
| | TC | 250 m | 0 | 5 m | 236 | |

Table 6. Continued.

Instrumentation Plan—Falcon 1

| Station | Instrument | x | y | z | S/N | Comments |
|---|---|---|---|---|---|---|
| | TC | 250 m | 0 | 11 m | 237 | |
| | MSA | 250 m | 0 | 1 m | 002 | |
| | MSA | 250 m | 0 | 11 m | 514 | |
| G19 | TC | 250 m | 28 m | 1 m | 201 | |
| | TC | 250 m | 28 m | 5 m | 207 | |
| | TC | 250 m | 28 m | 11 m | 209 | |
| | MSA | 250 m | 28 m | 5 m | 005 | |
| | MSA | 250 m | 28 m | 11 m | 516 | |
| G20 | TC | 250 m | 56 m | 1 m | 210 | |
| | TC | 250 m | 56 m | 5 m | 219 | |
| | TC | 250 m | 56 m | 11 m | 221 | |
| | MSA | 250 m | 56 m | 5 m | 003 | |
| | MSA | 250 m | 56 m | 11 m | 521 | |
| G21 | TC | 250 m | 84 m | 1 m | 222 | |
| | TC | 250 m | 84 m | 5 m | NSN | |
| | TC | 250 m | 84 m | 11 m | 224 | |
| | MSA | 250 m | 84 m | 1 m | 019 | |
| | MSA | 250 m | 84 m | 5 m | 008 | |
| | MSA | 250 m | 84 m | 11 m | 517 | |
| G22 | TC | -32 m | 0 | -10 cm | NSN | |
| | TC | -32 m | 0 | -5 cm | NSN | |
| | TC | -32 m | 0 | 5 cm | NSN | |
| | TC | -32 m | 0 | 15 cm | NSN | |
| | TC | -32 m | 0 | 1 m | NSN | |
| | TC | -2 m | 0 | -10 cm | NSN | |
| | TC | -2 m | 0 | -5 cm | NSN | DNF |
| | TC | -2 m | 0 | 5 cm | NSN | |
| | TC | -2 m | 0 | 15 cm | NSN | |
| | TC | -2 m | 0 | 1 m | NSN | |
| | TC | -2 m | 0 | 1 m | NSN | |
| | TC | -2 m | 0 | 2 m | NSN | |
| | TC | -2 m | 0 | 6 m | NSN | |
| | TC | -2 m | 0 | 10 m | NSN | |
| | TC | -2 m | 0 | 14 m | NSN | |
| | JPL-IR | -62 m | 20 m | 1 m | 001 | |
| G23 | TC | -64 m | 0 | 0 | NSN | |
| | TC | -76 m | 0 | 0 | NSN | |
| | TC | -88 m | 0 | 1 m | NSN | |
| | TC | -88 m | 0 | 2 m | NSN | |
| | TC | -88 m | 0 | 6 m | NSN | |
| | TC | -88 m | 0 | 10 m | NSN | |
| | TC | -88 m | 0 | 13 m | NSN | |
| | heat flux | -64 m | 0 | 0 | NSN | |
| | heat flux | -76 m | 0 | 0 | NSN | |
| | humidity | -2 m | 0 | 1 m | 389 | |
| | humidity | -32 m | 0 | 1 m | 394 | |
| | humidity | -64 m | 20 | 1 m | 387 | |
| | JPL-IR | -62 m | 0 | 1 m | 006 | DNF |

**Table 6.** Continued.

Instrumentation Plan—Falcon 1

| Station | Instrument | $x$ | $y$ | $z$ | S/N | Comments |
|---|---|---|---|---|---|---|
| G24 | TC | −130 m | −25 m | 0 | NSN | |
| | TC | −130 m | −25 m | 1 m | NSN | |
| | heat flux | −130 m | −25 m | 0 | NSN | |
| | bivane | −130 m | −25 m | 1 m | 382 | |
| | bivane | −130 m | −25 m | 4 m | 375 | |
| | bivane | −130 m | −25 m | 16 m | 374 | |
| (TCS) | RTD | −130 m | −25 m | 1 m | NSN | |
| | RTD | −130 m | −25 m | 2 m | NSN | |
| | RTD | −130 m | −25 m | 4 m | NSN | |
| | RTD | −130 m | −25 m | 8 m | NSN | |
| | RTD | −130 m | −25 m | 16 m | NSN | |
| G25 | TC | −64 m | 25 m | 1 m | NSN | |
| | TC | −64 m | 25 m | 2 m | NSN | |
| | TC | −64 m | 25 m | 4 m | NSN | |
| | TC | −64 m | 25 m | 8 m | NSN | |
| | TC | −64 m | 25 m | 11 m | NSN | |
| | TC | −64 m | 25 m | 17 m | NSN | |
| | bivane | 20 m | 0 | 1 m | 388 | |
| | bivane | 20 m | 0 | 5 m | 376 | |
| | bivane | 20 m | 0 | 11 m | 381 | |
| W01 | Met-One | −1000 m | 0 | 2 m | N/A | |
| W02 | Met-One | −600 m | −100 m | 2 m | N/A | |
| W03 | Met-One | −600 m | 100 m | 2 m | N/A | |
| W04 | Met-One | −300 m | −100 m | 2 m | N/A | |
| W05 | Met-One | −300 m | 100 m | 2 m | N/A | |
| W06 | Met-One | −44 m | 25 m | 2 m | N/A | ESD |
| W07 | Met-One | 50 m | −75 m | 2 m | N/A | |
| W08 | Met-One | 50 m | 0 | 2 m | N/A | |
| W09 | Met-One | 50 m | 75 m | 2 m | N/A | ESD |
| W10 | Met-One | 150 m | −150 m | 2 m | N/A | |
| W11 | Met-One | 150 m | −75 m | 2 m | N/A | |
| W12 | Met-One | 150 m | 0 | 2 m | N/A | |
| W13 | Met-One | 150 m | 75 m | 2 m | N/A | |
| W14 | Met-One | 150 m | 150 m | 2 m | N/A | |
| W15 | Met-One | 300 m | −150 m | 2 m | N/A | |
| W16 | Met-One | 300 m | −75 m | 2 m | N/A | |
| W17 | Met-One | 300 m | 0 | 2 m | N/A | |
| W18 | Met-One | 300 m | 75 m | 2 m | N/A | |
| W19 | Met-One | 300 m | 150 m | 2 m | N/A | |

**Remarks:**

1. Visual observation indicates significant overfilling of the vapor barrier structure causing exessive spillover early in the test.

**Table 6.** Continued.

Instrumentation Plan—Falcon 2

| Station | Instrument | $x$ | $y$ | $z$ | S/N | Comments |
|---|---|---|---|---|---|---|
| G01 | TC | 50 m | −66 m | 1 m | NSN | |
| | TC | 50 m | −66 m | 5 m | NSN | |
| | TC | 50 m | −66 m | 11 m | NSN | |
| | TC | 50 m | −66 m | 17 m | 215 | |
| | MSA | 50 m | −66 m | 17 m | 010 | |
| | LLNL-IR | 50 m | −66 m | 1 m | 031 | DNF |
| | LLNL-IR | 50 m | −66 m | 5 m | 029 | DNF |
| | LLNL-IR | 50 m | −66 m | 11 m | 022 | DNF |
| G02 | TC | 50 m | −44 m | 1 m | NSN | |
| | TC | 50 m | −44 m | 5 m | NSN | |
| | TC | 50 m | −44 m | 11 m | NSN | |
| | TC | 50 m | −44 m | 17 m | 216 | |
| | MSA | 50 m | −44 m | 17 m | 513 | |
| | LLNL-IR | 50 m | −44 m | 1 m | 033 | DNF |
| | LLNL-IR | 50 m | −44 m | 5 m | 004 | DNF |
| | LLNL-IR | 50 m | −44 m | 11 m | 009 | DNF |
| G03 | TC | 50 m | −22 m | 0 | NSN | |
| | TC | 50 m | −22 m | 1 m | NSN | |
| | TC | 50 m | −22 m | 5 m | NSN | |
| | TC | 50 m | −22 m | 11 m | NSN | |
| | TC | 50 m | −22 m | 17 m | 211 | |
| | MSA | 50 m | −22 m | 17 m | 172 | |
| | LLNL-IR | 50 m | −22 m | 1 m | 032 | DNF |
| | LLNL-IR | 50 m | −22 m | 5 m | 003 | DNF |
| | LLNL-IR | 50 m | −22 m | 11 m | 010 | DNF |
| | heat flux | 50 m | −22 m | 0 | NSN | |
| G04 | TC | 50 m | 0 | 1 m | NSN | |
| | TC | 50 m | 0 | 5 m | NSN | |
| | TC | 50 m | 0 | 11 m | NSN | |
| | TC | 50 m | 0 | 17 m | 212 | |
| | MSA | 50 m | 0 | 17 m | 522 | |
| | LLNL-IR | 50 m | 0 | 1 m | 036 | DNF |
| | LLNL-IR | 50 m | 0 | 5 m | 015 | DNF |
| | LLNL-IR | 50 m | 0 | 11 m | 013 | DNF |
| | bivane | 50 m | 0 | 1 m | 378 | |
| | bivane | 50 m | 0 | 5 m | 377 | |
| | bivane | 50 m | 0 | 11 m | 386 | |
| | humidity | 50 m | 0 | 1 m | 389 | |
| G05 | TC | 50 m | 22 m | 0 | NSN | |
| | TC | 50 m | 22 m | 1 m | NSN | |
| | TC | 50 m | 22 m | 5 m | NSN | |
| | TC | 50 m | 22 m | 11 m | NSN | |
| | TC | 50 m | 22 m | 17 m | 213 | |
| | MSA | 50 m | 22 m | 17 m | 012 | |
| | LLNL-IR | 50 m | 22 m | 1 m | 034 | DNF |
| | LLNL-IR | 50 m | 22 m | 5 m | 008 | DNF |
| | LLNL-IR | 50 m | 22 m | 11 m | 030 | DNF |
| | heat flux | 50 m | 22 m | 0 | 025 | |

**Table 6.** Continued.

Instrumentation Plan---Falcon 2

| Station | Instrument | $x$ | $y$ | $z$ | S/N | Comments |
|---|---|---|---|---|---|---|
| G06 | TC | 50 m | 44 m | 1 m | NSN | |
| | TC | 50 m | 44 m | 5 m | NSN | |
| | TC | 50 m | 44 m | 11 m | NSN | |
| | TC | 50 m | 44 m | 17 m | 214 | |
| | MSA | 50 m | 44 m | 17 m | 009 | |
| | LLNL-IR | 50 m | 44 m | 1 m | 037 | DNF |
| | LLNL-IR | 50 m | 44 m | 5 m | 016 | DNF |
| | LLNL-IR | 50 m | 44 m | 11 m | 006 | DNF |
| G07 | TC | 50 m | 66 m | 1 m | NSN | |
| | TC | 50 m | 66 m | 5 m | NSN | |
| | TC | 50 m | 66 m | 11 m | NSN | |
| | TC | 50 m | 66 m | 17 m | 201 | |
| | MSA | 50 m | 66 m | 17 m | 013 | |
| | LLNL-IR | 50 m | 66 m | 1 m | 035 | DNF |
| | LLNL-IR | 50 m | 66 m | 5 m | 017 | DNF |
| | LLNL-IR | 50 m | 66 m | 11 m | 014 | DNF |
| G08 | TC | 150 m | −75 m | 1 m | NSN | |
| | TC | 150 m | −75 m | 5 m | NSN | |
| | TC | 150 m | −75 m | 11 m | 217 | |
| | MSA | 150 m | −75 m | 11 m | 020 | |
| | LLNL-IR | 150 m | −75 m | 1 m | 028 | DNF |
| | LLNL-IR | 150 m | −75 m | 5 m | 005 | DNF |
| G09 | TC | 150 m | −50 m | 0 | NSN | |
| | TC | 150 m | −50 m | 1 m | NSN | |
| | TC | 150 m | −50 m | 5 m | NSN | |
| | TC | 150 m | −50 m | 11 m | 218 | |
| | MSA | 150 m | −50 m | 11 m | 519 | |
| | LLNL-IR | 150 m | −50 m | 1 m | 018 | DNF |
| | LLNL-IR | 150 m | −50 m | 5 m | 025 | DNF |
| | heat flux | 150 m | −50 m | 0 | 023 | |
| G10 | TC | 150 m | −25 m | 1 m | NSN | |
| | TC | 150 m | −25 m | 5 m | NSN | |
| [B | | | | | | |
| | TC | 150 m | −25 m | 11 m | 203 | |
| | TC | 150 m | −25 m | 17 m | 204 | |
| | MSA | 150 m | −25 m | 11 m | 004 | |
| | MSA | 150 m | −25 m | 17 m | 016 | |
| | LLNL-IR | 150 m | −25 m | 1 m | 021 | DNF |
| | LLNL-IR | 150 m | −25 m | 5 m | 002 | DNF |
| | bivane | 150 m | −25 m | 1 m | 384 | |
| | bivane | 150 m | −25 m | 5 m | 392 | |
| | bivane | 150 m | −25 m | 11 m | 387 | |
| G11 | MSA | 150 m | 0 | 11 m | 007 | |
| | MSA | 150 m | 0 | 17 m | 512 | |
| | LLNL-IR | 150 m | 0 | 1 m | 007 | DNF |
| | LLNL-IR | 150 m | 0 | 5 m | 026 | DNF |
| | bivane | 150 m | 0 | 1 m | 380 | |
| | bivane | 150 m | 0 | 5 m | 385 | |
| | bivane | 150 m | 0 | 11 m | 379 | |

**Table 6.** Continued.

Instrumentation Plan—Falcon 2

| Station | Instrument | $x$ | $y$ | $z$ | S/N | Comments |
|---|---|---|---|---|---|---|
| | RTD | 150 m | 0 | 1 m | 006 | |
| | RTD | 150 m | 0 | 2 m | 007 | |
| | RTD | 150 m | 0 | 4 m | 008 | |
| | RTD | 150 m | 0 | 8 m | 009 | |
| G12 | TC | 150 m | 25 m | 1 m | NSN | |
| | TC | 150 m | 25 m | 5 m | NSN | |
| | TC | 150 m | 25 m | 11 m | 205 | |
| | TC | 150 m | 25 m | 17 m | 206 | |
| | MSA | 150 m | 25 m | 11 m | 520 | |
| | MSA | 150 m | 25 m | 17 m | 515 | |
| | LLNL-IR | 150 m | 25 m | 1 m | 024 | DNF |
| | LLNL-IR | 150 m | 25 m | 5 m | 023 | DNF |
| | bivane | 150 m | 25 m | 1 m | 391 | |
| | bivane | 150 m | 25 m | 5 m | 389 | |
| | bivane | 150 m | 25 m | 11 m | 373 | |
| G13 | TC | 150 m | 50 m | 0 | NSN | |
| | TC | 150 m | 50 m | 1 m | NSN | |
| | TC | 150 m | 50 m | 5 m | NSN | |
| | TC | 150 m | 50 m | 11 m | 220 | |
| | MSA | 150 m | 50 m | 11 m | 011 | |
| | LLNL-IR | 150 m | 50 m | 1 m | 011 | DNF |
| | LLNL-IR | 150 m | 50 m | 5 m | 027 | DNF |
| | heat flux | 150 m | 50 m | 0 | 029 | |
| G14 | TC | 150 m | 75 m | 1 m | NSN | |
| | TC | 150 m | 75 m | 5 m | NSN | |
| | TC | 150 m | 75 m | 11 m | 230 | |
| | MSA | 150 m | 75 m | 11 m | 017 | |
| | LLNL-IR | 150 m | 75 m | 1 m | 012 | DNF |
| | LLNL-IR | 150 m | 75 m | 5 m | 019 | DNF |
| G15 | TC | 250 m | −84 m | 1 m | 225 | |
| | TC | 250 m | −84 m | 5 m | 226 | |
| | TC | 250 m | −84 m | 11 m | 227 | |
| | MSA | 250 m | −84 m | 1 m | 014 | |
| | MSA | 250 m | −84 m | 5 m | 006 | |
| | MSA | 250 m | −84 m | 11 m | 015 | |
| G16 | TC | 250 m | −56 m | 1 m | 228 | |
| | TC | 250 m | −56 m | 5 m | 229 | |
| | TC | 250 m | −56 m | 11 m | 231 | |
| | MSA | 250 m | −56 m | 5 m | 001 | |
| | MSA | 250 m | −56 m | 11 m | 018 | |
| G17 | TC | 250 m | −28 m | 1 m | 232 | |
| | TC | 250 m | −28 m | 5 m | 233 | |
| | TC | 250 m | −28 m | 11 m | 234 | |
| | MSA | 250 m | −28 m | 5 m | 173 | |
| | MSA | 250 m | −28 m | 11 m | 518 | |

**Table 6.** Continued.

Instrumentation Plan—Falcon 2

| Station | Instrument | $x$ | $y$ | $z$ | S/N | Comments |
|---|---|---|---|---|---|---|
| G18 | TC | 250 m | 0 | 1 m | 235 | |
| | TC | 250 m | 0 | 5 m | 236 | |
| | TC | 250 m | 0 | 11 m | 237 | |
| | MSA | 250 m | 0 | 1 m | 002 | |
| | MSA | 250 m | 0 | 11 m | 514 | |
| G19 | TC | 250 m | 28 m | 1 m | 201 | |
| | TC | 250 m | 28 m | 5 m | 207 | |
| | TC | 250 m | 28 m | 11 m | 209 | |
| | MSA | 250 m | 28 m | 5 m | 005 | |
| | MSA | 250 m | 28 m | 11 m | 516 | |
| G20 | TC | 250 m | 56 m | 1 m | 210 | |
| | TC | 250 m | 56 m | 5 m | 219 | |
| | TC | 250 m | 56 m | 11 m | 221 | |
| | MSA | 250 m | 56 m | 5 m | 003 | |
| | MSA | 250 m | 56 m | 11 m | 521 | |
| G21 | TC | 250 m | 84 m | 1 m | 222 | |
| | TC | 250 m | 84 m | 5 m | NSN | |
| | TC | 250 m | 84 m | 11 m | 224 | |
| | MSA | 250 m | 84 m | 1 m | 019 | |
| | MSA | 250 m | 84 m | 5 m | 008 | |
| | MSA | 250 m | 84 m | 11 m | 517 | |
| G22 | TC | −32 m | 0 | −10 cm | NSN | |
| | TC | −32 m | 0 | −5 cm | NSN | |
| | TC | −32 m | 0 | 5 cm | NSN | |
| | TC | −32 m | 0 | 15 cm | NSN | |
| | TC | −32 m | 0 | 1 m | NSN | |
| | TC | −2 m | 0 | −10 cm | NSN | |
| | TC | −2 m | 0 | −5 cm | NSN | DNF |
| | TC | −2 m | 0 | 5 cm | NSN | |
| | TC | −2 m | 0 | 15 cm | NSN | |
| | TC | −2 m | 0 | 1 m | NSN | |
| | TC | −2 m | 0 | 1 m | NSN | |
| | TC | −2 m | 0 | 2 m | NSN | DNF |
| | TC | −2 m | 0 | 6 m | NSN | |
| | TC | −2 m | 0 | 10 m | NSN | |
| | TC | −2 m | 0 | 14 m | NSN | |
| | JPL-IR | −62 m | 20 m | 1 m | 001 | |
| G23 | TC | −64 m | 0 | 0 | NSN | |
| | TC | −76 m | 0 | 0 | NSN | |
| | TC | −88 m | 0 | 1 m | NSN | |
| | TC | −88 m | 0 | 2 m | NSN | |
| | TC | −88 m | 0 | 6 m | NSN | |
| | TC | −88 m | 0 | 10 m | NSN | |
| | TC | −88 m | 0 | 13 m | NSN | |
| | heat flux | −64 m | 0 | 0 | NSN | |
| | heat flux | −76 m | 0 | 0 | NSN | |
| | humidity | −2 m | 0 | 1 m | 394 | DNF |
| | humidity | −32 m | 0 | 1 m | 387 | |

**Table 6.** Continued.

Instrumentation Plan—Falcon 2

| Station | Instrument | $x$ | $y$ | $z$ | S/N | Comments |
|---|---|---|---|---|---|---|
| | JPL-IR | −32 m | 0 | 1 m | 006 | |
| | JPL-IR | −62 m | 0 | 1 m | 002 | |
| G24 | TC | −130 m | −25 m | 0 | NSN | |
| | TC | −130 m | −25 m | 1 m | NSN | |
| | heat flux | −130 m | −25 m | 0 | NSN | |
| | bivane | −130 m | −25 m | 1 m | 382 | |
| | bivane | −130 m | −25 m | 4 m | 375 | |
| (TCS) | bivane | −130 m | −25 m | 16 m | 374 | |
| (TCS) | RTD | −130 m | −25 m | 1 m | NSN | |
| | RTD | −130 m | −25 m | 2 m | NSN | |
| | RTD | −130 m | −25 m | 4 m | NSN | |
| | RTD | −130 m | −25 m | 8 m | NSN | |
| | RTD | −130 m | −25 m | 16 m | NSN | |
| G25 | TC | −64 m | 25 m | 1 m | NSN | |
| | TC | −64 m | 25 m | 2 m | NSN | |
| | TC | −64 m | 25 m | 4 m | NSN | |
| | TC | −64 m | 25 m | 8 m | NSN | |
| | TC | −64 m | 25 m | 11 m | NSN | |
| | TC | −64 m | 25 m | 17 m | NSN | |
| | bivane | 20 m | 0 | 1 m | 388 | |
| | bivane | 20 m | 0 | 5 m | 376 | |
| | bivane | 20 m | 0 | 11 m | 381 | |
| W01 | Met-One | −1000 m | 0 | 2 m | N/A | |
| W01 | Met-One | −1000 m | 0 | 2 m | N/A | |
| W02 | Met-One | −600 m | −100 m | 2 m | N/A | |
| W03 | Met-One | −600 m | 100 m | 2 m | N/A | |
| W04 | Met-One | −300 m | −100 m | 2 m | N/A | |
| W05 | Met-One | −300 m | 100 m | 2 m | N/A | |
| W06 | Met-One | −44 m | 25 m | 2 m | N/A | ESD |
| W07 | Met-One | 50 m | −75 m | 2 m | N/A | |
| W08 | Met-One | 50 m | 0 | 2 m | N/A | ESD |
| W09 | Met-One | 50 m | 75 m | 2 m | N/A | |
| W10 | Met-One | 150 m | −150 m | 2 m | N/A | |
| W11 | Met-One | 150 m | −75 m | 2 m | N/A | |
| W12 | Met-One | 150 m | 0 | 2 m | N/A | |
| W13 | Met-One | 150 m | 75 m | 2 m | N/A | |
| W14 | Met-One | 150 m | 150 m | 2 m | N/A | |
| W15 | Met-One | 300 m | −150 m | 2 m | N/A | |
| W16 | Met-One | 300 m | −75 m | 2 m | N/A | |
| W17 | Met-One | 300 m | 0 | 2 m | N/A | |
| W18 | Met-One | 300 m | 75 m | 2 m | N/A | |
| W19 | Met-One | 300 m | 150 m | 2 m | N/A | |

**Remarks:**

1. LLL-IR sensors failed to take data due to internal software problems.

**Table 6.** Continued.

Instrumentation Plan—Falcon 3

| Station | Instrument | x | y | z | S/N | Comments |
|---|---|---|---|---|---|---|
| G01 | TC | 50 m | -66 m | 1 m | NSN | |
| | TC | 50 m | -66 m | 5 m | NSN | |
| | TC | 50 m | -66 m | 11 m | NSN | |
| | TC | 50 m | -66 m | 17 m | 215 | |
| | MSA | 50 m | -66 m | 17 m | 010 | |
| | LLNL-IR | 50 m | -66 m | 1 m | 031 | |
| | LLNL-IR | 50 m | -66 m | 5 m | 029 | |
| | LLNL-IR | 50 m | -66 m | 11 m | 022 | |
| G02 | TC | 50 m | -44 m | 1 m | NSN | |
| | TC | 50 m | -44 m | 5 m | NSN | |
| | TC | 50 m | -44 m | 11 m | NSN | |
| | TC | 50 m | -44 m | 17 m | 216 | |
| | MSA | 50 m | -44 m | 17 m | 513 | |
| | LLNL-IR | 50 m | -44 m | 1 m | 033 | |
| | LLNL-IR | 50 m | -44 m | 5 m | 004 | |
| | LLNL-IR | 50 m | -44 m | 11 m | 009 | |
| G03 | TC | 50 m | -22 m | 0 | NSN | |
| | TC | 50 m | -22 m | 1 m | NSN | |
| | TC | 50 m | -22 m | 5 m | NSN | |
| | TC | 50 m | -22 m | 11 m | NSN | |
| | TC | 50 m | -22 m | 17 m | 211 | |
| | MSA | 50 m | -22 m | 17 m | 172 | |
| | LLNL-IR | 50 m | -22 m | 1 m | 032 | |
| | LLNL-IR | 50 m | -22 m | 5 m | 003 | |
| | LLNL-IR | 50 m | -22 m | 11 m | 010 | |
| | heat flux | 50 m | -22 m | 0 | NSN | |
| G04 | TC | 50 m | 0 | 1 m | NSN | |
| | TC | 50 m | 0 | 5 m | NSN | |
| | TC | 50 m | 0 | 11 m | NSN | |
| | TC | 50 m | 0 | 17 m | 212 | |
| | MSA | 50 m | 0 | 17 m | 522 | |
| | LLNL-IR | 50 m | 0 | 1 m | 036 | |
| | LLNL-IR | 50 m | 0 | 5 m | 015 | |
| | LLNL-IR | 50 m | 0 | 11 m | 013 | |
| | bivane | 50 m | 0 | 1 m | 378 | |
| | bivane | 50 m | 0 | 5 m | 377 | |
| | bivane | 50 m | 0 | 11 m | 376 | |
| | humidity | 50 m | 0 | 1 m | 389 | |
| G05 | TC | 50 m | 22 m | 0 | NSN | |
| | TC | 50 m | 22 m | 1 m | NSN | |
| | TC | 50 m | 22 m | 5 m | NSN | |
| | TC | 50 m | 22 m | 11 m | NSN | |
| | TC | 50 m | 22 m | 17 m | 213 | |
| | MSA | 50 m | 22 m | 17 m | 012 | |
| | LLNL-IR | 50 m | 22 m | 1 m | 034 | |
| | LLNL-IR | 50 m | 22 m | 5 m | 008 | |
| | LLNL-IR | 50 m | 22 m | 11 m | 030 | |
| | heat flux | 50 m | 22 m | 0 | 025 | |

Table 6. Continued.

Instrumentation Plan—Falcon 3

| Station | Instrument | x | y | z | S/N | Comments |
|---|---|---|---|---|---|---|
| G06 | TC | 50 m | 44 m | 1 m | NSN | |
| | TC | 50 m | 44 m | 5 m | NSN | |
| | TC | 50 m | 44 m | 11 m | NSN | |
| | TC | 50 m | 44 m | 17 m | 214 | |
| | MSA | 50 m | 44 m | 17 m | 009 | |
| | LLNL-IR | 50 m | 44 m | 1 m | 037 | |
| | LLNL-IR | 50 m | 44 m | 5 m | 016 | |
| | LLNL-IR | 50 m | 44 m | 11 m | 006 | |
| G07 | TC | 50 m | 66 m | 1 m | NSN | |
| | TC | 50 m | 66 m | 5 m | NSN | |
| | TC | 50 m | 66 m | 11 m | NSN | |
| | TC | 50 m | 66 m | 17 m | 201 | |
| | MSA | 50 m | 66 m | 17 m | 013 | |
| | LLNL-IR | 50 m | 66 m | 1 m | 035 | |
| | LLNL-IR | 50 m | 66 m | 5 m | 017 | |
| | LLNL-IR | 50 m | 66 m | 11 m | 014 | |
| G08 | TC | 150 m | −75 m | 1 m | NSN | |
| | TC | 150 m | −75 m | 5 m | NSN | |
| | TC | 150 m | −75 m | 11 m | 217 | |
| | LLNL-IR | 150 m | −75 m | 1 m | 028 | |
| | LLNL-IR | 150 m | −75 m | 5 m | 005 | |
| G09 | TC | 150 m | −50 m | 0 | NSN | |
| | TC | 150 m | −50 m | 1 m | NSN | |
| | TC | 150 m | −50 m | 5 m | NSN | |
| | TC | 150 m | −50 m | 11 m | 218 | |
| | MSA | 150 m | −50 m | 11 m | 519 | |
| | LLNL-IR | 150 m | −50 m | 1 m | 018 | |
| | LLNL-IR | 150 m | −50 m | 5 m | 025 | |
| | heat flux | 150 m | −50 m | 0 | 023 | |
| G10 | TC | 150 m | −25 m | 1 m | NSN | |
| | TC | 150 m | −25 m | 5 m | NSN | |
| | TC | 150 m | −25 m | 11 m | 203 | |
| | TC | 150 m | −25 m | 17 m | 204 | |
| | MSA | 150 m | −25 m | 11 m | 004 | |
| | MSA | 150 m | −25 m | 17 m | 016 | |
| | LLNL-IR | 150 m | −25 m | 1 m | 021 | |
| | LLNL-IR | 150 m | −25 m | 5 m | 002 | |
| | bivane | 150 m | −25 m | 1 m | 384 | |
| | bivane | 150 m | −25 m | 5 m | 392 | |
| | bivane | 150 m | −25 m | 11 m | 387 | |
| G11 | MSA | 150 m | 0 | 11 m | 007 | |
| | MSA | 150 m | 0 | 17 m | 512 | |
| | LLNL-IR | 150 m | 0 | 1 m | 007 | |
| | LLNL-IR | 150 m | 0 | 5 m | 026 | |
| | bivane | 150 m | 0 | 1 m | 380 | |
| | bivane | 150 m | 0 | 5 m | 385 | |
| | bivane | 150 m | 0 | 11 m | 379 | |
| | RTD | 150 m | 0 | 1 m | 006 | |

**Table 6.** Continued.

Instrumentation Plan—Falcon 3

| Station | Instrument | $x$ | $y$ | $z$ | S/N | Comments |
|---|---|---|---|---|---|---|
| | RTD | 150 m | 0 | 2 m | 007 | |
| | RTD | 150 m | 0 | 4 m | 008 | |
| | RTD | 150 m | 0 | 8 m | 009 | |
| G12 | TC | 150 m | 25 m | 1 m | NSN | |
| | TC | 150 m | 25 m | 5 m | NSN | |
| | TC | 150 m | 25 m | 11 m | 205 | |
| | TC | 150 m | 25 m | 17 m | 206 | |
| | MSA | 150 m | 25 m | 11 m | 520 | |
| | MSA | 150 m | 25 m | 17 m | 515 | |
| | LLNL-IR | 150 m | 25 m | 1 m | 024 | |
| | LLNL-IR | 150 m | 25 m | 5 m | 023 | |
| | bivane | 150 m | 25 m | 1 m | 391 | |
| | bivane | 150 m | 25 m | 5 m | 389 | |
| | bivane | 150 m | 25 m | 11 m | 373 | |
| G13 | TC | 150 m | 50 m | 0 | NSN | |
| | TC | 150 m | 50 m | 1 m | NSN | |
| | TC | 150 m | 50 m | 5 m | NSN | |
| | TC | 150 m | 50 m | 11 m | 220 | |
| | MSA | 150 m | 50 m | 11 m | 011 | |
| | LLNL-IR | 150 m | 50 m | 1 m | 011 | |
| | LLNL-IR | 150 m | 50 m | 5 m | 027 | |
| | heat flux | 150 m | 50 m | 0 | 029 | |
| G14 | TC | 150 m | 75 m | 1 m | NSN | |
| | TC | 150 m | 75 m | 5 m | NSN | |
| | TC | 150 m | 75 m | 11 m | 230 | |
| | MSA | 150 m | 75 m | 11 m | 017 | |
| | LLNL-IR | 150 m | 75 m | 1 m | 012 | |
| | LLNL-IR | 150 m | 75 m | 5 m | 019 | |
| G15 | TC | 250 m | -84 m | 1 m | 225 | |
| | TC | 250 m | -84 m | 5 m | 226 | |
| | TC | 250 m | -84 m | 11 m | 227 | |
| | MSA | 250 m | -84 m | 1 m | 014 | |
| | MSA | 250 m | -84 m | 5 m | 006 | |
| G16 | TC | 250 m | -56 m | 1 m | 228 | |
| | TC | 250 m | -56 m | 5 m | 229 | |
| | TC | 250 m | -56 m | 11 m | 231 | |
| | MSA | 250 m | -56 m | 1 m | 015 | |
| | MSA | 250 m | -56 m | 5 m | 001 | |
| | MSA | 250 m | -56 m | 11 m | 018 | |
| G17 | TC | 250 m | -28 m | 1 m | 232 | |
| | TC | 250 m | -28 m | 5 m | 233 | |
| | TC | 250 m | -28 m | 11 m | 234 | |
| | MSA | 250 m | -28 m | 1 m | 173 | |
| | MSA | 250 m | -28 m | 5 m | 518 | |
| G18 | TC | 250 m | 0 | 1 m | 235 | |
| | TC | 250 m | 0 | 5 m | 236 | |

**Table 6.** Continued.

Instrumentation Plan—Falcon 3

| Station | Instrument | x | y | z | S/N | Comments |
|---|---|---|---|---|---|---|
| | TC | 250 m | 0 | 11 m | 237 | |
| | MSA | 250 m | 0 | 1 m | 002 | |
| | MSA | 250 m | 0 | 5 m | 020 | |
| | MSA | 250 m | 0 | 11 m | 514 | |
| G19 | TC | 250 m | 28 m | 1 m | 201 | |
| | TC | 250 m | 28 m | 5 m | 207 | |
| | TC | 250 m | 28 m | 11 m | 209 | |
| | MSA | 250 m | 28 m | 1 m | 516 | |
| | MSA | 250 m | 28 m | 5 m | 005 | |
| G20 | TC | 250 m | 56 m | 1 m | 210 | |
| | TC | 250 m | 56 m | 5 m | 219 | |
| | TC | 250 m | 56 m | 11 m | 221 | |
| | MSA | 250 m | 56 m | 11 m | 517 | |
| | MSA | 250 m | 56 m | 5 m | 003 | |
| | MSA | 250 m | 56 m | 11 m | 521 | |
| G21 | TC | 250 m | 84 m | 1 m | 222 | |
| | TC | 250 m | 84 m | 5 m | NSN | |
| | TC | 250 m | 84 m | 11 m | 224 | |
| | MSA | 250 m | 84 m | 1 m | 019 | |
| | MSA | 250 m | 84 m | 5 m | 008 | |
| G22 | TC | -32 m | 0 | 1 m | NSN | DNF |
| | TC | -32 m | 0 | 2 m | NSN | |
| | TC | -32 m | 0 | 4 m | NSN | |
| | TC | -32 m | 0 | 6 m | NSN | |
| | TC | -32 m | 0 | 1 m | NSN | |
| | TC | -2 m | 0 | -10 cm | NSN | |
| | TC | -2 m | 0 | -5 cm | NSN | |
| | TC | -2 m | 0 | 5 cm | NSN | |
| œ[B | | | | | | |
| | TC | -2 m | 0 | 15 cm | NSN | |
| | TC | -2 m | 0 | 1 m | NSN | |
| | TC | -2 m | 0 | 1 m | NSN | |
| | TC | -2 m | 0 | 2 m | NSN | |
| | TC | -2 m | 0 | 6 m | NSN | |
| | TC | -2 m | 0 | 10 m | NSN | |
| | TC | -2 m | 0 | 14 m | NSN | |
| | JPL-IR | -62 m | 20 m | 2 m | 001 | |
| G23 | TC | -64 m | 0 | 0 | NSN | |
| | TC | -76 m | 0 | 0 | NSN | |
| | TC | -88 m | 0 | 1 m | NSN | |
| | TC | -88 m | 0 | 2 m | NSN | |
| | TC | -88 m | 0 | 6 m | NSN | |
| | TC | -88 m | 0 | 10 m | NSN | |
| | TC | -88 m | 0 | 13 m | NSN | |
| | heat flux | -64 m | 0 | 0 | NSN | |
| | heat flux | -76 m | 0 | 0 | NSN | |
| | humidity | -2 m | 0 | 1 m | 392 | |
| | humidity | -32 m | 0 | 1 m | 394 | |
| | JPL-IR | -2 m | 0 | 1 m | 005 | |

**Table 6.** Continued.

Instrumentation Plan—Falcon 3

| Station | Instrument | $x$ | $y$ | $z$ | S/N | Comments |
|---|---|---|---|---|---|---|
| | JPL-IR | −32 m | 0 | 1 m | 006 | |
| | JPL-IR | −62 m | 0 | 2 m | 002 | |
| G24 | TC | −130 m | −25 m | 0 | NSN | |
| | TC | −130 m | −25 m | 1 m | NSN | |
| | heat flux | −130 m | −25 m | 0 | NSN | |
| | bivane | −130 m | −25 m | 1 m | 382 | |
| | bivane | −130 m | −25 m | 4 m | 375 | |
| | bivane | −130 m | −25 m | 16 m | 374 | |
| (TCS) | RTD | −130 m | −25 m | 1 m | NSN | |
| | RTD | −130 m | −25 m | 2 m | NSN | |
| | RTD | −130 m | −25 m | 4 m | NSN | |
| | RTD | −130 m | −25 m | 8 m | NSN | |
| | RTD | −130 m | −25 m | 16 m | NSN | |
| G25 | TC | −64 m | 25 m | 1 m | NSN | |
| | TC | −64 m | 25 m | 2 m | NSN | |
| | TC | −64 m | 25 m | 4 m | NSN | |
| | TC | −64 m | 25 m | 8 m | NSN | |
| | TC | −64 m | 25 m | 11 m | NSN | |
| | TC | −64 m | 25 m | 17 m | NSN | |
| | bivane | 20 m | 0 | 1 m | 388 | |
| | bivane | 20 m | 0 | 5 m | 376 | |
| | bivane | 20 m | 0 | 11 m | 381 | |
| W01 | Met-One | −1000 m | 0 | 2 m | N/A | |
| W01 | Met-One | −1000 m | 0 | 2 m | N/A | |
| W02 | Met-One | −600 m | −100 m | 2 m | N/A | |
| W03 | Met-One | −600 m | 100 m | 2 m | N/A | |
| W04 | Met-One | −300 m | −100 m | 2 m | N/A | |
| W05 | Met-One | −300 m | 100 m | 2 m | N/A | |
| W06 | Met-One | −44 m | 25 m | 2 m | N/A | DNF |
| W07 | Met-One | 50 m | −75 m | 2 m | N/A | |
| W08 | Met-One | 50 m | 0 | 2 m | N/A | ESD |
| W09 | Met-One | 50 m | 75 m | 2 m | N/A | |
| W10 | Met-One | 150 m | −150 m | 2 m | N/A | |
| W11 | Met-One | 150 m | −75 m | 2 m | N/A | |
| W12 | Met-One | 150 m | 0 | 2 m | N/A | |
| W13 | Met-One | 150 m | 75 m | 2 m | N/A | |
| W14 | Met-One | 150 m | 150 m | 2 m | N/A | |
| W15 | Met-One | 300 m | −150 m | 2 m | N/A | |
| W16 | Met-One | 300 m | −75 m | 2 m | N/A | |
| W17 | Met-One | 300 m | 0 | 2 m | N/A | |
| W18 | Met-One | 300 m | 75 m | 2 m | N/A | |
| W19 | Met-One | 300 m | 150 m | 2 m | N/A | |

**Remarks:**

1. Large RPT explosions occurred beginning at approximately $T = 60$ sec.

**Table 6.** Continued.

Instrumentation Plan—Falcon 4

| Station | Instrument | $x$ | $y$ | $z$ | S/N | Comments |
|---|---|---|---|---|---|---|
| G01 | TC | 50 m | −66 m | 1 m | NSN | |
| | TC | 50 m | −66 m | 5 m | NSN | |
| | TC | 50 m | −66 m | 11 m | NSN | |
| | TC | 50 m | −66 m | 17 m | 215 | |
| | MSA | 50 m | −66 m | 17 m | 010 | |
| | LLNL-IR | 50 m | −66 m | 1 m | 031 | |
| | LLNL-IR | 50 m | −66 m | 5 m | 029 | |
| | LLNL-IR | 50 m | −66 m | 11 m | 022 | |
| G02 | TC | 150 m | −50 m | 0 | NSN | |
| | TC | 150 m | −50 m | 1 m | NSN | |
| | TC | 150 m | −50 m | 5 m | NSN | |
| | TC | 150 m | −50 m | 11 m | NSN | |
| | TC | 150 m | −50 m | 17 m | 216 | |
| | MSA | 150 m | −50 m | 17 m | 513 | |
| | LLNL-IR | 150 m | −50 m | 1 m | 033 | |
| | LLNL-IR | 150 m | −50 m | 5 m | 004 | |
| | LLNL-IR | 150 m | −50 m | 11 m | 009 | |
| | heat flux | 150 m | −50 m | 0 | 023 | |
| G03 | TC | 50 m | −33 m | 0 | NSN | |
| | TC | 50 m | −33 m | 1 m | NSN | |
| | TC | 50 m | −33 m | 5 m | NSN | |
| | TC | 50 m | −33 m | 11 m | NSN | |
| | TC | 50 m | −33 m | 17 m | 211 | |
| | MSA | 50 m | −33 m | 17 m | 172 | |
| | LLNL-IR | 50 m | −33 m | 1 m | 032 | |
| | LLNL-IR | 50 m | −33 m | 5 m | 003 | |
| | LLNL-IR | 50 m | −33 m | 11 m | 010 | |
| | heat flux | 50 m | −33 m | 0 | NSN | |
| G04 | TC | 50 m | 0 | 1 m | NSN | |
| | TC | 50 m | 0 | 5 m | NSN | |
| | TC | 50 m | 0 | 11 m | NSN | |
| | TC | 50 m | 0 | 17 m | 212 | |
| | MSA | 50 m | 0 | 17 m | 522 | |
| | LLNL-IR | 50 m | 0 | 1 m | 036 | |
| | LLNL-IR | 50 m | 0 | 5 m | 015 | |
| | LLNL-IR | 50 m | 0 | 11 m | 013 | |
| | bivane | 50 m | 0 | 1 m | 378 | |
| | bivane | 50 m | 0 | 5 m | 377 | |
| | bivane | 50 m | 0 | 11 m | 376 | |
| | humidity | 50 m | 0 | 1 m | 389 | |
| G05 | TC | 50 m | 33 m | 0 | NSN | |
| | TC | 50 m | 33 m | 1 m | NSN | |
| | TC | 50 m | 33 m | 5 m | NSN | |
| | TC | 50 m | 33 m | 11 m | NSN | |
| | TC | 50 m | 33 m | 17 m | 213 | |
| | MSA | 50 m | 33 m | 17 m | 012 | |
| | LLNL-IR | 50 m | 33 m | 1 m | 034 | |
| | LLNL-IR | 50 m | 33 m | 5 m | 008 | |
| | LLNL-IR | 50 m | 33 m | 11 m | 030 | |
| | heat flux | 50 m | 33 m | 0 | 025 | |

**Table 6.** Continued.

Instrumentation Plan—Falcon 4

| Station | Instrument | x | y | z | S/N | Comments |
|---|---|---|---|---|---|---|
| G06 | TC | 150 m | 50 m | 0 | NSN | |
| | TC | 150 m | 50 m | 1 m | NSN | |
| | TC | 150 m | 50 m | 5 m | NSN | |
| | TC | 150 m | 50 m | 11 m | NSN | |
| | TC | 150 m | 50 m | 17 m | 214 | |
| | MSA | 150 m | 50 m | 17 m | 009 | |
| | LLNL-IR | 150 m | 50 m | 1 m | 037 | |
| | LLNL-IR | 150 m | 50 m | 5 m | 016 | |
| | LLNL-IR | 150 m | 50 m | 11 m | 006 | |
| | heat flux | 150 m | 50 m | 0 | 029 | |
| G07 | TC | 50 m | 66 m | 1 m | NSN | |
| | TC | 50 m | 66 m | 5 m | NSN | |
| | TC | 50 m | 66 m | 11 m | NSN | |
| | TC | 50 m | 66 m | 17 m | 201 | |
| | MSA | 50 m | 66 m | 17 m | 013 | |
| | LLNL-IR | 50 m | 66 m | 1 m | 035 | |
| | LLNL-IR | 50 m | 66 m | 5 m | 017 | |
| | LLNL-IR | 50 m | 66 m | 11 m | 014 | |
| G08 | TC | 150 m | −75 m | 1 m | NSN | |
| | TC | 150 m | −75 m | 5 m | NSN | |
| | TC | 150 m | −75 m | 11 m | 217 | |
| | MSA | 150 m | −75 m | 11 m | 117 | |
| | LLNL-IR | 150 m | −75 m | 1 m | 028 | |
| | LLNL-IR | 150 m | −75 m | 5 m | 005 | |
| G09 | TC | 150 m | −100 m | 1 m | NSN | |
| | TC | 150 m | −100 m | 5 m | NSN | |
| | TC | 150 m | −100 m | 11 m | 218 | |
| | MSA | 150 m | −100 m | 11 m | 519 | |
| | LLNL-IR | 150 m | −100 m | 1 m | 018 | |
| | LLNL-IR | 150 m | −100 m | 5 m | 025 | |
| G10 | TC | 150 m | −25 m | 1 m | NSN | |
| | TC | 150 m | −25 m | 5 m | NSN | |
| | TC | 150 m | −25 m | 11 m | 203 | |
| | TC | 150 m | −25 m | 17 m | 204 | |
| | MSA | 150 m | −25 m | 11 m | 004 | |
| | MSA | 150 m | −25 m | 17 m | 016 | |
| | LLNL-IR | 150 m | −25 m | 1 m | 021 | |
| | LLNL-IR | 150 m | −25 m | 5 m | 002 | |
| | bivane | 150 m | −25 m | 1 m | 384 | |
| | bivane | 150 m | −25 m | 5 m | 392 | |
| | bivane | 150 m | −25 m | 11 m | 387 | |
| G11 | MSA | 150 m | 0 | 11 m | 007 | |
| | MSA | 150 m | 0 | 17 m | 512 | |
| | LLNL-IR | 150 m | 0 | 1 m | 007 | |
| | LLNL-IR | 150 m | 0 | 5 m | 026 | |
| | bivane | 150 m | 0 | 1 m | 380 | |
| | bivane | 150 m | 0 | 5 m | 385 | |
| | bivane | 150 m | 0 | 11 m | 379 | |

**Table 6.** Continued.

Instrumentation Plan—Falcon 4

| Station | Instrument | x | y | z | S/N | Comments |
|---|---|---|---|---|---|---|
| | RTD | 150 m | 0 | 1 m | 006 | |
| | RTD | 150 m | 0 | 2 m | 007 | |
| | RTD | 150 m | 0 | 4 m | 008 | |
| | RTD | 150 m | 0 | 8 m | 009 | |
| G12 | TC | 150 m | 25 m | 1 m | NSN | |
| | TC | 150 m | 25 m | 5 m | NSN | |
| | TC | 150 m | 25 m | 11 m | 205 | |
| | TC | 150 m | 25 m | 17 m | 206 | |
| | MSA | 150 m | 25 m | 11 m | 520 | |
| | MSA | 150 m | 25 m | 17 m | 515 | |
| | LLNL-IR | 150 m | 25 m | 1 m | 024 | |
| | LLNL-IR | 150 m | 25 m | 5 m | 023 | |
| | bivane | 150 m | 25 m | 1 m | 391 | |
| | bivane | 150 m | 25 m | 5 m | 389 | |
| | bivane | 150 m | 25 m | 11 m | 373 | |
| G13 | TC | 150 m | 100 m | 1 m | NSN | |
| | TC | 150 m | 100 m | 5 m | NSN | |
| | TC | 150 m | 100 m | 11 m | 220 | |
| | MSA | 150 m | 100 m | 11 m | 011 | |
| | LLNL-IR | 150 m | 100 m | 1 m | 011 | |
| | LLNL-IR | 150 m | 100 m | 5 m | 027 | |
| G14 | TC | 150 m | 75 m | 1 m | NSN | |
| | TC | 150 m | 75 m | 5 m | NSN | |
| | TC | 150 m | 75 m | 11 m | 230 | |
| | MSA | 150 m | 75 m | 11 m | 017 | |
| | LLNL-IR | 150 m | 75 m | 1 m | 012 | |
| | LLNL-IR | 150 m | 75 m | 5 m | 019 | |
| G15 | TC | 250 m | -84 m | 1 m | 225 | |
| | TC | 250 m | -84 m | 5 m | 226 | |
| | TC | 250 m | -84 m | 11 m | 227 | |
| | MSA | 250 m | -84 m | 1 m | 014 | |
| | MSA | 250 m | -84 m | 5 m | 006 | |
| G16 | TC | 250 m | -56 m | 1 m | 228 | |
| | TC | 250 m | -56 m | 5 m | 229 | |
| | TC | 250 m | -56 m | 11 m | 231 | |
| | MSA | 250 m | -56 m | 1 m | 015 | |
| | MSA | 250 m | -56 m | 5 m | 001 | |
| | MSA | 250 m | -56 m | 11 m | 018 | |
| G17 | TC | 250 m | -28 m | 1 m | 232 | |
| | TC | 250 m | -28 m | 5 m | 233 | |
| | TC | 250 m | -28 m | 11 m | 234 | |
| | MSA | 250 m | -28 m | 1 m | 173 | |
| | MSA | 250 m | -28 m | 5 m | 518 | |
| G18 | TC | 250 m | 0 | 1 m | 235 | |
| | TC | 250 m | 0 | 5 m | 236 | |
| | TC | 250 m | 0 | 11 m | 237 | |

**Table 6.** Continued.

Instrumentation Plan—Falcon 4

| Station | Instrument | $x$ | $y$ | $z$ | S/N | Comments |
|---|---|---|---|---|---|---|
| | MSA | 250 m | 0 | 1 m | 002 | |
| | MSA | 250 m | 0 | 5 m | 020 | |
| | MSA | 250 m | 0 | 11 m | 514 | |
| G19 | TC | 250 m | 28 m | 1 m | 201 | |
| | TC | 250 m | 28 m | 5 m | 207 | |
| | TC | 250 m | 28 m | 11 m | 209 | |
| | MSA | 250 m | 28 m | 1 m | 516 | |
| | MSA | 250 m | 28 m | 5 m | 005 | |
| G20 | TC | 250 m | 56 m | 1 m | 210 | |
| | TC | 250 m | 56 m | 5 m | 219 | |
| | TC | 250 m | 56 m | 11 m | 221 | |
| | MSA | 250 m | 56 m | 1 m | 003 | |
| | MSA | 250 m | 56 m | 5 m | 521 | |
| | MSA | 250 m | 56 m | 11 m | 517 | |
| G21 | TC | 250 m | 84 m | 1 m | 222 | |
| | TC | 250 m | 84 m | 5 m | NSN | |
| | TC | 250 m | 84 m | 11 m | 224 | |
| | MSA | 250 m | 84 m | 1 m | 019 | |
| | MSA | 250 m | 84 m | 5 m | 008 | |
| G22 | TC | −32 m | 0 | 1 m | NSN | |
| | TC | −32 m | 0 | 2 m | NSN | |
| | TC | −32 m | 0 | 4 m | NSN | |
| | TC | −32 m | 0 | 6 m | NSN | |
| | TC | −32 m | 0 | 1 m | NSN | |
| | TC | −2 m | 0 | −10 cm | NSN | |
| | TC | −2 m | 0 | −5 cm | NSN | DNF |
| | TC | −2 m | 0 | 5 cm | NSN | |
| | TC | −2 m | 0 | 15 cm | NSN | |
| | TC | −2 m | 0 | 1 m | NSN | |
| | TC | −2 m | 0 | 1 m | NSN | |
| | TC | −2 m | 0 | 2 m | NSN | |
| | TC | −2 m | 0 | 6 m | NSN | |
| | TC | −2 m | 0 | 10 m | NSN | |
| | TC | −2 m | 0 | 14 m | NSN | DNF |
| | JPL-IR | −62 m | 20 m | 2 m | 001 | |
| G23 | TC | −64 m | 0 | 0 | NSN | |
| | TC | −76 m | 0 | 0 | NSN | |
| | TC | −88 m | 0 | 1 m | NSN | |
| | TC | −88 m | 0 | 2 m | NSN | |
| | TC | −88 m | 0 | 6 m | NSN | |
| | TC | −88 m | 0 | 10 m | NSN | |
| | TC | −88 m | 0 | 13 m | NSN | |
| | heat flux | −64 m | 0 | 0 | NSN | |
| | heat flux | −76 m | 0 | 0 | NSN | |
| | humidity | −2 m | 0 | 1 m | 392 | |
| | humidity | −32 m | 0 | 1 m | 394 | |
| | JPL-IR | −2 m | 0 | 1 m | 005 | |
| | JPL-IR | −32 m | 0 | 1 m | 006 | |
| | JPL-IR | −62 m | 0 | 2 m | 002 | |

Table 6. Continued.

Instrumentation Plan—Falcon 4

| Station | Instrument | $x$ | $y$ | $z$ | S/N | Comments |
|---|---|---|---|---|---|---|
| G24 | TC | −130 m | −25 m | 0 | NSN | |
| | TC | −130 m | −25 m | 1 m | NSN | |
| | heat flux | −130 m | −25 m | 0 | NSN | |
| | bivane | −130 m | −25 m | 1 m | 382 | |
| | bivane | −130 m | −25 m | 4 m | 375 | |
| | bivane | −130 m | −25 m | 16 m | 374 | |
| | RTD | −130 m | −25 m | 1 m | NSN | |
| | RTD | −130 m | −25 m | 2 m | NSN | |
| | RTD | −130 m | −25 m | 4 m | NSN | |
| | RTD | −130 m | −25 m | 8 m | NSN | |
| | RTD | −130 m | −25 m | 16 m | NSN | |
| G25 | TC | −64 m | 25 m | 1 m | NSN | |
| | TC | −64 m | 25 m | 2 m | NSN | |
| | TC | −64 m | 25 m | 4 m | NSN | |
| | TC | −64 m | 25 m | 8 m | NSN | |
| | TC | −64 m | 25 m | 11 m | NSN | |
| | bivane | 20 m | 0 | 1 m | 388 | |
| | bivane | 20 m | 0 | 5 m | 376 | |
| | bivane | 20 m | 0 | 11 m | 381 | |
| W01 | Met-One | −1000 m | 0 | 2 m | N/A | |
| W02 | Met-One | −600 m | −100 m | 2 m | N/A | |
| W03 | Met-One | −600 m | 100 m | 2 m | N/A | |
| W04 | Met-One | −300 m | −100 m | 2 m | N/A | |
| W05 | Met-One | −300 m | 100 m | 2 m | N/A | |
| W06 | Met-One | −44 m | 25 m | 2 m | N/A | DNF |
| W07 | Met-One | 50 m | −75 m | 2 m | N/A | |
| W08 | Met-One | 50 m | 0 | 2 m | N/A | ESD |
| W09 | Met-One | 50 m | 75 m | 2 m | N/A | |
| W10 | Met-One | 150 m | −150 m | 2 m | N/A | |
| W11 | Met-One | 150 m | −75 m | 2 m | N/A | |
| W12 | Met-One | 150 m | 0 | 2 m | N/A | |
| W13 | Met-One | 150 m | 75 m | 2 m | N/A | |
| W14 | Met-One | 150 m | 150 m | 2 m | N/A | |
| W15 | Met-One | 300 m | −150 m | 2 m | N/A | |
| W16 | Met-One | 300 m | −75 m | 2 m | N/A | |
| W17 | Met-One | 300 m | 0 | 2 m | N/A | |
| W18 | Met-One | 300 m | 75 m | 2 m | N/A | |
| W19 | Met-One | 300 m | 150 m | 2 m | N/A | |

**Table 6.** Continued.

Instrumentation Plan—Falcon 5

| Station | Instrument | x | y | z | S/N | Comments |
|---|---|---|---|---|---|---|
| G01 | TC | 50 m | −66 m | 1 m | 107 | |
| | TC | 50 m | −66 m | 5 m | 017 | |
| | TC | 50 m | −66 m | 11 m | NSN | |
| | TC | 50 m | −66 m | 17 m | 215 | |
| | MSA | 50 m | −66 m | 17 m | 010 | |
| | LLNL-IR | 50 m | −66 m | 1 m | 031 | |
| | LLNL-IR | 50 m | −66 m | 5 m | 029 | |
| | LLNL-IR | 50 m | −66 m | 11 m | 022 | |
| G02 | TC | 150 m | −50 m | 0 | 012 | |
| | TC | 150 m | −50 m | 1 m | 173 | |
| | TC | 150 m | −50 m | 5 m | 000 | |
| | TC | 150 m | −50 m | 11 m | 217 | |
| | TC | 150 m | −50 m | 17 m | 023 | |
| | MSA | 150 m | −50 m | 17 m | 513 | |
| | LLNL-IR | 150 m | −50 m | 1 m | 033 | |
| | LLNL-IR | 150 m | −50 m | 5 m | 004 | |
| | LLNL-IR | 150 m | −50 m | 11 m | 009 | |
| | heat flux | 150 m | −50 m | 0 | 023 | |
| | humidity | 150 m | −50 m | 1 m | 387 | |
| G03 | TC | 50 m | −33 m | 0 | 024 | |
| | TC | 50 m | −33 m | 1 m | 105 | |
| | TC | 50 m | −33 m | 5 m | 083 | |
| | TC | 50 m | −33 m | 11 m | 203 | |
| | TC | 50 m | −33 m | 17 m | 211 | |
| | MSA | 50 m | −33 m | 17 m | 172 | |
| | LLNL-IR | 50 m | −33 m | 1 m | 032 | |
| | LLNL-IR | 50 m | −33 m | 5 m | 003 | |
| | LLNL-IR | 50 m | −33 m | 11 m | 010 | |
| | heat flux | 50 m | −33 m | 0 | 024 | |
| G04 | TC | 50 m | 0 | 1 m | 058 | |
| | TC | 50 m | 0 | 5 m | 093 | |
| | TC | 50 m | 0 | 11 m | 074 | |
| | TC | 50 m | 0 | 17 m | 212 | |
| | MSA | 50 m | 0 | 17 m | 522 | |
| | LLNL-IR | 50 m | 0 | 1 m | 036 | |
| | LLNL-IR | 50 m | 0 | 5 m | 015 | |
| | LLNL-IR | 50 m | 0 | 11 m | 013 | |
| | bivane | 50 m | 0 | 1 m | 378 | |
| | bivane | 50 m | 0 | 5 m | 377 | |
| | bivane | 50 m | 0 | 11 m | 376 | |
| | humidity | 50 m | 0 | 1 m | 389 | |
| G05 | TC | 50 m | 33 m | 0 | 025 | |
| | TC | 50 m | 33 m | 1 m | 089 | |
| | TC | 50 m | 33 m | 5 m | 016 | |
| | TC | 50 m | 33 m | 11 m | 054 | |
| | TC | 50 m | 33 m | 17 m | 213 | |
| | MSA | 50 m | 33 m | 17 m | 012 | |
| | LLNL-IR | 50 m | 33 m | 1 m | 034 | |
| | LLNL-IR | 50 m | 33 m | 5 m | 008 | |

**Table 6.** Continued.

Instrumentation Plan—Falcon 5

| Station | Instrument | x | y | z | S/N | Comments |
|---|---|---|---|---|---|---|
| | LLNL-IR | 50 m | 33 m | 11 m | 030 | |
| | heat flux | 50 m | 33 m | 0 | 025 | |
| G06 | TC | 150 m | 50 m | 0 | 102 | |
| | TC | 150 m | 50 m | 1 m | 120 | |
| | TC | 150 m | 50 m | 5 m | 096 | |
| | TC | 150 m | 50 m | 11 m | 214 | |
| | TC | 150 m | 50 m | 17 m | 029 | |
| | MSA | 150 m | 50 m | 17 m | 009 | |
| | LLNL-IR | 150 m | 50 m | 1 m | 037 | |
| | LLNL-IR | 150 m | 50 m | 5 m | 016 | |
| | LLNL-IR | 150 m | 50 m | 11 m | 006 | |
| | heat flux | 150 m | 50 m | 0 | 029 | |
| G07 | TC | 50 m | 66 m | 1 m | 023 | |
| | TC | 50 m | 66 m | 5 m | 070 | |
| | TC | 50 m | 66 m | 11 m | 027 | |
| | TC | 50 m | 66 m | 17 m | 201 | |
| | MSA | 50 m | 66 m | 17 m | 013 | |
| | LLNL-IR | 50 m | 66 m | 1 m | 035 | |
| | LLNL-IR | 50 m | 66 m | 5 m | 017 | |
| | LLNL-IR | 50 m | 66 m | 11 m | 014 | |
| G08 | TC | 150 m | −75 m | 1 m | 032 | |
| | TC | 150 m | −75 m | 5 m | 029 | |
| | TC | 150 m | −75 m | 11 m | 217 | |
| | MSA | 150 m | −75 m | 11 m | 117 | |
| | LLNL-IR | 150 m | −75 m | 1 m | 028 | |
| | LLNL-IR | 150 m | −75 m | 5 m | 005 | |
| G09 | TC | 150 m | −100 m | 1 m | 125 | |
| | TC | 150 m | −100 m | 5 m | 026 | |
| | TC | 150 m | −100 m | 11 m | 218 | |
| | MSA | 150 m | −100 m | 11 m | 519 | |
| | LLNL-IR | 150 m | −100 m | 1 m | 018 | |
| | LLNL-IR | 150 m | −100 m | 5 m | 025 | |
| G10 | TC | 150 m | −25 m | 1 m | 122 | |
| | TC | 150 m | −25 m | 5 m | 101 | |
| | TC | 150 m | −25 m | 11 m | 203 | |
| | TC | 150 m | −25 m | 17 m | 204 | |
| | MSA | 150 m | −25 m | 11 m | 004 | |
| | MSA | 150 m | −25 m | 17 m | 016 | |
| | LLNL-IR | 150 m | −25 m | 1 m | 021 | |
| | LLNL-IR | 150 m | −25 m | 5 m | 002 | |
| | bivane | 150 m | −25 m | 1 m | 384 | |
| | bivane | 150 m | −25 m | 5 m | 392 | |
| | bivane | 150 m | −25 m | 11 m | 387 | |
| G11 | MSA | 150 m | 0 | 11 m | 007 | |
| | MSA | 150 m | 0 | 17 m | 512 | |
| | LLNL-IR | 150 m | 0 | 1 m | 007 | |
| | LLNL-IR | 150 m | 0 | 5 m | 026 | |

**Table 6.** Continued.

Instrumentation Plan—Falcon 5

| Station | Instrument | x | y | z | S/N | Comments |
|---|---|---|---|---|---|---|
| | bivane | 150 m | 0 | 1 m | 380 | |
| | bivane | 150 m | 0 | 5 m | 385 | |
| | bivane | 150 m | 0 | 11 m | 379 | |
| | RTD | 150 m | 0 | 1 m | 006 | |
| | RTD | 150 m | 0 | 2 m | 007 | |
| | RTD | 150 m | 0 | 4 m | 008 | |
| | RTD | 150 m | 0 | 8 m | 009 | |
| G12 | TC | 150 m | 25 m | 1 m | 011 | |
| | TC | 150 m | 25 m | 5 m | 019 | |
| | TC | 150 m | 25 m | 11 m | 205 | |
| | TC | 150 m | 25 m | 17 m | 206 | |
| | MSA | 150 m | 25 m | 11 m | 520 | |
| | MSA | 150 m | 25 m | 17 m | 515 | |
| | LLNL-IR | 150 m | 25 m | 1 m | 024 | |
| | LLNL-IR | 150 m | 25 m | 5 m | 023 | |
| | bivane | 150 m | 25 m | 1 m | 391 | |
| | bivane | 150 m | 25 m | 5 m | 389 | |
| | bivane | 150 m | 25 m | 11 m | 373 | |
| G13 | TC | 150 m | 100 m | 1 m | 052 | |
| | TC | 150 m | 100 m | 5 m | 066 | |
| | TC | 150 m | 100 m | 11 m | 220 | |
| | MSA | 150 m | 100 m | 11 m | 011 | |
| | LLNL-IR | 150 m | 100 m | 1 m | 011 | |
| | LLNL-IR | 150 m | 100 m | 5 m | 027 | |
| G14 | TC | 150 m | 75 m | 1 m | 040 | |
| | TC | 150 m | 75 m | 5 m | 024 | |
| | TC | 150 m | 75 m | 11 m | 230 | |
| | MSA | 150 m | 75 m | 11 m | 017 | |
| | LLNL-IR | 150 m | 75 m | 1 m | 012 | |
| | LLNL-IR | 150 m | 75 m | 5 m | 019 | |
| G15 | TC | 250 m | −84 m | 1 m | 225 | |
| | TC | 250 m | −84 m | 5 m | 226 | |
| | TC | 250 m | −84 m | 11 m | 227 | |
| | MSA | 250 m | −84 m | 1 m | 014 | |
| | MSA | 250 m | −84 m | 5 m | 006 | |
| G16 | TC | 250 m | −56 m | 1 m | 210 | |
| | TC | 250 m | −56 m | 5 m | 219 | |
| | TC | 250 m | −56 m | 11 m | 221 | |
| | MSA | 250 m | −56 m | 1 m | 015 | |
| | MSA | 250 m | −56 m | 5 m | 001 | |
| | MSA | 250 m | −56 m | 11 m | 018 | |
| G17 | TC | 250 m | −28 m | 1 m | 202 | |
| | TC | 250 m | −28 m | 5 m | 207 | |
| | TC | 250 m | −28 m | 11 m | 209 | |
| | MSA | 250 m | −28 m | 1 m | 173 | |
| | MSA | 250 m | −28 m | 5 m | 518 | |

Table 6. Continued.

Instrumentation Plan—Falcon 5

| Station | Instrument | x | y | z | S/N | Comments |
|---|---|---|---|---|---|---|
| G18 | TC | 250 m | 0 | 1 m | 235 | |
| | TC | 250 m | 0 | 5 m | 236 | |
| | TC | 250 m | 0 | 11 m | 237 | |
| | MSA | 250 m | 0 | 1 m | 002 | |
| | MSA | 250 m | 0 | 5 m | 020 | |
| | MSA | 250 m | 0 | 11 m | 514 | |
| G19 | TC | 250 m | 28 m | 1 m | 232 | |
| | TC | 250 m | 28 m | 5 m | 233 | |
| | TC | 250 m | 28 m | 11 m | 234 | |
| | MSA | 250 m | 28 m | 1 m | 516 | |
| | MSA | 250 m | 28 m | 5 m | 005 | |
| G20 | TC | 250 m | 56 m | 1 m | 228 | |
| | TC | 250 m | 56 m | 5 m | 229 | |
| | TC | 250 m | 56 m | 11 m | 231 | |
| | MSA | 250 m | 56 m | 1 m | 003 | |
| | MSA | 250 m | 56 m | 5 m | 521 | |
| | MSA | 250 m | 56 m | 11 m | 517 | |
| G21 | TC | 250 m | 84 m | 1 m | 225 | |
| | TC | 250 m | 84 m | 5 m | 226 | |
| | TC | 250 m | 84 m | 11 m | 227 | |
| | MSA | 250 m | 84 m | 1 m | 019 | |
| | MSA | 250 m | 84 m | 5 m | 008 | |
| G22 | TC | −32 m | 0 | 1 m | NSN | DNF |
| | TC | −32 m | 0 | 2 m | NSN | |
| | TC | −32 m | 0 | 4 m | NSN | |
| | TC | −32 m | 0 | 6 m | NSN | |
| | TC | −32 m | 0 | 1 m | NSN | DNF |
| | TC | −2 m | 0 | −10 cm | NSN | DNF |
| | TC | −2 m | 0 | −5 cm | NSN | DNF |
| | TC | −2 m | 0 | 5 cm | NSN | DNF |
| | TC | −2 m | 0 | 15 cm | NSN | DNF |
| | TC | −2 m | 0 | 1 m | NSN | DNF |
| | TC | −2 m | 0 | 1 m | NSN | DNF |
| | TC | −2 m | 0 | 2 m | NSN | DNF |
| | TC | −2 m | 0 | 6 m | NSN | DNF |
| | TC | −2 m | 0 | 10 m | NSN | DNF |
| | TC | −2 m | 0 | 14 m | NSN | DNF |
| | JPL-IR | −62 m | 20 m | 2 m | 001 | DNF |
| G23 | TC | −64 m | 0 | 0 | NSN | |
| | TC | −76 m | 0 | 0 | NSN | |
| | TC | −88 m | 0 | 1 m | NSN | DNF |
| | TC | −88 m | 0 | 2 m | NSN | |
| | TC | −88 m | 0 | 6 m | NSN | |
| | TC | −88 m | 0 | 10 m | NSN | |
| | TC | −88 m | 0 | 13 m | NSN | DNF |
| | heat flux | −64 m | 0 | 0 | NSN | |
| | heat flux | −76 m | 0 | 0 | NSN | |
| | humidity | −2 m | 0 | 1 m | 392 | DNF |
| | humidity | −32 m | 0 | 1 m | 388 | DNF |

**Table 6.** Continued.

Instrumentation Plan—Falcon 5

| Station | Instrument | $x$ | $y$ | $z$ | S/N | Comments |
|---|---|---|---|---|---|---|
| | JPL-IR | −2 m | 0 | 1 m | 005 | DNF |
| | JPL-IR | −32 m | 0 | 1 m | 006 | |
| | JPL-IR | −62 m | 0 | 2 m | 002 | DNF |
| G24 | TC | −130 m | −25 m | 0 | 030 | |
| | TC | −130 m | −25 m | 1 m | 223 | |
| | heat flux | −130 m | −25 m | 0 | 030 | |
| | bivane | −130 m | −25 m | 1 m | 382 | |
| | bivane | −130 m | −25 m | 4 m | 375 | |
| | bivane | −130 m | −25 m | 16 m | 374 | |
| | RTD | −130 m | −25 m | 1 m | NSN | |
| | RTD | −130 m | −25 m | 2 m | NSN | |
| | RTD | −130 m | −25 m | 4 m | NSN | |
| | RTD | −130 m | −25 m | 8 m | NSN | |
| | RTD | −130 m | −25 m | 16 m | NSN | |
| G25 | TC | −64 m | 25 m | 1 m | 000 | |
| | TC | −64 m | 25 m | 2 m | 000 | |
| | TC | −64 m | 25 m | 4 m | 000 | |
| | TC | −64 m | 25 m | 8 m | 000 | |
| | TC | −64 m | 25 m | 11 m | 000 | |
| | bivane | 20 m | 0 | 1 m | 388 | |
| | bivane | 20 m | 0 | 5 m | 376 | |
| | bivane | 20 m | 0 | 11 m | 381 | |
| W01 | Met-One | −1000 m | 0 | 2 m | N/A | |
| W02 | Met-One | −600 m | −100 m | 2 m | N/A | |
| W03 | Met-One | −600 m | 100 m | 2 m | N/A | |
| W04 | Met-One | −300 m | −100 m | 2 m | N/A | |
| W05 | Met-One | −300 m | 100 m | 2 m | N/A | |
| W06 | Met-One | −44 m | 25 m | 2 m | N/A | DNF |
| W07 | Met-One | 50 m | −75 m | 2 m | N/A | ESD |
| W08 | Met-One | 50 m | 0 | 2 m | N/A | ESD, DNF |
| W09 | Met-One | 50 m | 75 m | 2 m | N/A | |
| W10 | Met-One | 150 m | −150 m | 2 m | N/A | |
| W11 | Met-One | 150 m | −75 m | 2 m | N/A | |
| W12 | Met-One | 150 m | 0 | 2 m | N/A | |
| W13 | Met-One | 150 m | 75 m | 2 m | N/A | |
| W14 | Met-One | 150 m | 150 m | 2 m | N/A | |
| W15 | Met-One | 300 m | −150 m | 2 m | N/A | |
| W16 | Met-One | 300 m | −75 m | 2 m | N/A | |
| W17 | Met-One | 300 m | 0 | 2 m | N/A | |
| W18 | Met-One | 300 m | 75 m | 2 m | N/A | |
| W19 | Met-One | 300 m | 150 m | 2 m | N/A | |

**Remarks:**

1. Large RPT explosions began at approximately $T = 60$ sec.
2. Fire began at $T = 81$ sec.

## LEGEND

### Instrument Codes

| | |
|---|---|
| bivane | Gill bivane anemometer (see section 2.3.1.1). |
| heat flux | Commercially available heat flux plate (see section 2.3.1.5) |
| humidity | Ondyne dew point hygrometer (see section 2.3.1.6). |
| JPL-IR | Four channel infrared absorption sensor developed by the Jet Propulsion Laboratory (see section 2.3.2.2). |
| LLNL-IR | Four channel infrared absorption sensor developed by LLNL (see section 2.3.2.1). |
| Met-One | Cup and vane anemometer (see section 2.3.1.2) |
| MSA | Mine Safety Appliances catalytic gas sensor (see section 2.3.2.3) |
| TC | Thermocouple (see section 2.3.1.3). |
| RTD | Resistive temperature device (see section 2.3.1.4) |

### Function Codes

| | |
|---|---|
| DNF | Sensor failed to function, no data received. |
| HNL | High noise level. |
| ESD | Excessive standard deviation, local effects on flow. |
| EBD | Excessive baseline drift. |

## 4.0 The Meteorological Results

The data presented in this section include summaries of the approach atmospheric boundary layer conditions in effect during each spill, estimates of the centerline trajectory of the dispersing vapor cloud as predicted by the wind field data, and a measure of the atmospheric turbulence both upwind and downwind of the vapor barrier structure.

### 4.1 The Atmospheric Boundary Layer Data

A summary of the atmospheric boundary layer data for each of the five Falcon Series tests is included in Table 7 in the form of meteorological parameters commonly used to describe the atmospheric surface or boundary layer. The basis and physical significance of these meteorological parameters is adequately described elsewhere (Businger, 1973; Dyer, 1974; and Lettau, 1979). A brief description of what data were used, how they were handled, and how the parameters were calculated is presented in the following text.

The average wind speed and direction, and their standard deviations ($\sigma_\theta$ and $\sigma_u$) were taken from the wind field data collected by the array of 19 two-axis anemometers averaged over a three minute period starting at zero time (except Falcon 5, where three minutes prior to zero time was used). Station W6 was eliminated from all calculations, since the vapor curtain affected its response. Other stations were eliminated, as indicated in Table 7, due to large standard deviations in their directional readings caused either by proximity to structures or interference from highly-localized atmospheric disturbances, such as small "dust devils." Average direction variability was calculated as the square root of the sum of the squares of the standard deviations of the high and low frequency components of the wind variation. These quantities were taken as the values averaged over the individual stations of the 10 sec standard deviations (high frequency) and the standard deviation of the wind direction about its 3 min average direction (low frequency). The wind speed profile was calculated using the Gill bivane anemometer data from station G24 for the same 3 min time period (see Appendix B). The ambient temperature profile reflects data averaged over 3 min beginning at time zero from each of five RTD sensors on the upwind meteorological tower (station G24). Time history plots of each RTD reading are presented in Appendix D.

The friction velocity, $U_*$, scaling potential temperature, $\theta_*$, zero level potential temperature, $\theta_0$, and the Monin-Obukhov length, $L$, are determined from a least squares fit of the wind speed profile and potential temperature profile data to the assumed velocity profile function, Equation (1a), and potential temperature profile function, Equation (2a), as given below.

$$U(z) = \left(\frac{U_*}{k}\right) \cdot \left[\ln\left(\frac{z}{z_0}\right) - \psi_m\left(\frac{z}{L}\right)\right] \tag{1a}$$

$$\frac{dU(z)}{dz} = \frac{U_* \cdot \phi_m\left(\frac{z}{L}\right)}{k \cdot z} \tag{1b}$$

$$\theta(z) = \theta_0 + \left(\frac{\theta_*}{k}\right) \cdot \left[\ln\left(\frac{z}{z_0}\right) - \psi_h\left(\frac{z}{L}\right)\right] \tag{2a}$$

$$\frac{d\theta(z)}{dz} = \frac{\theta_* \cdot \phi_h\left(\frac{z}{L}\right)}{k \cdot z} \tag{2b}$$

**Table 7.** Falcon Series boundary layer data.

| | Test Name | | | | |
|---|---|---|---|---|---|
| | Falcon 1 | Falcon 2 | Falcon 3 | Falcon 4 | Falcon 5 |
| Array angle | 225°T | 225°T | 225°T | 225°T | 225°T |
| Average wind direction (@ 2 M) | 234.3°T | 227.0°T | 221.7°T | 230.6°T | 218.0°T |
| $\sigma_\theta$ | 5.46° | 8.27° | 8.41° | 5.82° | 7.70° |
| Average wind speed (@ 2 M) | 1.7 m/s | 4.7 m/s | 4.1 m/s | 5.2 m/s | 2.8 m/s |
| $\sigma_u$ | 0.20 m/s | 1.3 m/s | 0.56 m/s | 0.62 m/s | 0.41 m/s |
| Wind speed profile (G24) | | | | | |
| at 1.0 meters | $1.20 \pm 0.178$ m/s | $4.25 \pm 0.977$ m/s | $3.70 \pm 0.414$ m/s | $4.33 \pm 0.407$ m/s | $2.23 \pm 0.453$ m/s |
| at 4.0 meters | $2.20 \pm 0.142$ m/s | $5.25 \pm 1.24$ m/s | $4.53 \pm 0.367$ m/s | $5.93 \pm 0.448$ m/s | $3.40 \pm 0.498$ m/s |
| at 16.0 meters | $3.20 \pm 0.209$ m/s | $6.25 \pm 1.35$ m/s | $5.55 \pm 0.303$ m/s | $7.87 \pm 0.499$ m/s | $4.82 \pm 0.400$ m/s |
| $U_*$ | 0.0605 m/s | 0.3565 m/s | 0.3053 m/s | 0.3694 m/s | 0.1562 m/s |
| Temperature Profile (G24) | | | | | |
| at 1.0 meters | $32.2 \pm 0.14$°C | $31.8 \pm 0.05$°C | $35.0 \pm 0.05$°C | $30.8 \pm 0.11$°C | $31.1 \pm 0.20$°C |
| at 2.0 meters | $32.8 \pm 0.13$°C | $31.6 \pm 0.05$°C | $34.9 \pm 0.04$°C | $31.1 \pm 0.13$°C | $31.7 \pm 0.21$°C |
| at 4.0 meters | $33.4 \pm 0.13$°C | $31.5 \pm 0.06$°C | $34.8 \pm 0.03$°C | $31.4 \pm 0.15$°C | $32.2 \pm 0.21$°C |
| at 8.0 meters | $33.8 \pm 0.08$°C | $31.4 \pm 0.06$°C | $34.8 \pm 0.02$°C | $31.8 \pm 0.13$°C | $32.9 \pm 0.12$°C |
| at 16.0 meters | $34.1 \pm 0.06$°C | $31.2 \pm 0.06$°C | $34.7 \pm 0.04$°C | $32.0 \pm 0.08$°C | $33.4 \pm 0.06$°C |
| $\theta_*$ | 0.0577 K | −0.0964 K | −0.0175 K | 0.1521 K | 0.1379 K |
| Cloud cover | 1% | 1% | 5% | 10% | 20% |
| Absolute air pressure | 908.9 mb | 905.0 mb | 900.8 mb | 906.3 mb | 908.5 mb |
| Relative humidity | No data | No data | 4.0% | 12.0% | 13.7% |
| Dew point | No data | No data | −6.4°C | −0.3°C | 2.3°C |
| Stability class | G | D | D | D/E | E/F |
| Sensible heat flux | 3.64 W/m$^2$ | −3.57 W/m$^2$ | −5.46 W/m$^2$ | 58.70 W/m$^2$ | 22.52 W/m$^2$ |
| Momentum diffusivity (@ 2 M) | 0.0165 m$^2$/s | 0.313 m$^2$/s | 0.255 m$^2$/s | 0.265 m$^2$/s | 0.0740 m$^2$/s |
| Heat diffusivity (@ 2 M) | 0.0165 m$^2$/s | 0.335 m$^2$/s | 0.260 m$^2$/s | 0.265 m$^2$/s | 0.0740 m$^2$/s |
| Richardson number (@ 2 M) | 0.1337 | −0.0193 | −0.0047 | 0.0252 | 0.0844 |
| Monin-Obukhov length | 4.963 m | −103.4 m | −422.2 m | 69.38 m | 13.69 m |
| Roughness length | 0.008 m | 0.008 m | 0.008 m | 0.008 m | 0.008 m |

In the preceding equations, $U(z)$ is the wind speed at height $z$, $\theta(z)$ is the potential temperature at height $z$, and $k = 0.41$ is the Von Karman constant. The surface roughness value, $z_0$, was bracketed by plotting the zero wind speed intercept for each test. From the resulting range of values, several values were selected and used as $z_0$ values in the least squares fit for each test. The error in fit was plotted for each value of $z_0$ and each test and the minimum error (best fit) located. The results indicated $z_0 = 0.00775 \pm 0.0021$ m. This value was rounded to 0.008 m. For final computation of parameters for all tests.

The similarity functions used in Equations (1) and (2) are defined such that when $L \geq 0$:

$$\psi_m\left(\frac{z}{L}\right) = \psi_h\left(\frac{z}{L}\right) = -5 \cdot \frac{z}{L}$$

$$\phi_m\left(\frac{z}{L}\right) = \phi_h\left(\frac{z}{L}\right) = 1 + 5 \cdot \frac{z}{L} \quad , \tag{3a}$$

and when $L < 0$:

$$\begin{aligned}
\psi_m\left(\frac{z}{L}\right) &= 2 \cdot \ln\left[\frac{1+x}{2}\right] + \ln\left[\frac{1+x^2}{2}\right] - 2 \cdot \tan^{-1}(x) + \frac{\pi}{2} \\
\psi_h\left(\frac{z}{L}\right) &= 2 \cdot \ln\left[\frac{1+x^2}{2}\right] \\
\phi_m\left(\frac{z}{L}\right) &= \frac{1}{x} \\
\phi_h\left(\frac{z}{L}\right) &= \frac{1}{x^2} \quad ,
\end{aligned} \tag{3b}$$

where

$$x = \left(1 - \frac{16 \cdot z}{L}\right)^{1/4} \quad .$$

The parameters $U_*$, $\theta_*$, $\theta_0$, and $L$ are all related by the Monin-Obukhov length definition:

$$L = \frac{U_*^2 \cdot \theta_0}{g \cdot k \cdot \theta_*} \quad , \tag{4}$$

where $g = 9.8$ m/s$^2$ is the acceleration of gravity. Equation (4) is used as a constraint on the least squares fit of the profile data to the analytic curves of Equations (1a) and (2a).

The potential temperature is defined in terms of the actual ambient temperature and pressure to be:

$$\theta_0 = T_a \cdot \left(\frac{p_0}{p}\right)^{\mu} \quad , \tag{5a}$$

where

$T_a$ = actual ambient temperature

$p$ = ambient pressure

$p_0$ = standard pressure = 1000 mb

$\mu = R/C_p = 0.285$.

Differentiating Equation (5a) with respect to height $z$, using the hydrostatic approximation, $dp = -g \cdot \rho \cdot dz$, and the ideal gas law, $p = \rho \cdot R \cdot T$, assuming that the ratio, $\theta/T_a$, is essentially constant over the height range of interest, and then integrating with respect to height yields the following equation for potential temperature as a function of temperature and height.

$$\theta_0 = \left(\frac{p_0}{p_r}\right)^{\mu} \cdot [T_a + \gamma \cdot (z - z_r)] \quad , \tag{5b}$$

where

$$\gamma = \frac{g}{C_p}$$

and $r$ denotes reference value. Equation (5b) was used to calculate the potential temperature from the temperature data.

The sensible heat flux, $H$, defined to be negative upward, is calculated from:

$$H = \rho \cdot C_p \cdot U_* \cdot \theta_* \quad , \tag{6}$$

where $\rho$ = 1.13 kg/m$^3$ ($\pm$1% for 30 to 40°C) and $C_p$ = 1005W s/kg°C are, respectively, the density and specific heat of the ambient atmosphere. The momentum diffusivity, $K_m$, and the heat diffusivity $K_h$ are calculated from the formulas:

$$K_m(z) = \frac{U_* \cdot k \cdot z}{\phi_m(z/L)} \tag{7a}$$

$$K_h(z) = \frac{U_* \cdot k \cdot z}{\phi_h(z/L)} \quad . \tag{7b}$$

The Richardson number is defined and calculated from the similarity functions as follows:

$$R_i\left(\frac{z}{L}\right) = \frac{\frac{g}{T_0}\frac{dT}{dz}}{\left(\frac{dU}{dz}\right)^2} = \frac{\frac{z}{L} \cdot \phi_h\left(\frac{z}{L}\right)}{\phi_m^2\left(\frac{z}{L}\right)} \quad . \tag{8}$$

## 4.2 The Wind Field Data

The wind field was measured before, during, and after each Falcon Series spill test using an array of 19 Met-One cup and vane anemometers, each mounted at a height of 2 m above ground level. The array was distributed from 1000 m upwind of the spill point to 300 m downwind, and laterally to $\pm$150 m about the centerline, as shown in Figure 2. Each remote anemometer station measured wind speed and direction at a sampling rate of one sample per second for a period of 10 sec, then calculated mean values of wind speed and direction and RMS values ($\sigma_\theta$) about the mean wind direction over the 10 sec period, transmitted the calculated values to the CCDAS, and repeated the entire process throughout the test period.

The wind field provides the primary force for the dispersion of the LNG cloud after it exits the vapor barrier. In order to provide a preliminary estimate of cloud transport and dispersion, trajectory plots were constructed from the wind field data. Data from the 19 wind field stations were interpolated and extrapolated to a 400 m wide by 500 m long grid beginning at the spill point and straddling the array centerline. These data were then used to track hypothetical particles released every 10 sec during the spill. Since the vapor barrier was not a point source, but rather released the vapor cloud over its entire 44 m width (and also to some extent along its 88 m length) and also represented a major source of turbulence, the authors chose to plot three centerline trajectories from three different source points (one from the center and one from each edge of the downwind side of the vapor barrier). The interpolated 10 sec $\sigma_\theta$ data were ignored therefore the dispersion indicated by these plots arises strictly from variation in the trajectory of the gas cloud depending on where along the vapor curtain it was released. These computer-generated centerline trajectories at several selected times during each spill test are shown in Appendix A.

These results should approximate the position of the cloud as it passes through the sensor array. The location of the sensor array stations is shown on the trajectory plots.

### 4.3 The Turbulence Data

Turbulence data were recorded at a sampling rate of one sample per second at stations G04, G10, G11, G12, G24, and G25. Each station was equipped with three Gill bivane anemometers capable of measuring the wind speed and the horizontal and vertical components of wind direction. The anemometer data of station G24 were used to calculate the wind speed profiles of Table 7. The purpose of the other five stations was to determine if there was any measurable wind field displacement or turbulence perturbations due to the presence of the LNG cloud and/or the vapor barrier. Measurable turbulence damping was observable, particularly during Falcon 1, due to the presence of LNG vapors. Turbulence generated by the vapor barrier, damping out exponentially with distance, is readily observed in the data.

The anemometer data from all six turbulence stations for each spill test is shown in Appendix B. Vertical direction results have been shifted using 300 sec of data prior to zero time to establish a baseline value defined to be zero (to correct imbalances in sensor installation).

## 5.0 The Spill Area Results

In the spill area, measurements were taken of gas concentration, heat flux, dew point, and temperature. The number and distribution of these measurements varied from test to test due to sensor availability and in response to data from previous tests. These changes are reflected in sensor maps in Figures 3, 4, and 7 through 12. These data are expected to provide inputs to future analysis relevant to the design of effective vapor barrier mitigation systems. Thermocouple measurements taken above and below the water surface are to determine if the LNG is evaporating as rapidly as it is spilled. Gas concentration measurements are to establish actual source conditions and to correlate gas concentration with temperature in the contained vapor cloud. Elevated temperature measurements (up to 14 m) are intended to provide information on vapor density stratification within the barrier and on mixing of the atmosphere with the confined LNG vapor cloud.

Spill Area data are presented in Appendix C. Data are grouped by spill test in order of occurrence (Falcon 1–5). Data are organized within each spill test in the following sequence:

1. Gas sensor data are presented with collocated dew point and temperature data presented adjacent to the data from the applicable gas sensor.
2. Heat flux data are presented with collocated ground temperature data.
3. Temperature data below and above (>1 m height) the pond surface are presented grouped by $x$,$y$ coordinate.
4. Temperature data $\geq$1 m height are presented grouped by $x$,$y$ coordinate.

### 5.1 Spill Area Temperature Results

Temperature measurements in the spill area were performed using type $k$ thermocouples, as described in section 2.3. Since relative temperature measurement is more important than absolute temperature measurement to the analysis anticipated in the spill area, the thermocouples at 1 m or higher elevations were adjusted to the 100 sec pre-spill average of all spill area thermocouples (above 1 m). Relative temperature changes should be easily extracted from data plotted in this manner. No adjustments were applied to thermocouples reading pond temperature, ground temperature, or air temperature below 1 m in height. Accuracy of absolute temperature measurement in the spill area is believed to be $\pm 3°C$ and relative temperature measurements are believed accurate to $\pm 0.5°C$.

The presence of adverse conditions during Falcon 3 (RPTs) and Falcon 5 (RPTs and fire) disrupted measurements in the spill area. Data from these two tests often were truncated at between $t = 60$ sec and $t = 200$ sec because of these events. Similarly, on Falcon 2, station G22, channel A14, data were truncated at $t = 400$ sec due to the sudden (and as yet unexplained) failure of the sensor on that channel. Other data deleted from the data plots were due to sensor failure and are noted in Table 6.

### 5.2 Spill Area Heat Flux Results

Spill area heat flux data are presented together with collocated ground temperature data to provide a measure of cloud heating provided by the exposed ground surface inside the vapor barrier.

The two heat flux sensors were located one downwind and one upwind of the billboard structure to help understand the effects of that structure. Ground temperature measurements are not adjusted and are believed accurate to $\pm 3°C$ in absolute temperature, and $\pm 0.5°C$ in relative temperature. Heat flux measurements are given in Watts per $m^2$ with the sign convention chosen such that a *negative* reading indicates heat flow *into* the ground.

### 5.3 Spill Area Gas Sensor Results

Data from each JPL-IR sensor are presented in three plots showing percent by volume concentrations of methane, ethane, and total hydrocarbons. Immediately following the plots from each gas sensor is any collocated temperature and humidity data available. Collocated temperature data are intended to help establish the relationship between gas concentration and temperature for extrapolation to temperature/gas concentration profiles elsewhere within the vapor barrier. Collocated dew point data (samples were taken from the gas sampling tube at a point near the JPL-IR sensor, physically located outside the vapor barrier) are intended to help in establishing the energy balance due to the interaction between the cryogenic LNG and the water pond (i.e., water vapor in the cold cloud freezes and reduces the partial pressure of $H_2O$, allowing more water vapor to be introduced into the cloud from the pond. The vapor from the pond also freezes and the cycle continues transferring heat from the pond to the cloud). Temperature data are believed accurate to $\pm 3°C$ in absolute temperature, and to $\pm 0.5°C$ in relative temperature. Measurement of absolute dew point temperature was suspect throughout the test series. Three dew point hygrometers, all measuring samples taken from the same height within the vapor barrier during the last 100 sec prior to spill, showed variations on the order of $\pm 10°C$. Relative measurements are believed to be more accurate at $\pm 10\%$ of the recorded variation in dew point temperature.

JPL-IR gas sensors were individually calibrated prior to the test series and, where possible, after the test series was completed (some sensors could not be recalibrated due to the nature of their fire damage). Comparison of identical data plotted, using pre-test calibrations, post-test calibrations, and calibrations from previous test series, indicate an uncertainty of $\pm 5\%$ of the sensor reading for total hydrocarbons.

## 6.0 Vapor Dispersion Results

One major objective of the LNG vapor barrier verification field trials was to measure the atmospheric dispersion of LNG vapor released from a full-scale vapor barrier under actual atmospheric conditions, with emphasis on determining the range at which dilution below the lower flammability limit (LFL) is achieved. Comparison of the LFL dilution range from these tests with results of earlier free field dispersion tests provides the principle measure of the effectiveness of vapor barriers as mitigation devices for potential industrial LNG spills. It also provides the basic data to validate wind tunnel and computer models which can then be used to simulate a variety of plant site and meteorological conditions.

This objective was achieved by measuring the concentration of natural gas vapors at three or four levels (up to 17 m) at three rows of stations (each containing between 5 and 9 stations evenly spaced laterally at 50, 150, and 250 m downwind of the vapor barrier. This also allowed the height and lateral extent of the vapor cloud to be measured at each row. The locations of the various stations for the different tests are shown in Fig. 23 and Fig. 24. This section presents the gas concentration results, along with other measurements pertinent to understanding vapor cloud dispersion, including cloud temperature (at each gas sensor location), surface heat flux (at 50 and 150 m), surface temperature (at each heat flux sensor location), and humidity (where available).

### 6.1 Vapor Cloud Temperature Data

Vapor cloud temperature data are presented in Appendix D, grouped by test in the order of occurrence (Falcon 1–5). For each test the data from each tower (3 or 4 sensors) are displayed in a $2 \times 2$ array, each occupying one page of the report. The vertical scales are the same for each sensor on a given tower, allowing easy comparison and an overview of vertical gas concentration profile while retaining sufficient plot size to allow data extraction by the reader.

The temperature data have been adjusted by matching the pre-test average measurements to the pre-test average temperature profile measured by the RTDs on station G24 in order to eliminate baseline uncertainty inherent to thermocouples (uncertainties arise from variations in junction thickness, wire resistivity, etc.). RTD data from stations G11 and G24 are included as the last plots on each test for comparison purposes.

### 6.2 Ancillary Vapor Dispersion Data

This section presents data on surface heat flux (at 50 and 150 m), surface temperature (collocated with heat flux sensors), and dew point (where available), which are contained in Appendix E, grouped by test in order of occurrence (Falcon 1–5). For convenience in referencing data, each collocated heat flux and ground temperature data plot are presented immediately adjacent to one another. No adjustments have been made to the data presented in this section. These instruments are described in Section 2.3 and the station locations are defined in Table 6 (also in Figs. 23 and 24).

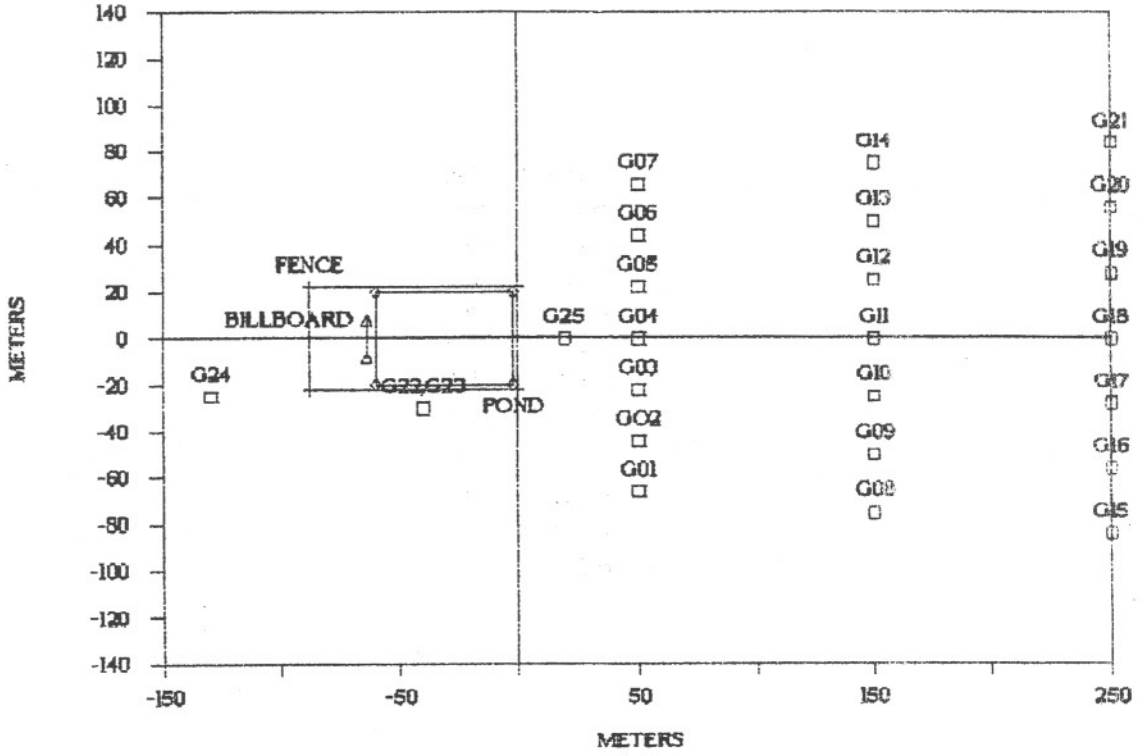


**Figure 23.** Falcon 1–3 FDAS station array.

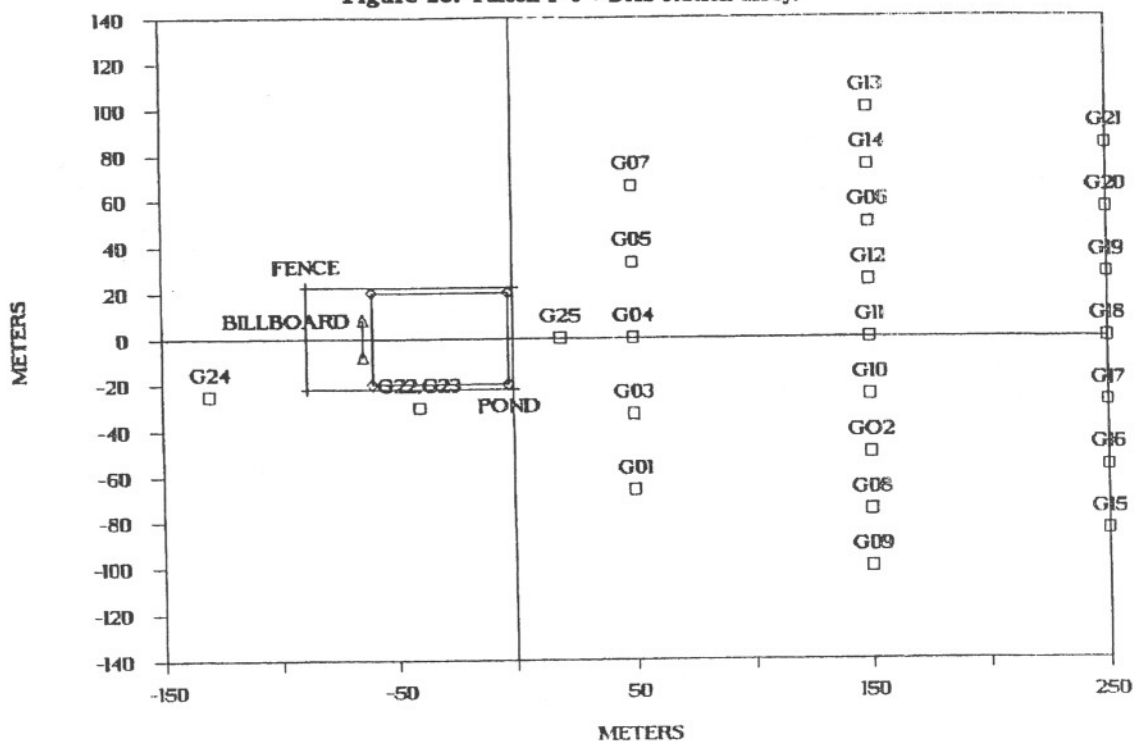


**Figure 24.** Falcon 4–5 FDAS station array.

## 6.3 LNG Vapor Concentration Data

LNG vapor concentration data were taken using LLNL-IR sensors and MSA catalytic sensors at up to four heights (1, 5, 11, and 17 m) on 21 towers emplaced in three lateral rows (50 m, 150 m, and 250 m) downwind of the vapor barrier, as shown in Figures 9–12. These data are presented in two forms: Vapor concentration time-history plots (see Appendix F), and vapor concentration vertical (crosswind) contour plots (see Appendix G).

Temporal concentration data are presented in the same manner as vapor cloud temperature data, by row and by sensor tower (see section 6.1). Each sensor was individually pre- and post-test calibrated with commercial gas calibration mixtures. Individual sensor data were processed using both calibrations, the data compared, and appropriate calibration coefficients selected and applied to the data presented. Data plots are concentration (percent by volume) vs time. The data were taken at the rate of one sample/sec, but were averaged over five seconds before plotting. The data on tape are at one sample/sec.

The LNG vapor concentration data were used to generate two-dimensional, vertical, crosswind contour plots at 20 sec time intervals during the experiments for the 150 m row and at 10 sec time intervals for Falcon II where the data at the 250 m row were plotted. Each contour plot is labeled by test name, time of the plot, and the concentration levels of each contour. The vertical contours are plotted as they would appear when looking towards the vapor barrier. The horizontal and vertical scales are not identical for the contour plots. The vertical scale is exaggerated, which makes the cloud appear to be higher than it actually was. Prior to each contour sequence is a vertical grid plot indicating the sensors which were operational during that particular test. Concentrations at locations where sensors were nonoperational were generated by linear interpolation and extrapolation of data from neighboring sensors. The two outside towers on each lateral boundary of the 150 m row were not instrumented at the 17-m height. Assigning zeros to these points would most likely be an underestimate. A more reasonable approach was taken by assigning two thirds and one third of the nearest 17-m sensor value to the adjacent and outer locations, respectively, at the 17-m height. The missing interior values for Falcon II Row 3 were plotted using linear interpolation of the horizontal values. The data were averaged for five seconds before contour plotting.

Contours were generated using linear interpolation in the horizontal direction, and both linear and quadratic interpolation in the vertical direction. In addition to the actual measured results at the three or four sensor heights at a tower location, the ground level was calculated using the following procedure to prevent contours from closing below the lowest level sensor. The ground level data were extrapolated using a quadratic fit (such that the concentration gradient was equal to zero at the ground) of the data from the sensors at the two lowest levels when the concentration at the second level was less than the concentration at the lowest level, or a linear fit if the concentration at the second level was greater than the concentration at the lowest level.

## 6.4 LNG Vapor Mass Flux Data and Calculations

The mass flux of the LNG vapor passing through the 150 m row was calculated using the LNG vapor concentration data and vapor cloud temperature data of section 6.3 and 6.1 along with the wind field data of section 4.2. Gas concentration data were the same as those used to construct contour plots presented in section 6.3, however additional interpolated concentration values were calculated for other heights, producing a total of 12 values per tower location. Gas concentration

was assumed to be zero at a height of 21 m. Below 1 m, the gas concentration profile was assumed to be quadratic approaching zero gradient at the ground if the vertical gradient was negative between 1 and 5 m; if the measured gradient was positive, a linear extrapolation was used below the 1-m height. These values were then interpolated horizontally at 9 intermediate locations between each pair of sensor towers. Temperature data interpolation was similar to that for gas concentration data, except that a logarithmic profile with height was assumed below 1 m. Wind speed interpolation was logarithmic in the vertical direction and linear in the horizontal direction. Time histories of calculated instantaneous and time-integrated (cumulative) mass flux are presented in Figures 25, 26 and 27.

The mass flux plots are consistent with spill parameters for the respective tests in two ways. First, the duration of cloud passage for the main cloud, that portion of the time history bounded by a rapid rise and then fall in the mass flux, is comparable to the duration of the respective spill events (valve open to valve closed); this is true even for Falcon 4, with its relatively low spill rate. Second, the peak mass flux in Falcon 3 and 4 is nearly the same as the spill rate, when converted to the same units. For Falcon 1, the peak mass flux is only about 40% of the spill rate; this is due to width of the cloud dramatically exceeding the width of the instrument array at 150 m.

Table 8 gives the specific numerical results of the mass balance calculations. The total amount of LNG spilled, assuming 430 kg per $m^3$, and the amount calculated from the mass flux results are given along with the ratio of these values. The rather low ratio of calculated to actual mass spilled in Falcon 1 is due primrily to the very low, wide cloud that resulted from the substantial LNG vapor overflow of the fence which occurred because of the high spill rate under low wind speed, stable conditions. As seen from the contour plots in Appendix G for Falcon 1, the cloud was primarily within 5 m of the ground; the values are rather constant in the horizontal, indicating tht the cloud edges were probably well beyond the array bounds. The array was widened on Falcon 4 and was successful in capturing the gas cloud, as seen in Appendix G. As a result, the mass calculated from the mass balance accounted for most of the actual mass spilled.

The calculated mass spilled for Falcon 3 was greater than the actual mass spilled by 18%. This was unexpected since the cloud exceeded the array on one side and then later on the other, as seen in the contour plots in Appendix G. A ratio of about 0.75 would be more plausible. The gas concentration, wind, and temperature data used in the calculations have been scrutinized, but no systematic source of error has emerged. The shape of the time history of mass flux seems reasonable, with perhaps slightly higher and more variable values after 400 seconds, when compared with Falcon 1 and 4. After 400 seconds, the cloud becomes elevated, as shown in Appendix G. The maximum concentration occurs at the 17-m height. In the mass balance calculations, the gas concentration is assumed to decrease linearly with height from 17 m to 21 m. If the cloud top were assumed to be at 17 m, with zero concentration above that, the calculated mass spilled is 24,380 kg, which gives a ratio of 1.12. This is, however, a rather unlikely scenario. Gas concentration data for Falcon 2 and 5 were insufficient for calculating mass balances.

**Table 8.** Summary of mass balance results.

| Test Name | Actual mass spilled | Calculated mass spilled | Ratio |
|---|---|---|---|
| Falcon 1 | 28,552 | 10160 | 0.36 |
| Falcon 3 | 21,801 | 25,830 | 1.18 |
| Falcon 4 | 19,307 | 16920 | 0.88 |

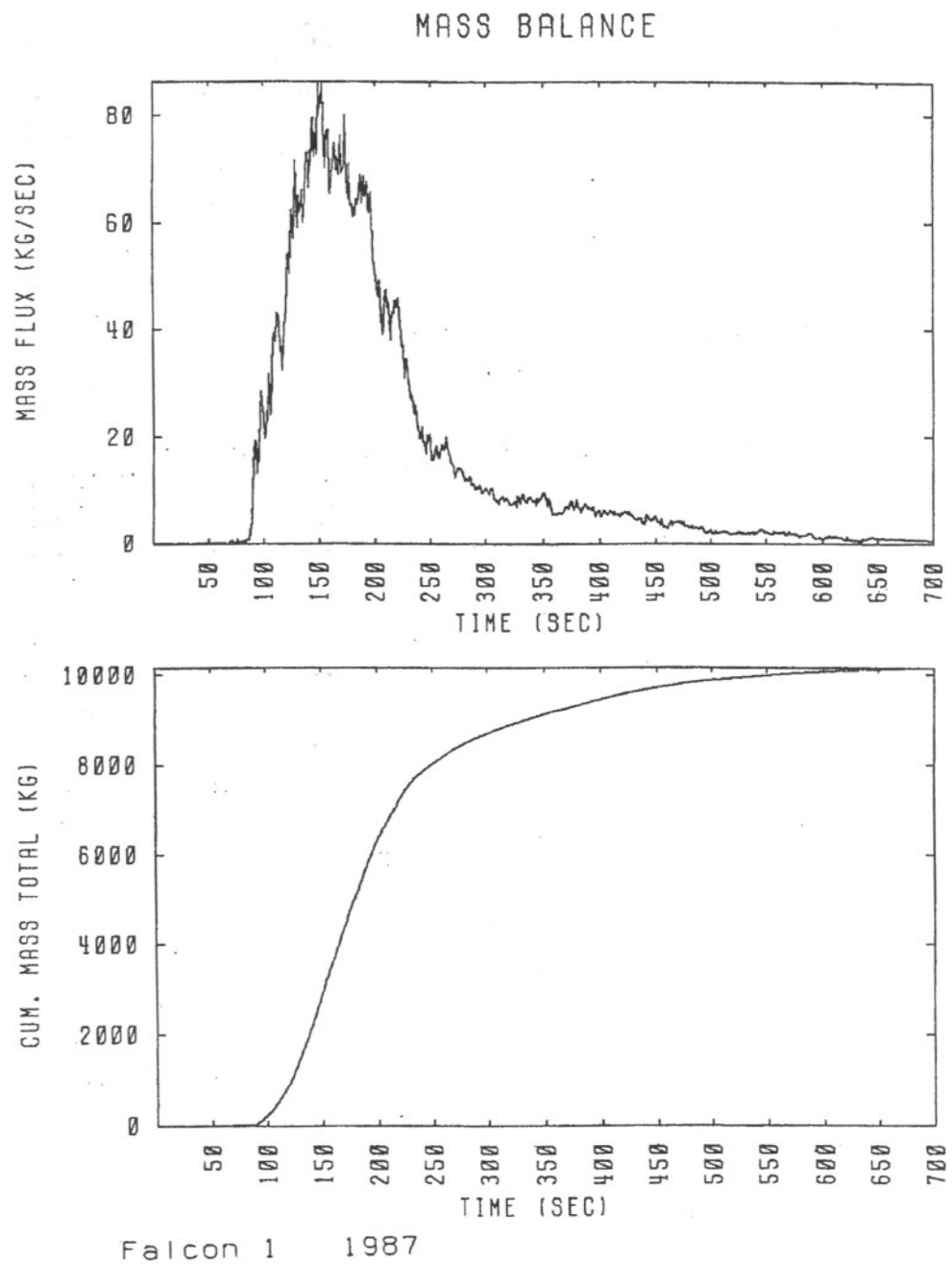


**Figure 25.** Falcon 1 mass flux data.

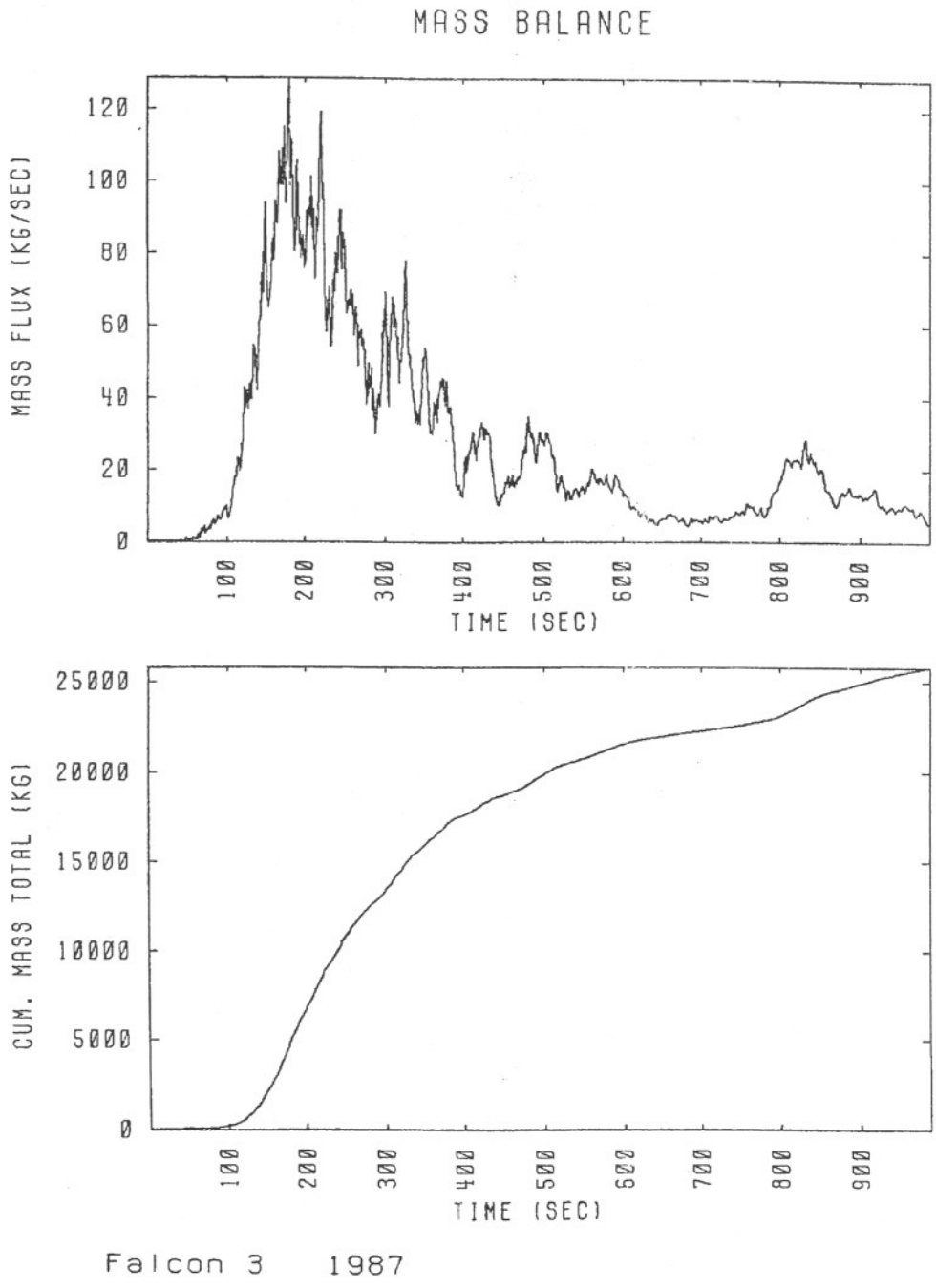


**Figure 26.** Falcon 3 mass flux data.

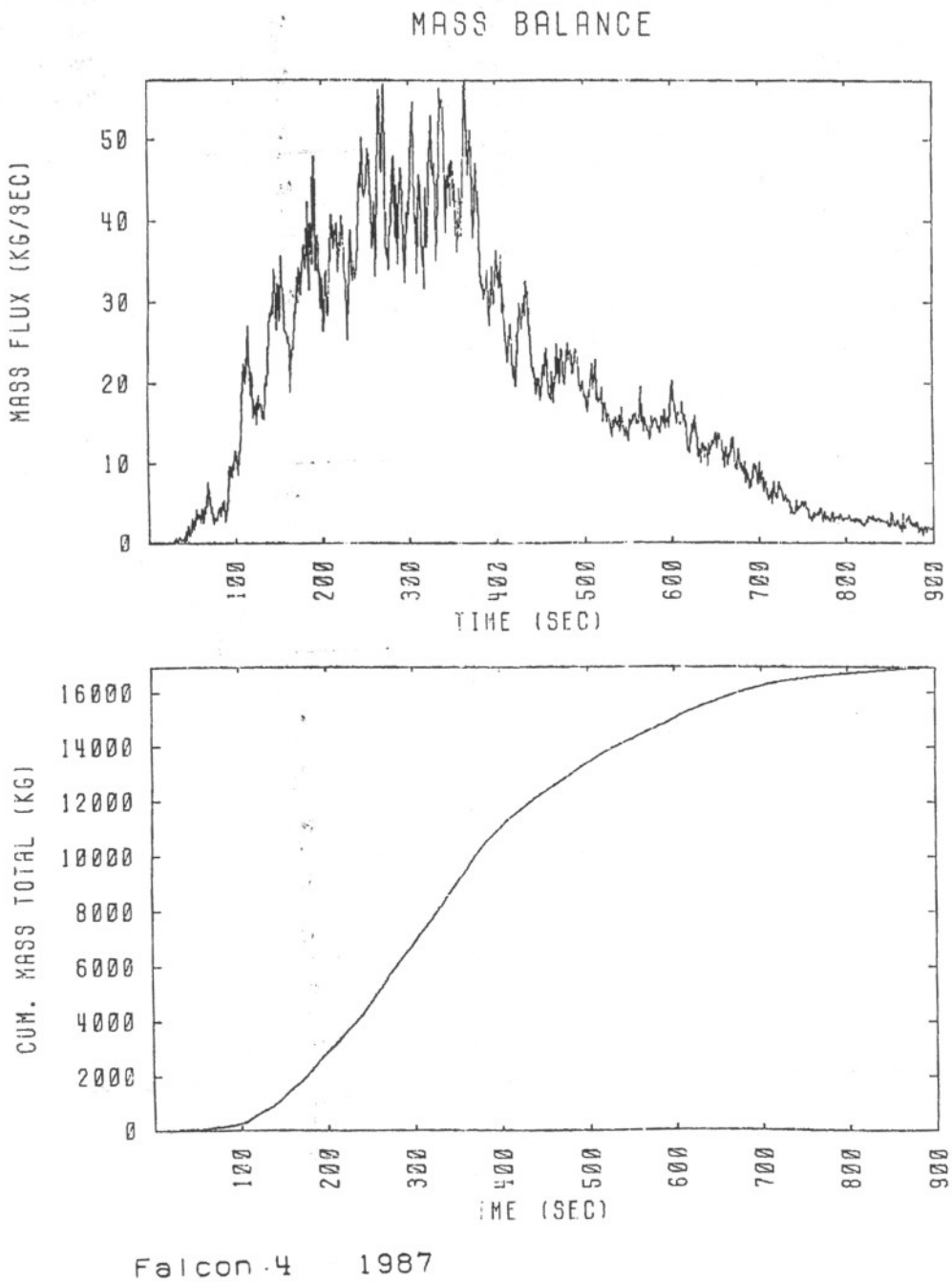


**Figure 27.** Falcon 4 mass flux data.

## Acknowledgments

The data reported here represent the work of many people from several different organizations. In particular, the authors wish to express their sincere thanks to Mr. Ted Williams and Dr. Steve Wiersma of the Gas Research Institute, and Mr. Walter Dennis of the Department of Transportation, for their contribution to the success of the field experiments. In addition, we would like to acknowledge the following individuals:

**LLNL/Livermore**
Chantel Aracne
Bruce Borman
Marilyn Borton
Bill Funkhauser
Gary Johnson
Chris Martin
Ralph Smith
Greg Soto
Myles Spann
Stan Trettenaro
Roland Wallstedt
Janet Welch
Steve Wofford

**EG&G Las Vegas**

Harold Gray
Lance Groft
Bill Huth
Monty Ortiz
John McEntire
Amaneo Sanchez, Jr.
Shirley Stutsman

**LLNL/NTS**
Bill Edwards
Terry Roy
Steve Stark
Pat Stathis

**NOAA/WSNSO**
Darryl Randerson
Pete Mueller

**REECo**
Dennis Finney

**DOE/NV**
Rudy Jezik
Don Martin
John Spahn
John Stewart

This work was performed for the United States Department of Transportation and the Gas Research Institute under the auspices of the US Department of Energy by the Lawrence Livermore National Laboratory (Contract No. W-7405-ENG-48).

# References


Baker, J., "The LLL Data Acquisition System for the Liquefied Gaseous Fuels Program," Lawrence Livermore National Laboratory, Livermore, CA, UCID-18576, March 1980.

Bingham, G.E., R.D. Kiefer, C.H. Gillespie, T.G. McRae, H.C. Goldwire, Jr., and R.P. Koopman, "Portable, Fast-Response Gas Sensor for Measuring Methane and Ethane in Liquefied Natural Gas Spills," *Rev. Sci. Instrum.* **54(10)**, 1356–1361, October 1983.

Brown, T.C., et al., *Test Plan LNG Vapor Barrier Verification Field Trials*, Prepared for the United States Department of Energy, Nevada Operations Office, May 1987.

Brown, T.C., et al., *Test Management Summary LNG Vapor Barrier Verification Field Trials*, Prepared for the United States Department of Energy, Nevada Operations Office, May 1987.

Brown, T.C., et al., *Safety Assessment Document LNG Vapor Barrier Verification Field Trials*, Prepared for the United States Department of Energy, Nevada Operations Office, May 1987.

Businger, J.A., "Turbulent Transfer in the Atmospheric Surface Layer," Chapter 2 in *Workshop on Micrometeorology*, Duane A. Haugen (ed.), American Meteorological Society, 1973.

Dyer, A.J., "A Review of Flux Profile Relationships," *Boundary-Layer Meteorology*, 7, 363–372, 1974.

Goldwire, H.C., Jr., H.C. Rodean, R.T. Cederwall, E.J. Kansa, R.P. Koopman, J.W. McClure, T.G. McCrae, L.K. Morris, L. Kamppinen, R.D. Kiefer, P.A. Urtiew, and C.D. Lind, "Coyote Series Data Report LLNL/NWC 1981 LNG Spill Tests Dispersion, Vapor-Burn, and Rapid-Phase-Transition," Lawrence Livermore Laboratory, Livermore, CA, UCID-19953, October 1983.

Goldwire, H.C., Jr., T.G. McRae, G.W. Johnson, D.L. Hipple, R.P. Koopman, J.W. McClure, L.K. Morris, R.T. Cederwall, "Desert Tortoise Series Data Report 1983 Pressurized Ammonia Spills," Lawrence Livermore National Laboratory, Livermore, CA, UCID-20562, December 1985.

Johnson, G.W., "The LGF Data Acquisition System 1983 Update," Lawrence Livermore National Laboratory, Livermore, CA, UCID-20138, August 1984.

Johnson, G.W., and D.W. Thompson, "Liquified Gaseous Fuels Spill Test Facility Facility Description," Lawrence Livermore National Laboratory, Livermore, CA, UCID-20291, Rev. 1, 1986.

Koopman, R.P., J. Baker, R.T. Cederwall, H. C. Goldwire, Jr., W.J. Hogan, L.M. Kamppinen, R.D. Kiefer, J.W. McClure, T.G. McRae, D.L. Morgan, L.K. Morris, M.W. Spahn, Jr., and C.D. Lind, "Burro Series Data Report LLNL/NWC 1980 LNG Spill Tests," Lawrence Livermore National Laboratory, Livermore, CA, UCID-19075, December 1982.

Lettau, H.H., "Wind and Temperature Profile Prediction for Diabatic Surface Layers Including Strong Inversion Cases," *Boundary-Layer Meteorology*, *17*, 443–464, 1979.

Mann, D., general editor, *LNG Materials and Fluids*, National Bureau of Standards, Boulder, CO, 1977.

McRae, T.G., R.T. Cederwall, D.L. Ermak, H.C. Goldwire, Jr, D.L. Hipple, G.W. Johnson, R.P. Koopman, J.W. McClure, and L.K. Morris, "Eagle Series Data Report 1983 Nitrogen Tetroxide Spills," Lawrence Livermore National Laboratory, Livermore, CA, UCID-20063, Rev. 1, March 1987.

Patton, S.E., M.G. Novo, and J.H. Shinn, *Environmental Assessment for the LGF Spill Test Facility at Frenchman Flat, Nevada Test Site*, United States Department of Energy, Nevada Operations Office, DOE/EA-3009, June 1986.

# Falcon Series Data Report

# Appendix A. Wind Field Data